

**DOKUZ EYLÜL UNIVERSITY**  
**GRADUATE SCHOOL OF NATURAL AND APPLIED SCIENCES**

**ENGINEERING GEOLOGY OF**  
**THE HARMANDALI (İZMİR) WASTE DISPOSAL**  
**SITE**

by  
**Lina PAZARBAŞI**

**July, 2018**  
**İZMİR**

**ENGINEERING GEOLOGY OF  
THE HARMANDALI (İZMİR) WASTE DISPOSAL  
SITE**


**A Thesis Submitted to the  
Graduate School of Natural and Applied Sciences of Dokuz Eylül University  
In Partial Fulfillment of the Requirements for the Degree of Master of  
Science in Geological Engineering, Applied Geology Program**

**by  
Lina PAZARBAŞI**

**July, 2018  
İZMİR**

**M.Sc THESIS EXAMINATION RESULT FORM**


We have read the thesis entitled “ENGINEERING GEOLOGY OF THE HARMANDALI (İZMİR) WASTE DISPOSAL SITE” completed by LINA PAZARBAŞI under supervision of ASSOC. PROF. DR. CEM KINCAL AND PROF. DR. GÖKHAN GÖKTÜRKLER and we certify that in our opinion it is fully adequate, in scope and in quality, as a thesis for the degree of Master of Science.

  
.....  
Assoc.Prof.Dr.Cem KINCAL

Supervisor

  
.....  
Prof.Dr.Gökhan GÖKTÜRKLER

Supervisor

  
.....  
Prof. Dr. M. Yılmaz Koc

(Jury Member)

  
.....  
Doç. Dr. Alper Sezer

(Jury Member)

  
.....  
Doç. Dr. Meriç Aziz BERGE

(Jury Member)

  
.....

Prof.Dr. Latif SALUM

Director

Graduate School of Natural and Applied Sciences

## ACKNOWLEDGEMENT

Firstly, I would like to express my special thanks of gratitude to the most generous person I have ever met...

To the person who knows the real meaning of Human and Humanity...

To the person who was always helping me in everything during three years without any complaints...

To the person who supports me a lot in my thesis and study...

My supervisor:

(Assoc. Prof. Cem KINCAL)

I am really grateful for your infinite kindness, supports and helps.

Also, my sincere thanks and gratitude go to my supervisor Prof. Dr. Gökhan GÖKTÜRKLER who was always helping me to overcome all the obstacles that faced me during the research. I would like to thank you so much for your guidance, patience and supports. I would also like to show gratitude and thanks to Instructor. Zulfikar ERHAN for his supports and helps in the field and geophysical analysis. I thank the staff in Izmir Metropolitan Municipality for being helpful to collect information about the study site. Besides, I would like to thank Assoc. Prof. Mümtaz Calok, Prof. Dr. Mehmet Yalçın KOCA and Prof. Dr. Ali Bahadır YAVUZ for their assistances, advices, helps and immense knowledge in the first year of my Master degree. Also I would like to thank eng. Amir Alboukhari for his supports. My grateful thanks go to my Tunisian twins Amna KHILA for her helps and supports in my thesis and I want to say that you are great faith and gift from Allah. I would like to thank my great friend Rabiye DAĞ for her supports and helps. I also would like to thank my sister and antim in alienation Rahma SHASHAA who was supporting me spiritually every time.

I would like to thank my great Syrian parents (MHD Amin & Suhair) for their infinite encouragefrom birth till now. Also, I would like to thank my sister (NOUR) for sharing all my problems and obstacles with me. I want to tell you that: I am so proud that you are my family and my soul which I live with.

I would also like to thank my Turkish parents (Ali Naci Ülkü & Nalan) who they received me first arrived to Turkey and teach me Turkish letters and how to deal with people here. I would to say thanks to you for fiving me the feel that I was reborn in Turkey with great family. My grateful thanks go to my great and dear aunts who are the best spiritually supporter for continuing my thesis. I would like to thank whole my family and friends in Syria and Turkey.

At last and not least, thanks for my cheerleader in this life, for my inspirational person, for my only and one, for my O<sub>2</sub>: (Imad Al- RAWI).



# **ENGINEERING GEOLOGY OF THE HARMANDALI (İZMİR) WASTE DISPOSAL SITE**

## **ABSTRACT**

Harmandalı (İzmir) waste disposal site has been put into service on 1996 and managed by the Metropolitan Municipality of Izmir and waste management office.

In February 2013, a landslide hit Harmandalı waste disposal site and affected the administration buildings and a truck scale in this area. Also, in March 2016 another landslide occurred in the area. These events resulted in mass movement in the Harmandalı landfill site. As well as, this mass movement reactivates by new external and internal factors for instance rainfall, seismic activity, earthquakes, etc. Two geophysical methods were conducted in the area in order to determine the sliding surface in Harmandalı waste disposal site; Electrical Resistivity Tomography (ERT) and Multichannel Analysis of Surface Waves (MASW). Surveys included two lines of Electrical Resistivity Tomography surveys which laid out parallel and perpendicular to landslide direction. Two ERT profiles were conducted to map resistivity distribution of the surface. The resistivities were classified into three categories; low, middle and high values. Comparing with geological studies, the low values of resistivity was indicated to leachate, water and clay. The second geophysical method MASW was carried out in the area using 7 profiles to obtain Rayleigh wave dispersion curves for estimation of shear wave velocity profiles to 30 m depth of the area. Three of the MASW profiles were parallel to the landslide direction and four of them were perpendicular to the landslide direction. The results of MASW surveys included seven of 1D S-wave velocity profiles and two of 2D S-wave velocity profiles. The results indicated that there are three velocity zones in the area; high, moderate and low values. The low values of velocity from the MASW surveys refer to sliding surfaces which were affected by existence of water and high plasticity clay.

According to the geophysical results, the essential depth of the sliding surface in the study area is about 9 meter in SK-8, 22 meter in SK-3, 15 meter in SK-5 and 10 m in SK-2.

**Keywords:** Landslide, electrical resistivity, tomography, MASW, waste disposal site, Harmandalı, İzmir



# HARMANDALI İZMİR ATIK DEPOLAMA SAHASININ MÜHENDİSLİK JEOLJİSİ

## ÖZ

Harmandalı (İzmir) katı atık sahası 1996 yılında hizmete girmiştir, İzmir Büyükşehir Belediyesi atık yönetim ofisi tarafından yönetilmektedir. Şubat 2013'te, Harmandalı katı atık sahasında gerçekleşen heyelan bu bölgedeki idari binaları ve bir kamyon kantarını etkilemiştir. Ayrıca Mart 2016'da bölgede başka bir heyelan daha meydana gelmiştir. Bu olaylar Harmandalı katı atık depolama sahasında kütle hareketleri ile sonuçlanmıştır. Bunun yanı sıra, kütle hareketleri yağış, sismik aktivite, deprem vb. gibi iç ve dış faktörler tarafından yeniden tekrarlanabilir. katı atık sahasında kayma yüzeyini belirlemek amacıyla inklinometre ölçümlerinin yansira iki farklı jeofizik yöntem uygulanmıştır. Bu yöntemleri Çok Kanallı Yüzey Dalgası Analizi (MASW) ve Elektrik Rezistivite Tomografi (ERT). Saha çalışmaları içerisinde, heyelan doğrultusuna paralel ve dik yönde yerleştirilmiş iki adet Elektrik Rezistivite Tomografi araştırması yer almış olup, yeraltının rezistivite (özdirenç) dağılımı için ERT profillerinden iki tanesi elde edilmiş ve rezistivite düşük, orta ve yüksek değerlerle üç kategoriye ayrılmıştır. Jeolojik çalışmalarla karşılaştırıldığında, düşük özdirenç değerleri su sızıntısı, su ve kil içeriğine işaret etmektedir. Saha çalışmalarında kullanılan ikinci jeofizik yöntem MASW, Rayleigh dalga dispersiyon (dağılım) eğrilerini elde etmek için 7 profil kullanılarak bölgenin 30 m derinliğindeki makaslama dalga hız profilleri elde edilmiştir, kullanılan MASW profillerinden üçü heyelana paralelken dördü heyelana diktir. MASW saha araştırmasının sonuçları, 1D S-dalgası hız profillerinden yedisini ve derinliğe sahip 2D S-dalgası ise hız profilinin ikisini içermiştir. Jeofizik çalışmaların sonuçlara göre, bölgede düşük, orta ve yüksek değerlerdeki hız zonlarına işaret etmekle birlikte kayma yüzeyine etki eden su ve yüksek plastisiteli killer düşük değerler vermiştir.



Jeofizik yöntemlerin sonuçlarına göre, çalışma alanındaki kayma yüzeyinin yaklaşık derinliği 9 meter (SK-8), 22 meter (SK-3), 15 meter (SK-5) ve 10 m (SK-2).

**Anahtar kelimeler:** Heyelan, elektrik resistivite, tomografi, MASW, ERT, Harmandalı, İzmir



## CONTENTS

	<b>Page</b>
M.Sc THESIS EXAMINATION RESULT FORM.....	ii
ACKNOWLEDGEMENT .....	iii
ABSTRACT .....	v
ÖZ .....	vii
LIST OF FIGURES .....	xiii
LIST OF TABLES .....	xvii
<b>CHAPTER ONE – INTRODUCTION .....</b>	<b>1</b>
1.1 Introduction.....	1
<b>CHAPTER TWO – LANDSLIDE .....</b>	<b>3</b>
2.1 Introduction.....	3
2.2 Landslide Definition.....	3
2.3 Landslide Classification .....	4
2.4 Mechanism of Landslide Occurrence.....	6
2.5 Landslide Causes and Effects.....	7
2.6 Landslide History in the World.....	10
2.6.1 Landslide Triggered by Earthquakes (Diexi landslide) .....	12
2.6.2 Landslide Triggered by Earthquakes (Khait landslide) .....	12
<b>CHAPTER THREE - LANDSLIDES TRIGGERED BY SOLID WASTE IN LANDFILLS.....</b>	<b>14</b>
3.1 Introduction.....	14
3.2 Landfill Linear and Cover System .....	15
3.2.1 Single System.....	15
3.2.2 Composite System.....	15
3.2.3 Double- Linear System .....	16

3.3 Leachate Collection Systems .....	17
3.4 Landfill Failure Risk Assessment .....	17
3.5 Landfill Failure Modes.....	19
3.6 Landslide Triggered by Solid Waste Landfill.....	21
3.6.1 Dona Juana Landslide .....	22
3.6.2 Payatas Landslide (Philippines) .....	23
3.6.3 Lewigajah Landslide (Indonesia).....	24
3.6.4 Ümraniye – Hekimbaşı Landslide (Turkey) .....	25
<b>CHAPTER FOUR - GEOPHYSICAL INVESTIGATION METHODS.....</b>	<b>27</b>
4.1 Introduction .....	27
4.2 Electrical Resistivity Method.....	28
4.2.1 Apparent Resistivity.....	29
4.2.2 Electrical Resistivity Properties of the Rocks.....	30
4.2.2.1 Porosity .....	30
4.2.2.2 Rock Types and Soil .....	31
4.2.2.3 Water Content and Salinity .....	32
4.2.2.4 Clay Contents .....	33
4.2.3 Types of Electrical Resistivity Method.....	33
4.2.3.1 Vertical Electrical Sounding (VES).....	34
4.2.3.2 Horizontal Profiling Electrical Resistivity .....	34
4.2.4 Types of Electrical Resistivity Arrays .....	35
4.2.4.1 Wenner Array.....	35
4.2.4.2 Schlumberger Array .....	35
4.2.4.3 Dipole - dipole Array .....	36
4.2.4.4 Wenner- Schlumberger Array .....	37
4.3 Electrical Resistivity Tomography (ERT) .....	37
4.3.1 2D and 3D Electrical Resistivity Tomography Survey.....	38
4.4 ERT data Analyses and software .....	40
4.4.1 Forward Modeling.....	41
4.4.2 Inversion Modeling .....	42

4.5 Seismic Methods .....	44
4.5.1 Elastic theory.....	45
4.5.1.1 Stress and Strain.....	45
4.5.1.2 Hooke's Law.....	46
4.5.1.3 Elastic Constants .....	47
4.5.2 Seismic Waves .....	48
4.5.2.1 Body waves .....	49
4.5.2.2 Surface Wave .....	50
4.5.2.2.1 Love Wave .....	50
4.5.2.2.2 Rayleigh Wave .....	50
4.5.3 Dispersion of Surface Wave.....	52
4.6 Surface Wave Methods for Estimating the Stiffness of Soil .....	53
4.6.1 Multi-channel Analysis of Surface Wave (MASW).....	54
4.6.1.1 Passive and Active MASW Sources .....	55
<b>CHAPTER FIVE - CASE STUDY HARMANDALI WASTE DISPOSAL SITE, İZMİR- TURKEY .....</b>	<b>58</b>
5.1 Study area.....	58
5.2 Propose of Study .....	59
5.3 Method .....	59
5.4 Previous Studies and History of the Landslide in the Study Area .....	60
5.5 Geological Settings .....	64
5.5.1 Bornova Flysch Formation.....	64
5.5.2 Yamanlar volcanic rocks.....	65
5.5.3 Slopewash .....	66
5.5.4 Faults .....	66
5.6 Solid Waste and Landslide in Harmandalı Landfill.....	68
5.7 Boreholes Data Results and Experiments .....	70
5.8 Buffer Zone and Requirements for MSW Placing.....	74

<b>CHAPTER SIX - FIELD WORKS AND INSTRUMENTS.....</b>	<b>76</b>
6.1 ERT Field Measurements.....	76
6.1.1 Data Acquisition and Processing .....	80
6.1.2 DC2DinvRes Software.....	80
6.2 MASW Field Measurements.....	80
6.2.1 Data Acquisition and Processing .....	80
6.2.2 Fieldwork and Instruments ( Hardware and Software).....	81
6.2.2.1 Smartseis ST Device .....	81
6.2.2.2 4.5 Hz Geophones .....	82
6.2.2.3 SeisImager Software .....	83
6.3 MASW Data Analysis.....	84
6.4 Inversion Analysis.....	85
<b>CHAPTER SEVEN - RESULTS AND DISSCUSSION.....</b>	<b>95</b>
7.1 ERT Investigations - Results and Discussion .....	95
7.2. MASW Investigations - Results and Discussion .....	99
<b>CHAPTER EIGHT – CONCLUSION AND DISSCUSSION.....</b>	<b>115</b>
8.1 Conclusion .....	115
8.2 Discussion and Suggestions .....	116
<b>REFERENCES.....</b>	<b>117</b>

## LIST OF FIGURES

	<b>Page</b>
Figure 2.1 Landslide types .....	5
Figure 2.2 Explanation of landslide mechanism occurrences .....	6
Figure 2.3 Diexi country map in China.....	12
Figure 2.4 Tien Shan mountain – Tajikistan map. And Figure View of Khait Landslide .....	13
Figure 3.1 Illustration of single linear system in the landfill .....	15
Figure 3.2 Illustration of composite linear system in the landfill .....	16
Figure 3.3 Illustration of double linear system in the landfill.....	16
Figure 3.4 Leachate collection systems .....	17
Figure 3.5 Landfill section and design .....	19
Figure 3.6 Landfill failure modes.....	21
Figure 3.7 Dona Juana sanitary landfill in Bogota.....	22
Figure 3.8 Payatas landfill in Quezon- Philippine .....	23
Figure 3.9 Leuwigajah, Bandung landfill .....	25
Figure 3.10 Ümraniye - Hekimbaşı landfill .....	26
Figure 4.1 Distribution of the potential in half-homogenous medium .....	29
Figure 4.2 The resistivity values of the rocks and groundwater .....	33
Figure 4.3 Arrangement of electrodes in Wenner array.....	35
Figure 4.4 Arrangement of electrodes in Schlumberger array.....	36
Figure 4.5 Arrangement of electrodes in in Dipole-dipole array .....	36
Figure 4.6 Arrangement of electrodes in Wenner- Schlumberger array .....	37
Figure 4.7 2D electrical resistivity tomography survey .....	38
Figure 4.8 Example of 2D ERT data coverage in the Blue Ridge mountain area in eastern USA for groundwater exploration using dipole-dipole configuration .....	38
Figure 4.9 The set of the electrode in (X,Y) directions in 3D ERT.....	39
Figure 4.10 Example of 3D ERT model for studying dam structure in ural municipality of Cordeirópolis in the State of São Paulo by using wenner configuration .....	39
Figure 4.11 The mesh types of FD and FEM technique .....	40

Figure 4.12 The iteration circle for inversion procedures.....	42
Figure 4.13 The apparent resistivity rectangular blocks grid- model before Inversion .....	43
Figure 4.14 The relation between stress and strain .....	46
Figure 4.15 The Longitudinal and lateral strain.....	47
Figure 4.16 The particle motion of Love wave.....	50
Figure 4.17 The particle motion of Rayleigh wave.....	52
Figure 4.18 The relation between wavelength of Rayleigh wave and the depth .....	52
Figure 4.19 Dispersion curve (phase velocity versus frequency) .....	52
Figure 4.20 The difference in propagation of surface waves in a vertically homogeneous medium and non- homogeneous medium.....	53
Figure 4.21 The active source of MASW Survey .....	55
Figure 4.22 Schematic of passive remote and roadside MASW field survey.....	57
Figure 5.1 Harmandalı Location Map.....	59
Figure 5.2 Electrical resistivity tomography surveys in Harmandalı waste disposal Site .....	60
Figure 5.3 Multichannel analysis of surface wave surveys in Harmandalı waste disposal site.....	60
Figure 5.4 Geological Section for landslide body in SE- NW direction.....	63
Figure 5.6 Bornova flysch formation in the Harmandalı waste disposal site .....	65
Figure 5.6 The volcanic rocks in The Harmandalı waste disposal site.....	66
Figure 5.7 Geological map of Harmandalı waste disposal site.....	67
Figure 5.8 The administration buildings in The Harmandalı waste disposal site and landslide direction NW-SE .....	69
Figure 5.9 The cracks and fractures which occurred resulting from landslide event in the Harmandalı waste disposal site .....	70
Figure 5.10 The cracks and fractures which occurred resulting from landslide event in the Harmandalı waste disposal site .....	70
Figure 5.11 The landslide effects in the Harmandalı waste disposal site .....	71
Figure 5.12 The inclinometer profile belonging to the SK-2 (INK-2) borehole.....	72
Figure 5.13 The leachate which occurred because of the waste in the Harmandalı Waste disposal site .....	74

Figure 5.14 Sarlak Dere leachate in the Harmandalı waste disposal site.....	75
Figure 6.1 ERT-1 profile with NW-SE direction parallel to landslide body .....	76
Figure 6.2 ERT-2 profile with NE-SE direction perpendicular to landslide body.....	77
Figure.6.3 RVA-1 resistivity instrument for ERT investigation.....	77
Figure 6.4 The technique of RVA-1 resistivity equipment working .....	78
Figure 6.5 Wenner- Schlumberger configuration for 2D ERT investigation surveys .....	79
Figure 6.6 Location map of boreholes and MASW profiles in Harmandalı waste disposal site.....	81
Figure 6.7 SMARTSEIS ST Device .....	82
Figure 6.8 4.5 Hz vertical geophone .....	83
Figure 6.9 The dispersion image for the first survey of MASW .....	85
Figure 6.10. The dispersion curve for the first survey of MASW .....	86
Figure 6.11 Illustration of the 1D S- wave velocity model for the first MASW Survey before (on the left) and after iteration (on the right) and dispersion curve.....	87
Figure 6.12 Illustration of the 1D S- wave velocity model for the second MASW survey before (on the left) and after iteration (on the right) and dispersion curve .....	88
Figure 6.13 Illustration of the 1D S- wave velocity model for the third MASW survey before (on the left) and after iteration (on the right) and dispersion curve .....	89
Figure 6.14 Illustration of the 1D S- wave velocity model for the fourth MASW survey before (on the left) and after iteration (on the right) and dispersion curve .....	90
Figure 6.15 Illustration of the 1D S- wave velocity model for the fourth MASW survey before (on the left) and after iteration (on the right) and dispersion curve .....	91
Figure 6.16 Illustration of the 1D S- wave velocity model for the fifth MASW Survey before (on the left) and after iteration (on the right) and dispersion curve .....	92



Figure 6.17 Illustration of the 1D S- wave velocity model for the sixth MASW survey before (on the left) and after iteration (on the right) and dispersion curve .....	93
Figure 6.18 Illustration of the 1D S- wave velocity model for the seventh MASW dispersion curve .....	94
Figure 7.1 ERT-1 NW-SE (a) measured data. (b) Calculated data. (c) Data Misfit. (d) Resistivity model with topography.....	96
Figure 7.2 ERT-2 NE-SW (a) measured data. (b) Calculated data. (c) Dats Misfit (d) Resistivity model with topography .....	98
Figure 7.3 Comparison between ERT-1 profile and boreholes in the site.....	107
Figure 7.4 Comparison between the first survey of MASW and borehole SK-2 ....	108
Figure 7.5 Comparison between the second survey of MASW and borehole SK-3 .....	109
Figure 7.6 Comparison between the third survey of MASW and borehole SK8.....	111
Figure 7.7 Comparison between the fourth survey of MASW and borehole SK-3 .....	110
Figure 7.8 Comparison between the fifth survey of MASW and borehole SK-4 .....	111
Figure 7.9 Comparison between the sixth survey of MASW and borehole SK-3 .....	111
Figure 7.10 Comparison between the seventh survey of MASW and borehole SK-3 .....	112
Figure 7.11 S- wave profile with depth parallel to landslide direction (NW-SE) .....	113
Figure 7.12 S- wave profile with depth perpendicular to landslide direction (NE-SW) .....	114

## LIST OF TABLES

	<b>Page</b>
Table 2.1 Landslide classification.....	4
Table 2.2 Landslide worldwide with causes and occurrence mechanisms .....	7
Table 2.3 Landslide events worldwide between the years 1900 – 2011 with the losses and damages results .....	10
Table 2.4 Comparison between the numbers of landslide events in the continents...	10
Table 4.1 Some application for MASW and resistivity method in geophysical investigations .....	28
Table 4.2 The resistivity values for some rocks	
Table 5.1 Types and amount of solid waste in Harmandali waste disposal site.....	30
Table 5.1 Types and amount of solid waste in Harmandali waste disposal site .....	65
Table 5.2 Some values for stability given by D.E.U. project.....	68
Table 6.1 Passive source acquisition parameters .....	79
Table 6.2 Initial model for vs.....	81
Table 7.1 ERT-1 field and inversion Parameters .....	90
Table 7.2 ERT-2 field and inversion Parameters .....	91
Table 7.3 The inversion results of the first survey of MASW .....	95
Table 7.4 The inversion results of the second survey of MASW .....	95
Table 7.5 The inversion results of the third survey of MASW .....	96
Table 7.6 The inversion results of the fourth survey of MASW .....	97
Table 7.7 The inversion results of the fifth survey of MASW.....	97
Table 7.8 The inversion results of the sixth survey of MASW.....	98
Table 7.9 The inversion results of the seventh survey of MASW .....	98

# **CHAPTER ONE**

## **INTRODUCTION**

### **1.1 Introduction**

Landslide phenomenon is a hazardous event which threatens life being human and environment due to the fact that landslide leads to catastrophic failures and instability in the affected areas. There are many types of landslides which are classified based on movement and materials (Varnes, 1978). The main factors which result in instability of the rocks and soil are; hydrogeological condition, groundwater table, angle of the slope and clay content. Landslide may happen due to many reasons such as earthquake, separation of large glacier, instance rainfall and human causes (extra loading on the slope, deforestation, etc.).

The slope failures occurred in the solid waste disposal sites are one of the most important types of failures and attracted the attention of researches in the last 20 years due to the urbanization and rising in population worldwide. The essential parameters which control this types of instability are; the protection system which shall be applied in the site before landfill establishment, groundwater and the leachate which result from the waste and gradient of the slopes (Slope angles). For the landslide investigations, there are many non-invasive geophysical techniques which are widely used for determination of the rock properties underlying the site as well as landslide parameters. These methods were applied in the field for estimation of the physical properties, lithology and hydrogeological conditions in the landslide areas and determining the geometry of sliding mass and slope failures. Some examples are given in this study; electrical resistivity tomography (ERT) method investigations which rely on assessments of resistivity values and its distribution in the landslide area. ERT method provides useful information in landslide investigations by imaging the subsurface of the earth. By interpreting 2D and 3D ERT images for resistivity distribution the geometry of landslide, the thickness of the layers, the lithology of the landslide area and water content can be easily determined. ERT measurements have been widely used in many landslide areas (Göktürkler et al., 2008, Darhor et al., 2006, Popescu, 2014, Al-Diabat et al., 2002, Mondal et al.,

2006). In order to collect information about the geometric, physical properties and water content in landslide areas then comparing the results with geological settings and previous studies. The procedures of ERT investigation in landslide sites start by choosing the type of the electrodes configuration as the first step then using multi-electrode cable and more than 30 - 40 electrodes. The current (I) will be applied to the earth and the voltage (V) will be measured. Calculating the apparent resistivity is the next step after measuring (I) and (V) and that enable us to obtain an approximate image for the subsurface apparent resistivity values (Perrone et al., 2014). Other examples for non-invasive geophysical method is multi-channel analysis of surface wave method (MASW) which use surface wave method for estimating shear wave velocity (Vs) profiles. This method depends on Rayleigh wave dispersion curves in order to determine s<sub>wave</sub> velocities in the site which provide us information about physical properties of materials in the site. In MASW method two of sources are used; active and passive sources. 12 – 24 geophones with multiple seismograms are used in the field. MASW measurements for landslide had been performed in many areas such as Romania and Brazil (Junior et al., Mihai et al.). There are mainly three procedures are included in MASW method; Acquisition of field data for Rayleigh wave, determination of the dispersion curve and finally estimation of S- wave velocity profiles depending on inversion methods.

The study aims to assess the stability of the Harmandalı waste disposal site in İzmir where a landslide had occurred and determine waste, landslide materials, rock properties and water effect in the study area. Multichannel Analysis of Surface Waves (MASW) and Electrical Resistivity Tomography (ERT) were used. By comparing the results of geophysical methods with previous studies which were previously performed in the study site; International Karst Water Resources Application and Research Center (Hacettepe University) (UKAM, 1990) and Dokuz Eylul University- Geological Engineering Dept. researches an assessment was made concerning the instability and failures potential of the Harmandalı waste disposal site was determined (DEU,2016).

## **CHAPTER TWO**

### **LANDSLIDE**

#### **2.1 Introduction**

Landslide is the most common mass movement in the waste disposal sites. It affects the human life and damages the environment. Between the years 1900 and 2009, the landslide phenomena resulted in 61,000 killed people and by landslide hazard assessments could prevent the majority of past landslide worldwide.

Landslide phenomena were also named by many other terms such as sliding, slope failure, mass movements (Varnes and IAEG ([1984](#)), Brusden ([1984](#)), Crozier ([1986](#))), etc. These terms depend on the materials and the kind of movement. The landslide may occur in the high steep slopes also if these slope areas are exposed to the earthquake risk that increase in the landslide occurrence probability. In addition, the other and most important triggers of the landslide are soil strength, seasonal fluctuations of groundwater levels and the type of rock units.

#### **2.2 Landslide Definition**

Landslide is the movement of soil and rock materials influencing by gravity. The term of landslide is defined as the downward and outward of slope forming material, natural rocks, soils and artificial fills. The landslide can be replaced by other terms depending on many factors such as movement types, sliding plane types, geological and geomorphological factors (Keith et al., 1996). The slope failure can be affected by many factors such as tectonic, increasing and decreasing in water level, earthquake, volcanic and human activities.

Landslide was firstly defined by Varnes (1958) as; "A downward and outward movement of slope forming materials under the influence of gravity". In 1978, the landslide had a new classification depending on two terms material and movement types (Varnes, 1978). The movement of the landslide can be classified to fast and

slow movements. The rapid movement of the rock material is more risky and lead to huge disasters because of unexpected displacing (Guzzetti, 2000).

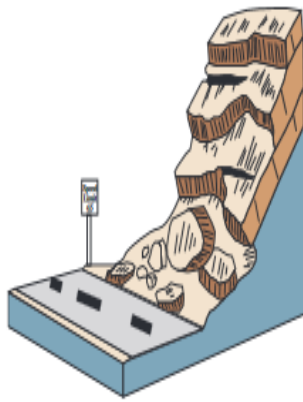
Water is a major factor in most landslides. However, surface water lead to creeks and fissures caused by earth movement instability

### 2.3 Landslide Classification

The landslide can be classified depending on the movement and material content in the sliding mass. The movement types of the landslide named by fall, topple, slide, spread and flow while the materials of the landslide are rock, earth, soil, mud and debris. If we banded two terms together we get the landslide classification (USGS, 2004). The landslide classification was given in Table 2.1 and Figure 2.1.

Table 2.1 Landslide classification (USGS, 2004)

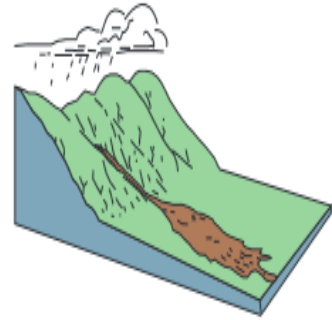
TYPE OF MOVEMENT		TYPE OF MATERIAL		
		BEDROCK	ENGINEERING SOILS	
			Predominantly coarse	Predominantly fine
FALLS		Rock fall	Debris fall	Earth fall
TOPPLES		Rock topple	Debris topple	Earth topple
SLIDES	ROTATIONAL	Rock slide	Debris slide	Earth slide
	TRANSLATIONAL			
LATERAL SPREADS		Rock spread	Debris spread	Earth spread
FLOWS		Rock flow (deep creep)	Debris flow (soil creep)	Earth flow
COMPLEX		Combination of two or more principal types of movement		



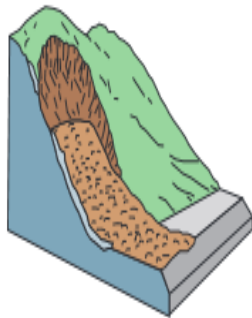
**Rockfall**



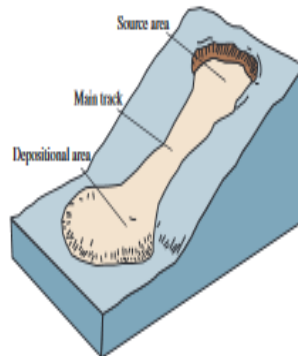
**Topple**



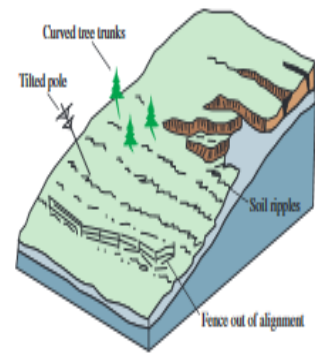
**Debris flow**



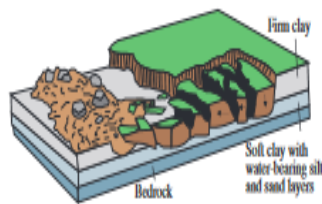
**Debris avalanche**



**Earthflow**



**Creep**



**Lateral spread**

Figure 2.1 Landslide Types (USGS, 2004)

## 2.4 Mechanism of Landslide Occurrence

The stability of slopes is affected by two forces shear strength and shear stress. If the shear stress of the material is greater than shear strength, the landslide occurs in that area. There are many parameters controlling the change in shear stress values. The geological movements and earthquake, slope degree, erosion and increasing of the loads on the steep slope are the fundamental reasons for instability (Duncan et al., 2014).

Ratio between shear strength and shear stress defined by factor of safety (F). If the value of the (F) is greater or equal to 1, it is understood that a cross section under consideration is stable (Shanmugam and Wang, 2015).

$$F = \frac{\text{Shear strength}}{\text{shear stress}} = \frac{S}{t} \quad (2.1)$$

Where,

F: The factor of safety

Shear strength: It is the force that defined as the resistance to shearing

Shear stress: It is the force that acts a parallel to the surface.

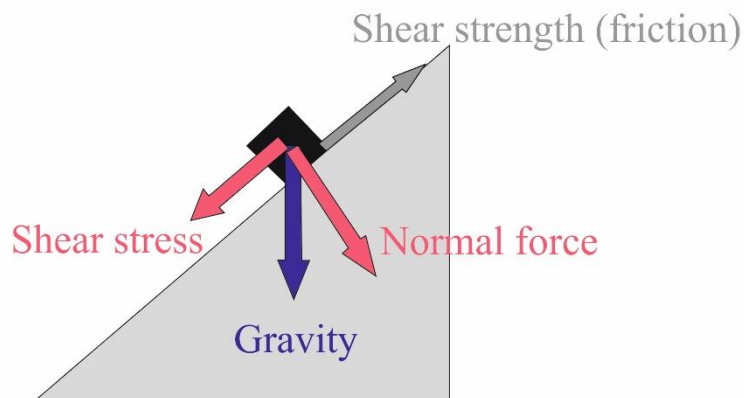


Figure 2.2 Explanation of landslide mechanism occurrences (Dawson, 2016)



## 2.5 Landslide Causes and Effects

The landslide phenomenon is influenced by many factors such as geology, geomorphology, seismology, etc. In order to make slope stability protection system, we should have information about the soil resistance and the parameters which deeply affect the stability of the materials (Shanmugam and Wang, 2015).

The fundamental causes and effects of the landslide will be explained in this section.

- 1- Groundwater and pore water pressure
- 2- Slope angle and slope height
- 3- Rock and soil types and fracturing system (Development of discontinuities in rocks).
- 4- Geological movements and earthquake
- 5- Seasonal rainfall (The most important factors that has activated or accelerated the movement of the sliding mass).

The occurrence mechanism and causes of landslide worldwide are shown in Table 2.2. The landslide mechanism were classified to landslide that triggering by mechanism such as earthquake, failure, volcanic, glacier and rainfall.

Table 2.2 Landslide worldwide with causes and occurrence mechanisms (Shanmugam & Wang, 2015)

<b>Year</b>	<b>Location</b>	<b>Landslide name and type</b>	<b>Triggering mechanism</b>	<b>Size, damage, and loss of human life</b>
1911	Tajikistan	Usoy MTD	Usoy earthquake, magnitude 7.4	2,000,000,000 m 354 deaths
1914	Argentina	Rio Barrancas and Rio Colorado	Failure of ancient MTD dam	2,000,000 m 3 Length of flow: 300 km

Table 2.2 continues

1919	Indonesia (Java)	Kelut MTD	Eruption of Kelut Volcano	185 km (length) Lahars caused 5,110 deaths, and destroyed or damaged 104 villages
1920 Haiyuan	China (Gansu), Haiyuan	Loess flows, MTD	earthquake, magnitude 8.5	50,000 km 2 (area) 100,000+ deaths
1920	Mexico	Rio Huitzilapan debris flows	Earthquake, magnitude 6.5- 7.0	> 40 km (length) 600 - 870 deaths
1933	China (Sichuan)	Deixi MTD Deixi	earthquake, magnitude 7.5	> 150,000,000 m 3 2,500 deaths

Table 2.2 continues

1938	Japan (Hyogo)	Mount Rokko MTD	Rainfall	505 deaths or missing, 130,000 homes were destroyed or badly damaged.
1941	Peru	Huaraz debris flow	Failure of moraine dam	10,000,000 m <sup>3</sup> 4,000-6,000 deaths
1949	Tajikistan (Tien Shan Mtns.)	Khait MTD	Khait earthquake, magnitude 7.4	245,000,000 m 3 7,200 deaths
1985	Colombia (Tolima)	Nevado del Ruiz debris flows	Eruption of Nevado del Ruiz volcano	23,000 deaths
1987	Colombia	Villa Tina MTD	Pond leakage	20,000,000 m 3 217 deaths
1991	China	(Zhaotong, Yunan) Touzhai MTD	Rainfall	18,000,000 m 3 216 deaths

Table 2.2 continues

2002	Russia	(North Ossetia) Kolka Glacier debris flows	Detachment of large glacier, causing a debris flow	Travel distance: 19.5 km; 110,000,000 m <sup>3</sup> volume of glacial ice deposited 2,000,000-5,000,000 m <sup>3</sup> of ice debris at end of runout; 125 death
2006	Philippines	(Leyte) MTD	Rainfall	15,000,000 m <sup>3</sup> 1,100 deaths
2008	China	(Sichuan) MTD Wenchuan	earthquake, magnitude 8.0	15,000 MTD, and 20,000 deaths Still being assessed
2008	Egypt	(East Cairo) Al Duwayqa MTD	Destabilization due to man-made construction	Affected area was 6,500 m <sup>3</sup> volume and rocks weighed about 18,000 tons. 107 deaths.

## 2.6 Landslide History in the World

There are many geological and environmental causes affect the rock masses and lead to landslide in the areas. The landslide and mass movements can be classified into many types such as `debris flows`, `avalanches` and `toppling failures` depending on the reason of the occurrence. Tectonic and seismicity, the type of the rock and the climate and the level of groundwater are the basic factors of landslide causes. This kind of risks results in a huge economic losses in the invasive areas. Table 2.3 showed the number of landslide events which happened between (1900–

2011) and the rate of economic losses which result from the destruction of the areas which exposed to these disasters (Ayala, 2014).

Table 2.3 Landslide events worldwide between the years 1900 – 2011 with the losses and damages results (Ayala, 2014)

<b>Disaster Types</b>	<b>Event Number</b>	<b>Killed People</b>	<b>Affected People</b>	<b>Estimated damage (US\$,000)</b>
Landslides	40	64089	13656983	8653598
Drought	616	11708271	2139534240	98147906
Earthquake	1198	2563226	170648422	735935084
Flood	3998	6929305	3461636168	559237000
Storm	3469	1380151	902827403	844179677

Table 2.4 showed that 53% of landslides in between 1900–2011 had been happened in Asia then American continent which occupies a second tier with landslide disasters (Ayala, 2014).

Table 2.4 Comparison between the numbers of landslide events in the continents (Ayala, 2014)

<b>Region</b>	<b>Number of Event</b>	<b>Killed People</b>	<b>Affected People</b>
Africa	31	1334	45032
America	177	22176	5518459
Asia	337	23252	8023397
Europe	76	16755	48780
Oceania	19	572	21315
Total	640	64089	13656983

The landslide phenomena have been recognized in several areas around the world owing to many reasons and causes. The strongest and most affective landslide events in the world history will be discussed in this chapter.

### ***2.6.1 Landslide Triggered by Earthquakes (Diexi landslide)***

On August 25, 1933, an earthquake (M 7.5) hit Diexi, Mao County, Szechwan, China which was later named as Diexi earthquake. This earthquake resulted in a massive landslide in the area which consider as one of the most serious mass movement in the world. Because of the mass movement in this area, three lakes were formed. Diexi landslide led to more than 6.000 deaths and totally destroying for 12 villages and towns (Lan & Xu, 2016).

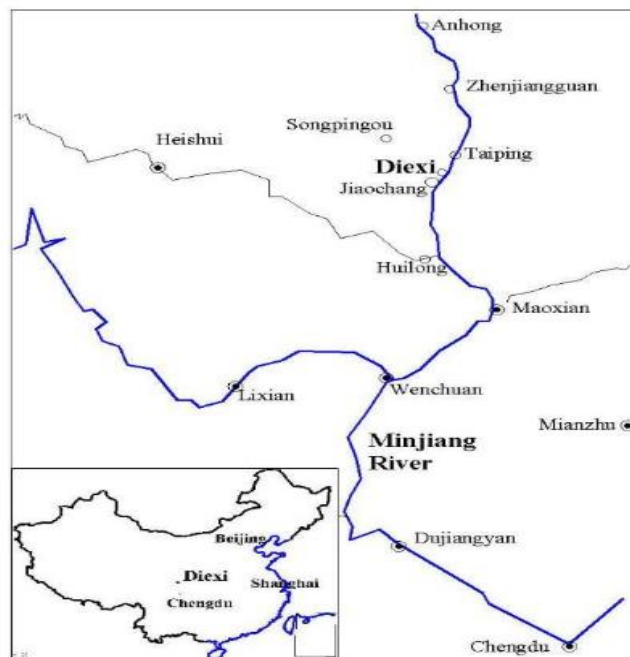


Figure 2.3 Diexi country map in China (Lan & Xu, 2016)

### ***2.6.2 Landslide Triggered by Earthquakes (Khait landslide)***

On 10th July, 1949 an earthquake (M=7.4) occurred in north of Tajikistan and named by Khait. Khait earthquake happened in Tien Shan Mountain. This mountain is known as mountains of Heaven because of the high which is about 7400 m (Jia, Fu, Jolivet and Zheng, 2015). Besides, Tien Shan represents one of the biggest systems of mountains in central of Asia. The southwestern of this mountain is located in Tajikistan and characterized by faults thrusting. Khait earthquake occurred in the southern part of Tien Shan and had huge effects on Gharm Oblast city - Khait (or

Hoit district). Many landslides followed by the earthquake. For instance, the landslide which happened in Yasman River valley which result in slow mass movement in the beginning of Obi-dara valley (characterized by flowslides) then started with rapidly mobility (loess landslides) in the sides and bottom of the valley (Havenith et al., 2015)

The distance covered by flow movements was about 11 km with 30 m/s velocity which led to 20,000 killed and burying of 23 villages (Havenith and Bourdeau, 2010). View of the Khait landslide (Figure 2.4) showing the scar on Chokrak Mountain and the landslide that overwhelmed the village of Khait (Jia et al., 2015).

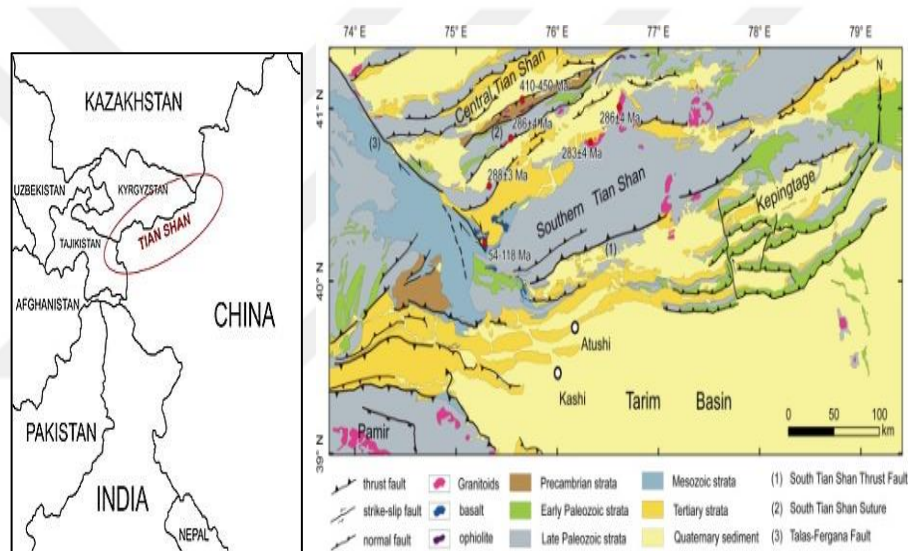


Figure 2.4 Tien Shan mountain – Tajikistan map. And Figure View of Khait landslide (Jia et al., 2015)

## **CHAPTER THREE**

### **LANDSLIDES TRIGGERED BY SOLID WASTE IN LANDFILLS**

#### **3.1 Introduction**

The instability of landfills around the world becomes an annoying issue because of slide and failures events which had been happened in the last 20 years. Because of the fact that population and construction of buildings in modern cities are increasing day by day, solid waste disposal sites constructions are also becoming increasingly common because of its large effects on the environments and result in water and air pollutions. Solid waste can be classified into three categories according to their composition and sources:

-Municipal Solid Waste (MSW): defined as the waste that generated from houses , establishments, debris, food wastes and paper.

-Industrial Wastes: This kind of the waste include wood, paints , cloth and plastic

-Hazardous waste: defined by the waste that harms the human and the environment. This waste characterized by ignitability, corrosively, reactivity and toxicity (Links, 2006).

The rate of landslides and mass movement which happened in the solid waste disposal site increased between 1977 and 2005 and led to many deaths and economic losses. There were many reasons for these kinds of failures such as fractured sedimentary rocks, groundwater levels, existing of clay materials, saturated soil and permeability. The most essential factors that control the slope stability in solid waste sites are the gradient of slope (e.g Istanbul, Payatas, Bandung), the greater the gradient of slope the lower the stability, the compaction of the waste; decrease in the degree of compaction of waste causes increase in infiltration of water, consequently, reduction in shear strength of the solid waste, water pressure; this factor also resulting in reducing in shear strength, the continuous rainfall leads into leachate creation and excessing in pore water pressure (ex: Bogota landfill) (Jahanfar et al., 2014).



## 3.2 Landfill Liner and Cover System

In the past, the landfill liner system design was boxed in single layer of clay. In 1982, double liner system started to be used. Generally, liner system is constructed in the site in order to separate the solid waste from the environment and prevent the ground water pollution and collect the leachate, water as well. There are three categories of landfill liner system; single, double and composite system.

### 3.2.1 Single System

Single system (Figure 3.1) is widely used in the landfills which contain debris and demolition materials (wood, asphalt, shingles, and glass). Clay liner and a geosynthetic clay liner (or geomembrane- polymers) are involved in single system and this kind of landfill design is cheaper than other options because of single linear containment. The construction of single system should not contain liquid tar, paint or any matters that could harm the environment (Hughes et al., 2005).

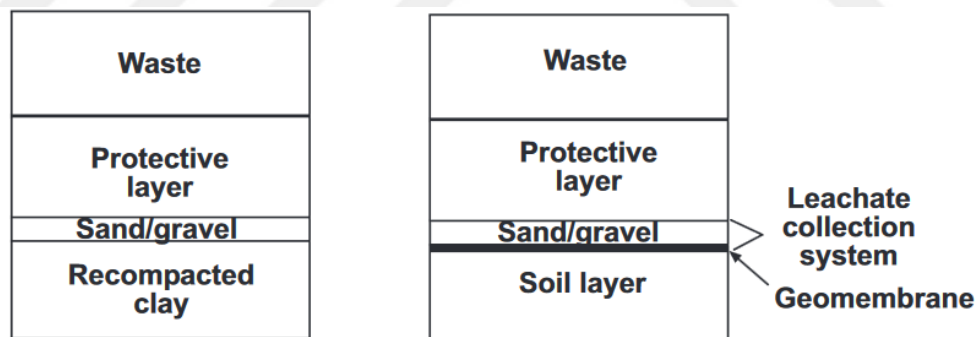


Figure 3.1 Illustration of single linear system in the landfill (Hughes et al., 2005)

### 3.2.2 Composite System

Composite system (Figure 3.2) is widely used for municipal solid waste (MSW) landfills due to the combination of clay and geomembrane are involved in composite liner system, this liner system has more efficacious in prevention of leachate water migration preventing (Hughes et al., 2005).

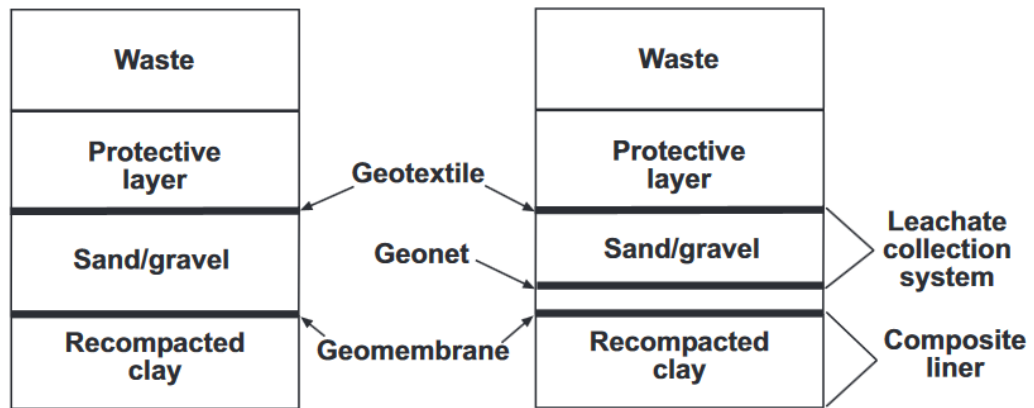


Figure 3.2 Illustration of composite liner system in the landfill (Hughes et al., 2005)

### 3.2.3 Double-Liner System

Double-liner system (Figure 3.3) is widely used in hazardous waste landfills. Double liner system involves two liners, a primary liner layer and secondary liner (two single liners, two composite liners, or a single and a composite liner.). The primary liner is the upper one and has an effective role in leachate water collecting whereas the secondary liner or lower has a role in water leakage detection (Hughes et al., 2005).

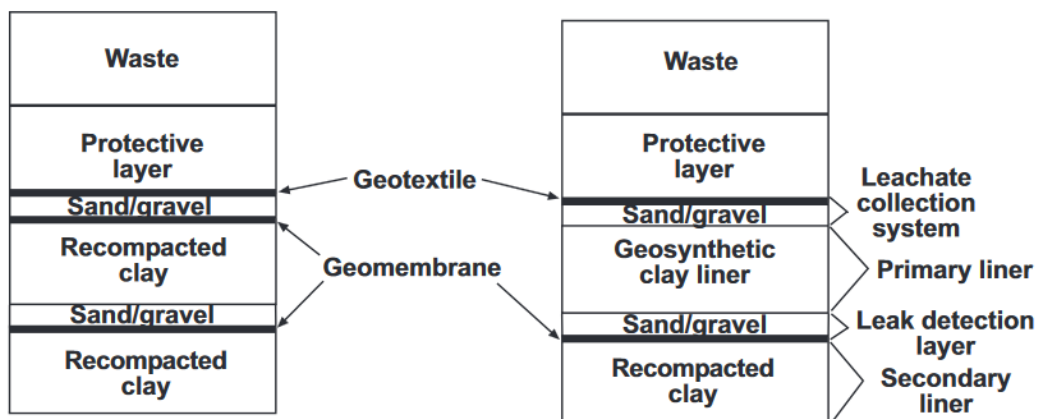


Figure 3.3 Illustration of double liner system in the landfill (Hughes et al., 2005)

### 3.3 Leachate Collection Systems

Leachate collection system (Figure 3.4) is located above the liner system designed in the landfill site aiming to manage and collect the water which could be generated in the site because of many factors (waste decomposition, rainfall, etc.) and removes the liquid from the landfill. Leachate system should be provided by permeable drainage layers and pipes to drain the water out of the landfill. Leachate system provides us the stability of waste and prevents the pollution of groundwater and other water sources (Ramke, 2008).

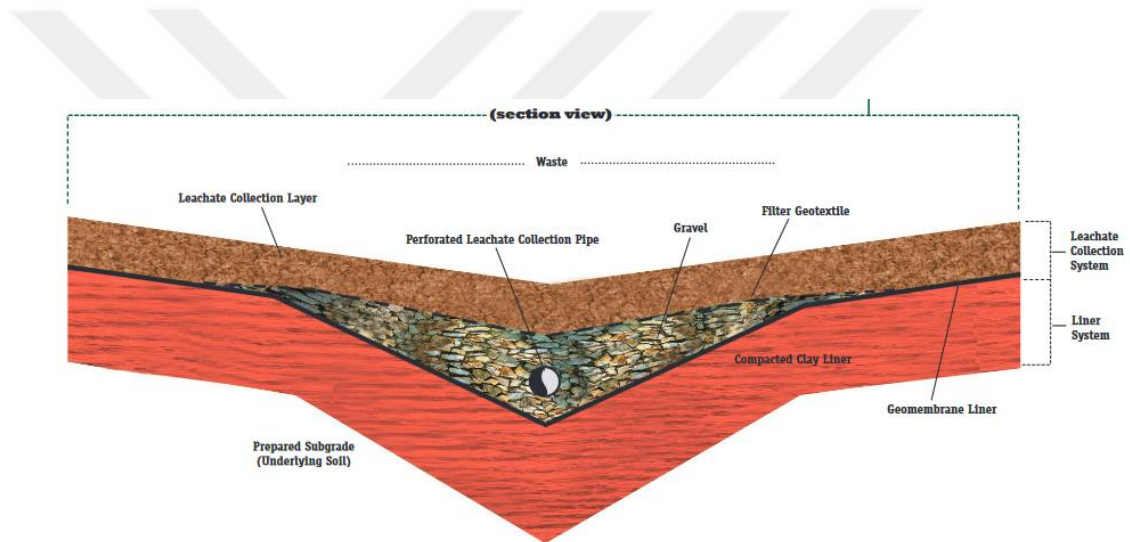


Figure 3.4 Leachate collection systems (Ramke, 2008)

### 3.4 Landfill Failure Risk Assessment

Risk assessment is defined by the event of the failure (processes) multiplied by the effects, losses and results (consequences). Risk assessment of the landfill failures includes the annual frequency of instability causes. In the landfill sites there should be a balance between increasing the capacity and the stability of the landfill.

Risks taken to the account in landfill sites:

- Gas producing: Methane and carbon dioxide producing risk is very high in landfill site resulting from the decomposition of solid waste material. Gas producing risk could lead to explosions and consequently waste displacement in the landfill site (Umraniye landfill 1993).
- Leachate production: the continuous rainfall and the decomposition of solid waste cause formation of leachate in the landfill and that cause a reduction in shear strength of the solid waste and increasing in pore water pressure
- Appropriate Site selection: The buffer zone location shall be far from landfill footprint at least 50 m. The distance between the landfills and planned areas (offices, houses, schools, etc.) should be about 500 m and shouldn't be located in 100 m near to archaeological site.
- The landfill selection site should be 8 km far away from the airports because of the landfill attraction for the birds and that fact deeply affect the taking of and landing of the planes.
- Landfills shouldn't be at least 300 m faraway from water collection points or water sources areas at least (300 m) far away.
- Also, the geological and geotechnical studies should be carried out in the site before landfill building up. The landfills should be located in stable geological area and far away from unstable areas such as sites that characterized by faults, active landslide, seismic zones and alluvial fans (about 100 m).
- And one of the most essential hydrogeological factors which must be taken to the account before construction of landfill is the groundwater level. The solid waste at least should be 1.5 m above the aquifers.
- Before construction of the landfills, geological studies should be carried out in the chosen areas. The most essential geological studies are soil stability, clay and organic material contents (British Colombia Bc Ministry of Environment, 2016).

Figure 3.5 showed the rules of landfill design in the world which was given by British Colombia Ministry of Environment.

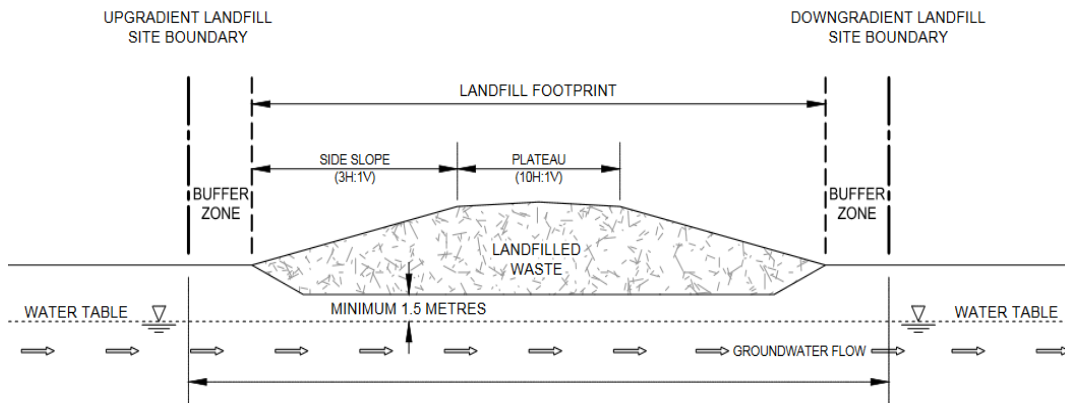


Figure 3.5 Landfill section and design (British Colombia Bc Ministry of Environment, 2016)

### 3.5 Landfill Failure Modes

Landfill failures have significant economic and environmental impacts in the affected areas and lead to massive movement of solid waste. The stability of landfills influenced by the height of slope and the inclination as inverse relationship shall be between the height and the angle of the slope. If the height of slope is high, slope angle should be decreased (Stark, 1999).

There are six modes of landfill failure (Figure 3.6) classified by Stark (1999). The failure could happen in the soils, waste and linear system (final cover system and leachate collection system). Strength, water sources, gas pressure and the weight of the waste are basic factors that affect the strength behavior of landfill areas.

The failure of landfills includes rotational and translational modes for the both natural and geosynthetics materials (Stark, 1999). Most of the failures are experienced as translational mode. Rotational failure is generally seen in homogenous materials in the curved surfaces such as clay and soil. Translational failure generally affects the weak surfaces and geosynthetics materials. The mass in the translational failure mode is moving down separating from the original slope. In

this case, the driving force is bigger than shear strength and that lead to mass movements. Rotational failure may also happen in the soil, in the waste or in the linear system.

Translational failure may happen in the landfill areas when a massive mass move laterally and occurs especially in the linear system (Savoikar and Choudhury, 2011). Linear system exposed to this types of failure because of the interfaces of different layers which make it less resistance. If the failure occurs in the leachate collection system that will result in a lot of cost for reconstruction on the other hand if the failure occurs in the final cover system that may require replacing the soil. In the translational failure mode the movement of the mass is fast and the mass separates completely from the slide surface while moving without any internal deformation. Generally, the slide surfaces are planar in this mode of failure. In the rotational failure, the movement of the mass occurs in the curved surfaces and it is slower than the translational failure with a little of internal deformations (Varnes, 1978). Translational failure mode is more risky than rotational mode in the slopes with great inclination due to the great driving force and open space for sliding (Stark, 1999).

The failure modes depend on the ratio between the thicknesses of the failed mass to the failed length. For rotational failure, the ratio ranges between 0.15-0.33. On the other hand, the ratio for translational failure is less than 0.1.

There are three types of circular and non- circular rotational failure modes which happened in the curved slopes; Base failure, toe slide and slope slide. If there is intersection between the slope and the surface of failure, so the failure is called by slope failure (or face failure). If the failure surface crosses the toe of the slope, the slide is known as toe failure. For the base failure, the intersection between failure surface and slope occur below the toe.

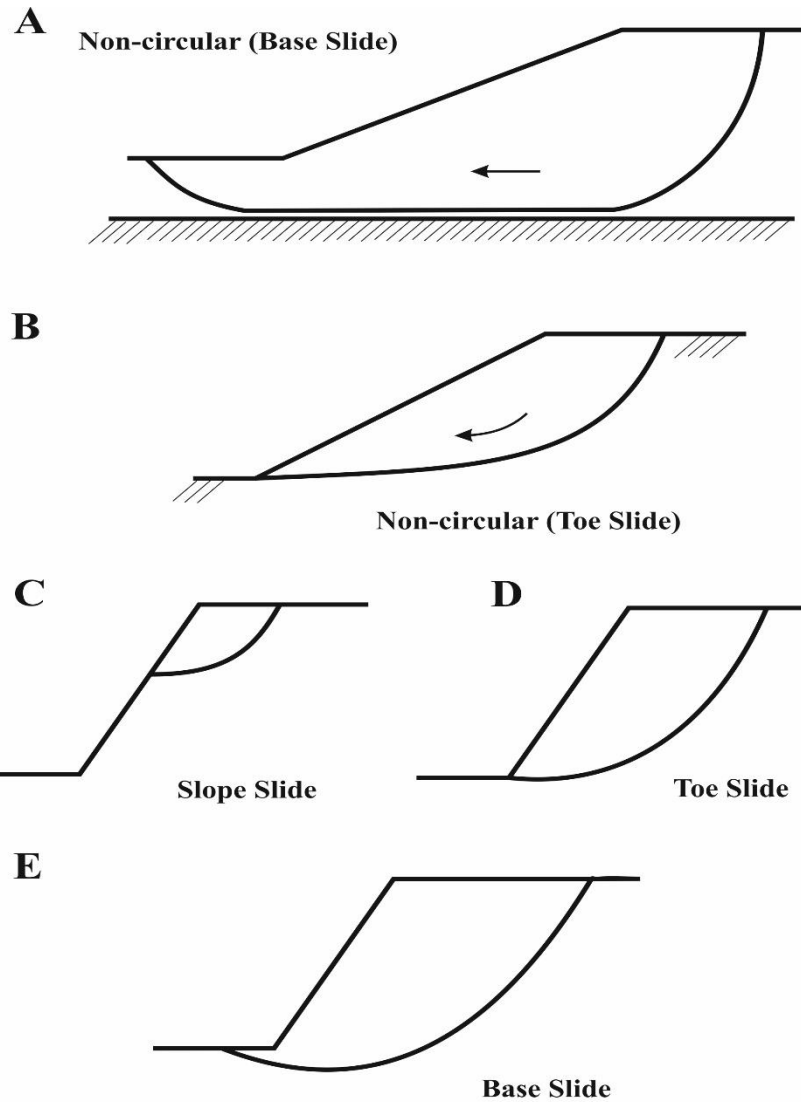


Figure 3.6 Landfill failure modes (Stark, 1999)

### 3.6 Landslide Triggered by Solid Waste Landfill

Because of the fact that population and buildings constructions in the modern cities are increasing day by day, solid waste disposal sites constructions are also becoming increasingly common because of its large effects on the environments and result in water and air pollutions. The rate of landslides and mass movement which happened in the solid waste disposal site was increased between 1977 and 2005 and led to many deaths and economic losses. There were many reasons for these kinds of

failures such as fractured sedimentary rocks, groundwater levels, existing of clay materials, saturated soil and permeability.

### 3.6.1 Dona Juana Landslide

Dona Juana is a sanitary landfill in Bogota, Colombia (Figure 3.7). This landfill is receiving 5000 tons per a day of solid waste from 1989. In September 1997, a huge landslide hit the area and result in 800.000 tons of waste fills sliding. Dona Juana landfill was constructed in a valley between Andes Mountains. The basic geological materials which the valley consists of are sandstone and shale pore pressure was the main reason for the failure in the waste site (Caicedo et al., 2002). This landslide just resulted in environmental destroying without and deaths (Blight, 2008) and waste dam had been generated in the river resulting in water pollution (Jahanfar et al., 2016).

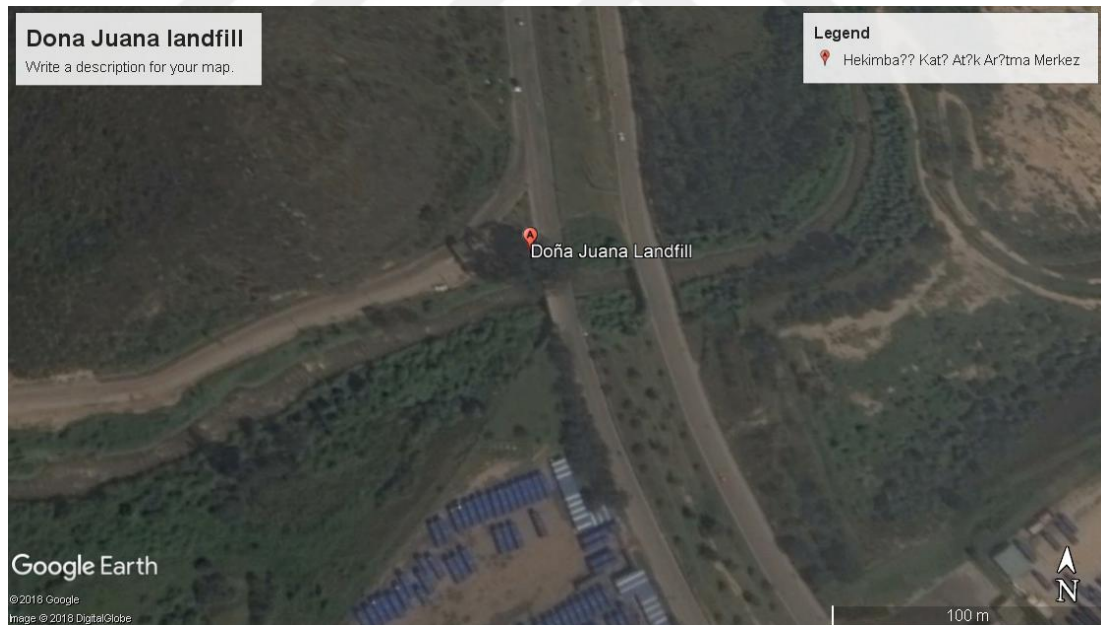


Figure 3.7 Dona Juana sanitary landfill in Bogota (Google Earth, 2018)



### 3.6.2 Payatas Landslide (Philippines)

The landslide which happened in Payatas landfill (Figure 3.8) on 10 July 2000 which located in Quezon- Philippines killed more than 200 people. Payatas landfill built up in 1973 and was receiving about 1000 tons per a day of solid waste (Koelsch, 2001). Owing to closing the Smokey Mountain Landfill in Manila, Payatas landfill receiving for the solid waste had been increased to 6000 tons per a day in the last 5 years before landslide event in the area (Jafari et al., 2013).

Many causes for the instability were observed in Payatas landfill. The main reason was defined by the low density of solid waste which triggered by very lightweight material (generally plastic materials) resulting in greater amount of leakage for the water into the layers. Second reason was because of two storms hit the area month ago before the landslide event and high precipitation and that led to presence of two leachates in the landfill site. The steep slope degree for the landfill is  $40^{\circ}$  to  $70^{\circ}$ . All these factors result in reducing in shear strength and massive landslide (Jafari et al., 2013).



Figure 3.8 Payatas landfill in Quezon- Philippine (Jafari et al., 2013)

### ***3.6.3 Leuwigajah landslide (Indonesia)***

Leuwigajah landfill which located between Bandung and Cimahi city, Indonesia (Figure 3.9), has been putted to the service in 1986. On 21 February 2005, a catastrophic landslide hit Leuwigajah landfill resulting from heavy rainfalls and that led to economical and human losses (143 deaths and 71 buried houses). Approximately 2,7 million cubic meter waste moved down. Bandung landfill failure is considered as the second deadliest landslide in the world after Payatas landfill failure (Lavigne et al., 2014).

Leuwigajah was the largest landfill in Bandung city. Leuwigajah landfill was managed by three authorities that have poor experience about solid waste managements. Leuwigajah is an open dumping filling can be easily affected by environmental conditions. The hydrogeological studies were carried out in the valley where Leuwigajah landfill were constructed and gave positive results. The slope of steep was between 30° and 45°. Heavy rain had been happened and affected the stability of the area and resulted in a high water level and pore water pressure.3 days before the landslide event. Moreover, the Leuwigajah landfill had been exposed to explosion resulting from methane gas which always generated by the waste and led to instability in the landfill area.

Solid waste sliding occurrence took just minutes as the sliding of the solid waste was going so quickly and resulted in 2.7 million cubic meters of waste collapsing (Koelsch et al., 2005).



Figure 3.9 Leuwigajah, Bandung landfill (Lavigne et al., 2014)

#### 3.6.4 Ümraniye - Hekimbaşı landslide (Turkey)

Istanbul landfill which named by Ümraniye - Hekimbaşı is located in the Asian side of Istanbul (Figure 3.10). This dump had been putted into service since 1976 and was receiving 1500-2000 tons per a day of solid waste. On 28 April 1993 a great waste movement happened (Approx 350,000 m<sup>3</sup>) resulting from explosion of gases compressed. The main reason of the instability in Ümraniye - Hekimbaşı dump was the gradient of slope which was about 33°. This landslide resulted in 39 deaths and 11 destroyed houses (Kanat, 2010).



Figure 3.10 Ümraniye – Hekimbaşı landfill (Google Earth, 2018)

## CHAPTER FOUR

### GEOPHYSICAL INVESTIGATION METHODS

#### 4.1 Introduction

Multichannel analysis of surface waves (MASW), shallow seismic refraction and reflection methods, Refraction micro-tremor (ReMi) and electrical resistivity methods consider as non-invasive geophysical surveying techniques. These techniques consume less time and cost as well as don't cause any damage in the site of study. There are many applications for these methods in geophysics; estimating the material properties, mapping the lithology and bedrock topography, hydrogeological studies and landslide investigations, etc. Table 4.1 illustrated some application for MASW and resistivity methods (X refer to Minor application and M refer to major application) (Anderson, Croxton, Hoover, & Sirles, 2008).

Table 4.1 Some applications for MASW and resistivity method in geophysical investigations (Anderson, Croxton, Hoover, & Sirles, 2008)

Applications	Methods	
	MASW	Resistivity
Mapping lithology (<30-ft >30) depth)	M	X
Mapping top of ground water surface	X	M
Mapping bedrock topography	M	X
Delineating steeply dipping geologic contacts (<30-ft depth)	X	M
Determining in situ rock properties (bulk, shear, and Young's moduli)	M	-
Mapping air-filled cavities, tunnels	X	M
Estimating in situ rock properties (saturation, porosity, permeability)	-	M
Landslide site evaluation	X	M

Electrical resistivity tomography Method (ERT) and multi-channel analyses of surface waves (MASW) will be widely discussed in this chapter.

## 4.2 Electrical Resistivity Method

Electric resistivity method assumes that geological layers have a variation in resistivity values. As a result, geological material properties can be determined by these differences between resistivity. ER surveys can be carried out multiple techniques for determining the resistivity variation in the rocks. Electrical resistivity method is performed in the field by applying electrical direct current (I) between two electrodes (AB) and measure the potential difference ( $\Delta V$ ) between the voltage electrodes (MN) (Figure 4.1). Electrical resistivity measurements always made using multiple electrode configurations in non- homogeneous medium and that result in apparent resistivity  $\rho_a$  which expressed by ohm meters. We can obtain the values of apparent resistivity from the potential values according to the following relationship: (Telford, Geldart, & Sheriff, 1991)

$$\rho_a = K \frac{\Delta V}{I} \quad (4.1)$$

Where,

K: is a factor depending on electrode configuration.

I: is the electrical direct current.

$\Delta V$ : is the potential difference.

Then the interpretation of field study is made depending on resistivity values which refer to the geological medium taking to the account previous geological study in the field.

### 4.2.1 Apparent Resistivity

Apparent resistivity (Figure 4.1) is the most important parameter in electrical resistivity survey.

For homogenous medium, the potential difference can be calculated by the following formula ( $\rho$  here is real resistivity):

$$\Delta V = \frac{I\rho}{2\pi} \left( \frac{1}{C_1P_1} - \frac{1}{C_1P_2} - \frac{1}{C_2P_1} + \frac{1}{C_2P_2} \right) \quad (4.2)$$

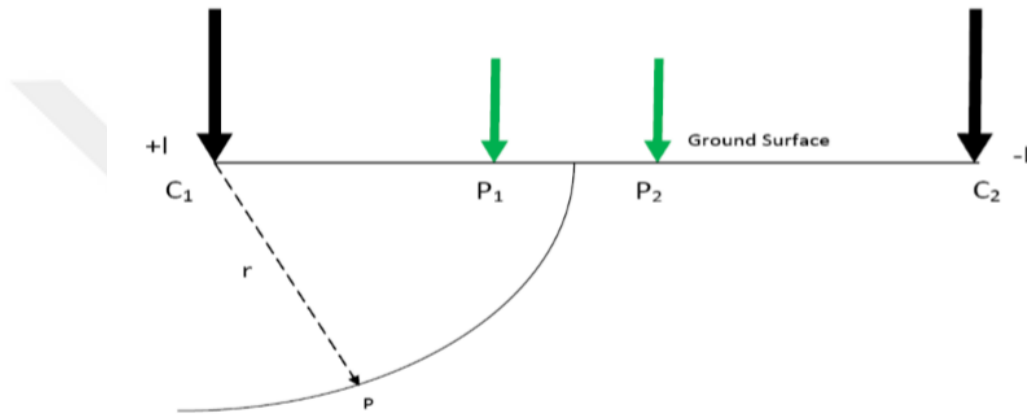


Figure 4.1 Distribution of the potential in half-homogenous medium (Aizebeokhai, 2010)

For non-homogeneous medium, the measured resistivity is not considered as the true resistivity because of the different distribution in the medium. In order to measure apparent resistivity values, we need four electrodes in the measurements two of them for conducting the current into the earth and the other for measuring potential difference. Apparent resistivity influenced by many factors such as the applied current to the earth, the geometric factor of the arrays, the geological structure in the field and the rock types (Robert, Nostrand, & Cook, 1966).

And geometric factor is given by the following formula: (Aizebeokhai, 2010)

$$G = 2\pi I \left( \frac{1}{C_1P_1} - \frac{1}{C_1P_2} - \frac{1}{C_2P_1} + \frac{1}{C_2P_2} \right) \quad (4.3)$$

## 4.2.2 Electrical Resistivity Properties of the Rocks

Rock resistivity associated with multiple parameters such as mineral content, stiffness and rigidity of rock materials, porosity and permeability, dissolved salts and water saturation. These previous factors play a great role in determining resistivity values in the rocks. In this chapter we will mention some essential electrical properties of the rocks which have large effects on the resistivity.

### 4.2.2.1 Porosity

Porosity is defined as the ratio between pore volumes ( $V_p$ ) to the total bulk volume ( $V_t$ ). We can formulate it as follows: (Lawrence, & Jiang 2017);

$$\varphi = \frac{V_p}{V_t} = \frac{V - V_s}{V_t} \quad (4.4)$$

The inverse of resistivity is conductivity

$$1/\varphi = \sigma \quad (4.5)$$

There are many types of the rock porosity (Gibb, Barcelona Ritchey, & LeFavre 1984):

- Primary porosity: It is formed at the same time with rock deposition.
- Secondary porosity: It is formed in the rock after deposition and sedimentation operations.
- Total porosity: This defined as the ratio between all pores and spaces in the rock to the total bulk volume.
- Effective porosity: is defined as the ratio between the whole effective pores which enable the fluid to transmit easily in the rock to the total bulk volume.



The resistivity value is deeply influenced by the porosity of the rocks. The relationship between the resistivity and porosity which state by Archie is given by (Loke, 2015):

$$\rho_r = a \rho_w \varphi^{-m} \quad (4.6)$$

Where,

$\rho_r$ : is rock resistivity

$\rho_w$ : is fluid resistivity

$\Phi$ : The porosity

a and m: Geometric parameters.

a and m are geometric parameters which depend on many factors such as pores, shape of the rock and grain size. For instance, if the grain size is small the particles of the rock will be closer to each other and that will result in low porosity. On the contrary, the larger the particles the greater the porosity because when we have large grain size more unfilled spaces will be existed in the rock and that will lead to high ratio of porosity (Zohdy, Eaton, & Mabey, 1974)

#### *4.2.2.2 Rock Types and Soil*

Rock resistivity` is associated with the degree of porosity, pore volume and fracturing. Generally, sedimentary rocks have low resistivity values comparing to igneous and metamorphic rocks because of high pore ratio, water and contents. Resistivity values of igneous and metamorphic rocks reach over 1000 ohm.m while the values of resistivity for sedimentary rocks range between 10 – 1000 ohm.m and have great dependence on pore, porosity and water content. On the other hand, the resistivity of soil is lower than the resistivity of rocks because of cementation and consolidation of the grains which lead to decrease in porosity (Figure 4.2).

The great resistivity values in the rocks which showed in Table 4.2 are obtained by decreasing the salinity and water content and increasing the cementation degree which lead to less of pores (Loke, 2000).

Table 4.2 The resistivity values for some rocks (Loke, 2000)

Material	Resistivity ( $\Omega.m$ )	Conductivity (Siemen/m)
<b>Igneous and Metamorphic Rocks</b>		
Granite	$5 \times 10^3 - 10^6$	$10^{-6} - 2 \times 10^{-4}$
Slate	$6 \times 10^2 - 4^{10}$	$2.5 \times 10^{-8} - 1.7 \times 10^{-3}$
Marble	$10^2 - 2.5 \times 10^8$	$4 \times 10^{-9} - 10^{-2}$
Quartzite	$10^2 - 2 \times 10^8$	$5 \times 10^{-9} - 10^{-2}$
<b>Sedimentary Rocks</b>		
Sandstone	$8 - 4 \times 10^3$	$2.5 \times 10^{-4} - 0.125$
Shale	$20 - 2 \times 10^3$	$5 \times 10^{-4} - 0.05$
Limestone	$50 - 4 \times 10^2$	$2.5 \times 10^{-3} - 0.02$
<b>Soils and water</b>		
Clay	1 - 100	0.01 - 1
Alluvium	10 - 800	$1.25 \times 10^{-3} - 0.1$
Groundwater (fresh)	10 - 100	0.01 - 0.1
Sea water	0.2	5

#### 4.2.2.3 Water Content and Salinity

Generally, the resistivity in the rocks associated with the type of water content. If the groundwater is fresh, the resistivity has high values (10 - 100 ohm.m.). For the salty groundwater, the resistivity values are low when the aquifers contain on saline water 1- 10 ohm.m (Loke, 2004).

#### 4.2.2.4 Clay Contents

Clay resistivity is ranging from 1 to 10 ohm.m. If the sediments contain clay that will lead to low values of resistivity as the decreasing in the clay content in the rock result in increasing in resistivity (Loke, 2004).

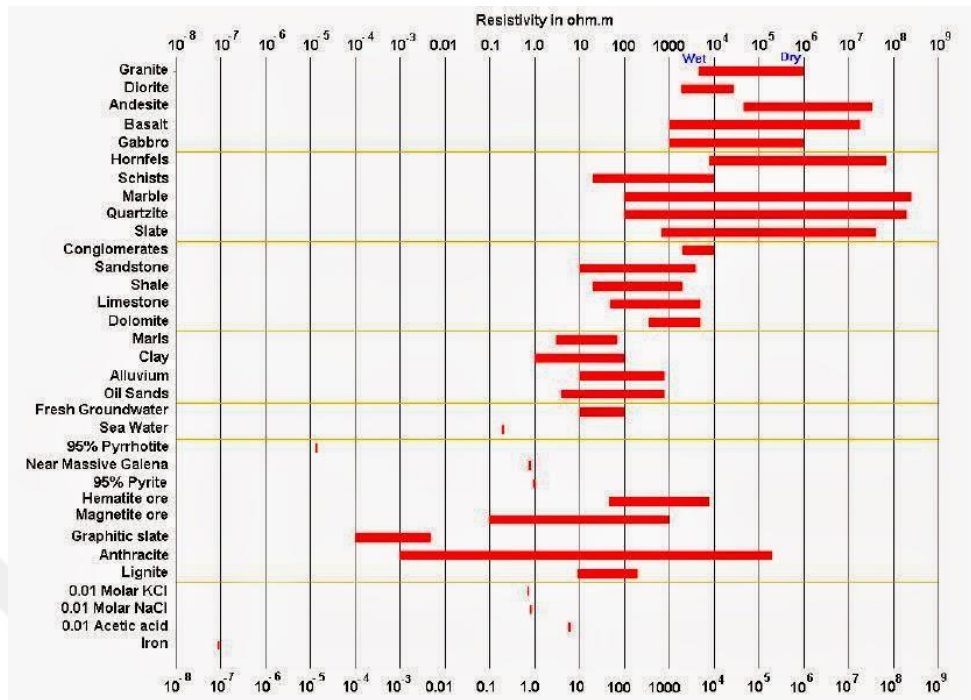


Figure 4.2 The resistivity values of the rocks and groundwater (Loke, 2004)

### 4.2.3 Types of Electrical Resistivity Method

There are two types of electrical resistivity surveys; vertical electrical sounding and profiling methods. Sounding surveys are used for delineating the vertical variations of the resistivity in the study area. The space between electrodes in this survey is increased in order to detect resistivity changes with the depth. Greater the space between the electrodes, greater the depth of penetration. On the other hand, the space between the electrodes in profiling electrical surveys is kept constant without change and this survey is used for detecting the lateral variation of resistivity.

#### 4.2.3.1 Vertical Electrical Sounding (VES)

It is one of geoelectrical resistivity survey and used for detecting the variation of resistivity with the depth. This detection can be achieved by moving the current electrodes in each measurement. These techniques of survey enable us to determine the horizontal structure also it is widely used in groundwater exploration. Vertical electrical resistivity data can be interpreted by qualitative and quantitative

interpretation techniques. Quantitative technique depends on master curve matching in the interpretation and computer-based methods then the thickness and resistivities of the layers will be delineated. On the other hand the qualitative interpretation depends on the number of layer models (Karanth,1987).

#### *4.2.3.2 Horizontal profiling Electrical Resistivity (EP)*

This kind of survey is sensitive to lateral variations (vertical structure) and in this technique of electrical resistivity measurements, the space between the electrodes kept fix while moving. Wenner configuration is the most famous array which is widely used in profiling measurements and the depth of investigation is considered as moderate and constant. The results of measurements are presented in resistivity maps and generally the most common used interpretation technique is qualitative interpretation (Karanth, 1987).

#### *4.2.4 Types of Electrical Resistivity Arrays*

Electrical resistivity surveys can be performed in the field using many types of configurations and arrays. These configurations are differing from each other in their electrode set arrangements. The most commonly used configurations in geoelectrical methods are Wenner, Schlumberger, dipole-dipole, pole-pole and pole-dipole arrays. Choosing the arrangement of the electrodes in the fieldwork is depending on our target in the study area and associate with many factors such as the type of structure, horizontal and vertical sensitivity in the subsurface and the required depth penetration. For example if our aim is to identify the lateral variation, it is preferred to use Wenner set. On the other hand when we want to determine the vertical variation of electrical resistivity with the depth Schlumberger array is more recommended (Loke, 2000).

#### 4.2.4.1 Wenner Array

Wenner configuration design consist of four electrodes are laid in the field as straight line. Two of them are current electrodes (outer electrodes) and the potential electrodes in the mid of the arrangement. In wenner array the distance between the four electrodes are equal to each other and the electrodes places should to be changed in every survey. Because of the fixed distance using the depth penetration is consider to be moderate comparing to other arrays The geometric factor for this array is  $k = 2\pi a$  and the apparent resistivity is expressed in:

$$\rho_a = 2\pi a \frac{V}{I} \quad (4.7)$$

Wenner configuration (Figure 4.3) is used for vertical variation detection (the horizontal structure) also has strong signal strength as we can use it in the places which characterized by high noise (Loke, 2000).

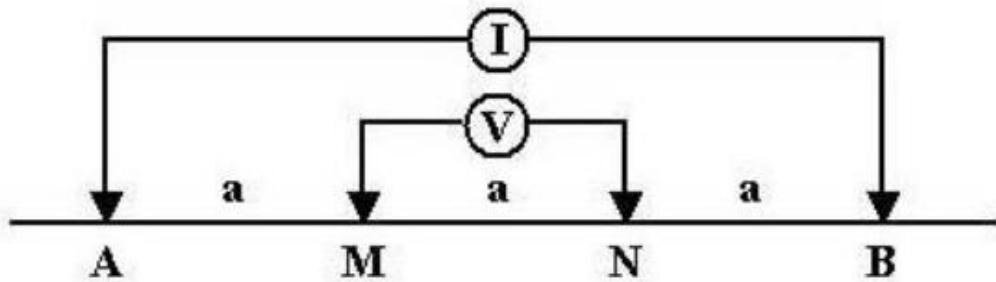


Figure 4.3 Arrangement of electrodes in Wenner array (Garofalo, 2014)

#### 4.2.4.2 Schlumberger Array

The four electrodes in the Schlumberger array are placed also in straight line but the space between the electrodes is not equal to each other. The distance between potential electrodes is smaller than the distance between the current electrodes. In the

field measurements, the potential electrodes are kept fixed in all measurements till reaching to too small voltage values however the current electrodes are moved increasingly and that lead to less time consuming during the measurements (Figure 4.4). The geometric factor for this array is  $k = \pi \frac{b(b+a)}{a}$  and the apparent resistivity expressed in:

$$\rho_a = \pi \frac{b(b+a)}{a} \cdot \frac{V}{I} \quad (4.8)$$

Schlumberger array (Figure 4.4) is widely used in detecting horizontal variation as it has high vertical resolution (vertical structure detection) (Adeyemo, Ojo, & Raheem, 2017).

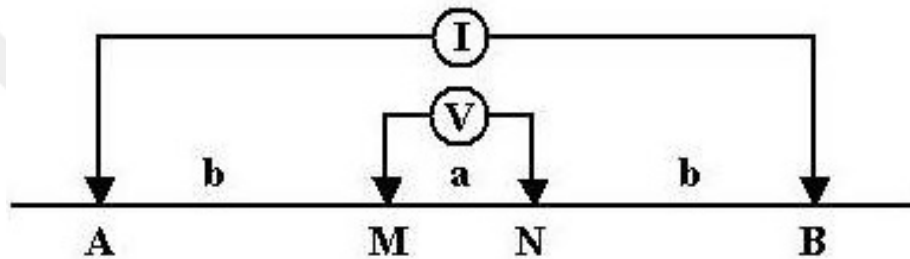


Figure 4.4 Arrangement of electrodes in Schlumberger array (Garofalo, 2014)

#### 4.2.4.3 Dipole - dipole Array

The arrangement of the electrodes in this array is different from previous arrays. In this configuration the current electrodes (AB) are placed at the beginning and the potential electrodes (MN) are placed in the end of the survey and the space between current and potential electrodes ( $n=1-6$ ) (Figure 4.5). In order to reach great depth penetration, the  $n$  values should be increase. Dipole-dipole array is more sensitive to horizontal changes (vertical structure) than the vertical one and has small signal strength when  $n$  has great values (Loke, 2000).

The geometric factor for this array is  $k = \pi a n(n + 1)(n + 2)$  and the apparent resistivity is expressed in:

$$\rho_a = \pi a n(n + 1)(n + 2) \cdot \frac{V}{I} \quad (4.9)$$

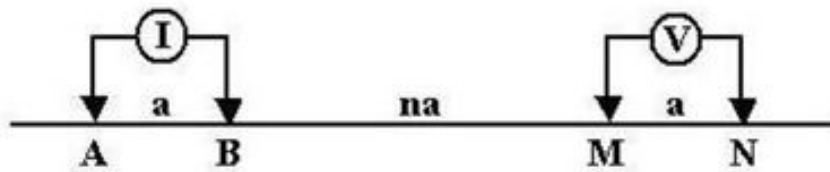


Figure 4.5 Arrangement of electrodes in Dipole-dipole array (Garofalo, 2014)

#### 4.2.4.4 Wenner- Schlumberger Array

This array is widely used in electrical resistivity tomography method. It is integrated technique between Wenner and Schlumberger arrays and provides both of vertical and horizontal sensitivity. The depth penetration in Wenner- Schlumberger configuration (Figure 4.6) is bigger than which achieved by Wenner array. The geometric factor for this array is  $k= xn (n+1) a$  and the apparent resistivity is expressed in:

$$\rho_a = xn (n + 1) \cdot \frac{V}{I} \quad (4.10)$$

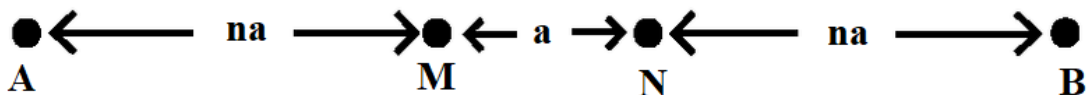


Figure 4.6 Arrangement of electrodes in Wenner- Schlumberger array (Garofalo, 2014)

### 4.3 Electrical Resistivity Tomography (ERT)

(ERT) is a geophysical method and electrical imaging technique. This method identifies the resistivity contrast in the test site using number of electrodes and cables also provides us 2D and 3D resistivity models depending on inversion methods. Electrical resistivity tomography method is modified from vertical electrical sounding techniques VES. This method can detect the horizontal and vertical variations in resistivity values by imaging the subsurface while VES method can

determine just the vertical differences of the electrical resistivity. ERT investigations are widely used in lithological properties determination, natural geo-hazards, such as slope stability and landslide taking into the account the changing in resistivity values. ERT surveys can be carried out in the field by several configuration types using multi electrode such as dipole-dipole, Wenner, Schlumberger, wenner - Schlumberger etc. The electrodes will be injected to the ground in order to send electric current and generate voltage signals.

#### 4.3.1 2D and 3D Electrical Resistivity Tomography Survey

Contrary to traditional electrical resistivity surveys which provide us 1D image for the earth, ERT survey provides 2D and 3D image for mapping the structure of the subsurface as it is very useful technique in lateral and vertical variations determination. However, 1D electrical survey is still widely used when the greater penetration depth is requested in the site investigation (Loke, 2015)

2D electrical resistivity tomography survey is carried out in the site investigation by using profiling and sounding electrical resistivity survey in order to provide a great coverage for the study site. Different separations between the electrodes and midpoints are used in 2D ERT survey (Figure 4.7). In general, the lateral coverage in this technique is bigger than the coverage with the depth (Adeyemo, Ojo, & Raheem, 2017).

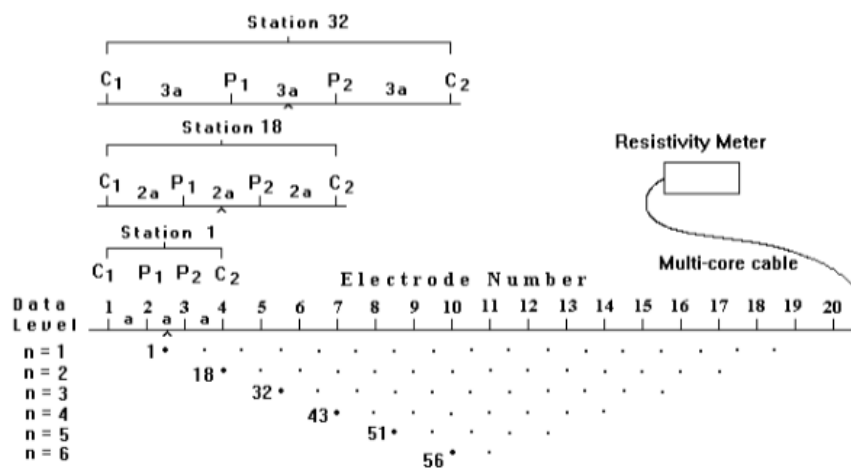


Figure 4.7 2D electrical resistivity tomography survey (Garofalo, 2014)



Figure 4.8 illustrate example of 2D ERT data coverage in the Blue Ridge mountain area in eastern USA for groundwater exploration using dipole-dipole configuration.

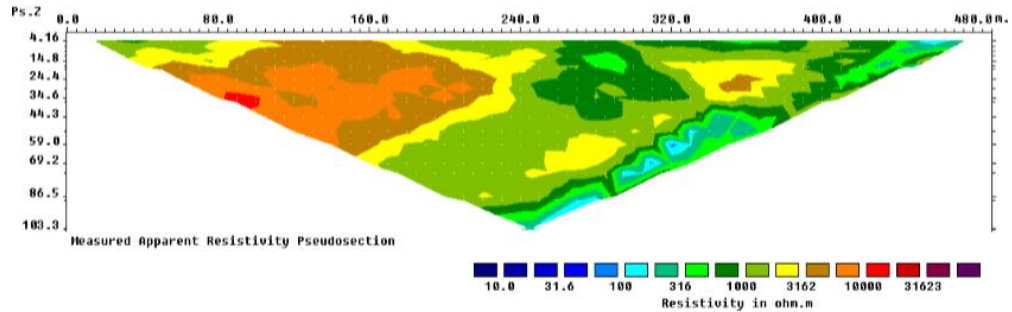


Figure 4.8 Example of 2D ERT data coverage in the Blue Ridge mountain area in eastern USA for groundwater exploration using dipole-dipole configuration (Loke, 2015)

Sometimes 2D survey gives us unreal features and that result in inaccurate interpretations. By providing 3D model for the resistivity variation in (X, Y, Z) directions more reliable results can be achieved (Adeyemo, Ojo, & Raheem, 2017). 3D ERT survey is widely used in mineral exploration, environmental and engineering investigations. In this 3D method, Roll-Along technique is the most famous technique in 3D electrical resistivity tomography investigation. In this technique, parallel survey lines are laid in the site investigation and the measurements are taken in the X and Y directions (Figure 4.8) in order to obtain great and sufficient amount of data (Chávez, Cifuentes-Nava, Tejero, , Hernández-Quintero, & Geofísica, 2014).

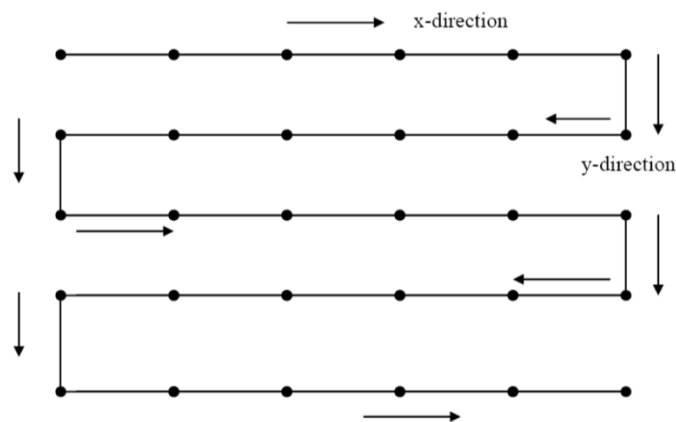


Figure 4.9 The set of the electrode in (X,Y) directions in 3D ERT (Adeyemo, Ojo, & Raheem, 2017)

Two of techniques were developed for reducing the number of obtaining data with keeping the quality and accuracy of the site investigation. The first one is named by cross-diagonal survey and has been developed by Loke and Barker (1996). In this survey, the potential electrodes are lined crossing the current electrodes in horizontal, vertical and diagonal directions (Loke & Barker, 1996).

The second technique named by maximum yield grid which depend on reducing the using the number of current electrodes (Capizzi, Martorana, Messina, & Cosentino, 2012). Recently, many types of instruments and inversion software are founded for ERT data collecting and analyses. By using the computer, the electrodes and the kind of configuration can be chosen for 2D and 3D (Figure 5.9) coverage of the site investigation (Loke, 2015).

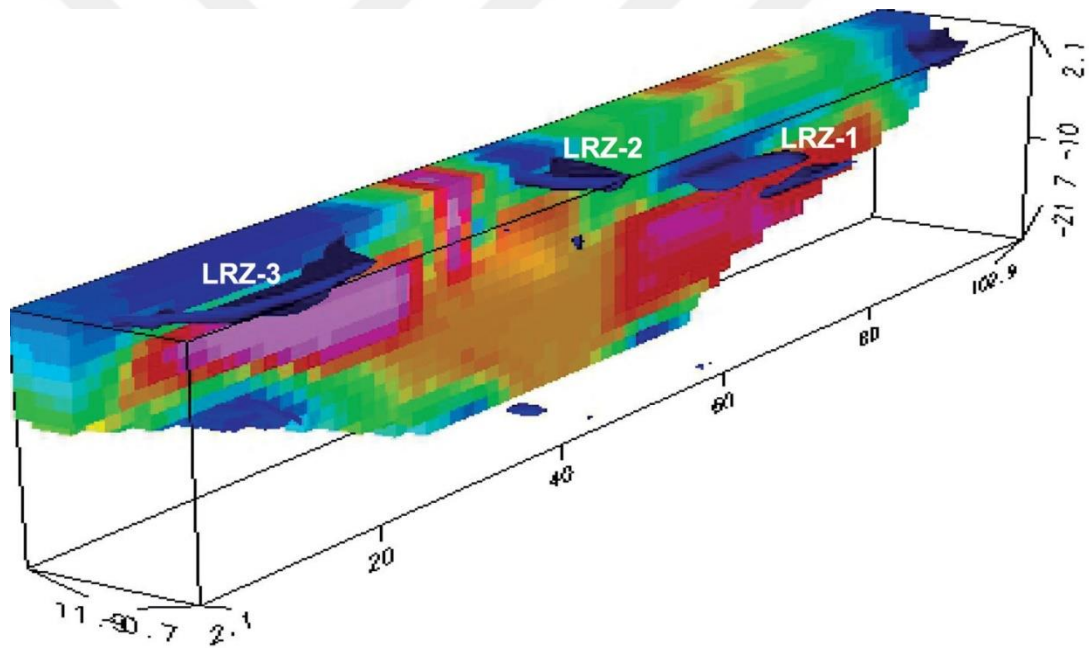


Figure 4.10 Example of 3D ERT model for studying dam structure in ural municipality of Cordeirópolis in the State of São Paulo by using wenner configuration (Camarero & Moreira, 2017)

#### 4.4 ERT data Analyses and software

The apparent resistivity data which obtained from the field investigation should be inverted using inversion techniques and software. Electrical resistivity tomography

software is used for inverting ERT data and making 2D model for the distribution values of the real resistivity (Hellman, Johansson, Olsson, & Dahlin, 2016). All the software which are used in ERT data interpretation are provided by two types of routine, forward and inversion. Forward modeling is applied for deriving the real resistivity values from the apparent resistivity. In the second step, the inversion modeling will be applied using iteration technique for obtaining 2D resistivity model that provide the best fitting between the calculated and the observed resistivity values. Forward modeling is time consuming and sometimes gives us difficult interpretation models as it needs a big experience from the interpreters. Non-linear least square method is used in inversion routine (Loke & Barker, 1996). The most common used inversion resistivity softwares are Res2Dinv (Loke et al. 1996; Loke et al. 2003), Aarhusinv (Auken et al. 2015; Fiandaca et al. 2013) and BERT (Rücker et al, 2006)

#### **4.4.1 Forward Modeling**

The solution of forward problem start with following the following equation: (Pasierb, 2015)

$$\frac{d}{dx} \left( \sigma \frac{dV}{dx} \right) + \frac{d}{dz} \left( \sigma \frac{dV}{dz} \right) - K_l^2 \sigma V = -\frac{I}{2} \delta(x) \delta(z) \quad (4.11)$$

Where,

$\sigma$ : electrical conductivity [S/m].

V: electrical potential [V].

I: current [A].

$K_l$ : wave number.

$\delta$ : Dirac delta

The previous equation can be solved by two numerical technique finite differences (FD) (Dey & Morrison, 1979) and finite element (FEM) approaches. FD approach is a fast technique but it does not take the topography to the account and that will lead

to inaccurate results. FEM approach is largely used when the data consists of topography. Although FEM provides us smaller error (Pasierb, 2015) but it is not applicable to large number of data. FD and FEM meshes are illustrated in Figure 4.11.

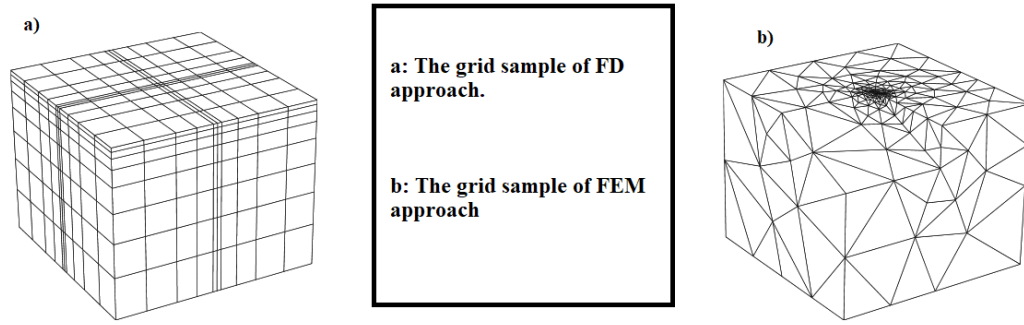


Figure 4.11 The mesh types of FD and FEM technique (Pasierb, 2015)

#### 4.4.2 Inversion Modeling

The inversion procedures (Figure 4.12) start with choosing the initial model of resistivity  $q_0$ . During initial step all the rectangular values will be equal to each other (Figure 4.13). Then, the new model parameter calculation will start using the following equation:

$$q_i = q_{i+1} \Delta q \quad (4.12)$$

Previous step will be repeated until reaching the best fitting between the calculated and observed resistivity values. The number of iteration in this algorithm is ranging between 3 – (Loke, 2015). Finally the smallest values of root-mean squared (RMS) error will be achieved by using the following formula:

$$RMS_j = \sqrt{\frac{1}{M} \sum_{i=1}^m \left( \frac{\rho_i^o - \rho_i^c}{\rho_i^c} \right)^2} \times 100\% \quad (4.13)$$

Where,

M: is the number of observed data.

$\rho^o$  and  $\rho^c$ : are the observed and calculated data.

i: denotes each observation.

j: denotes iteration.

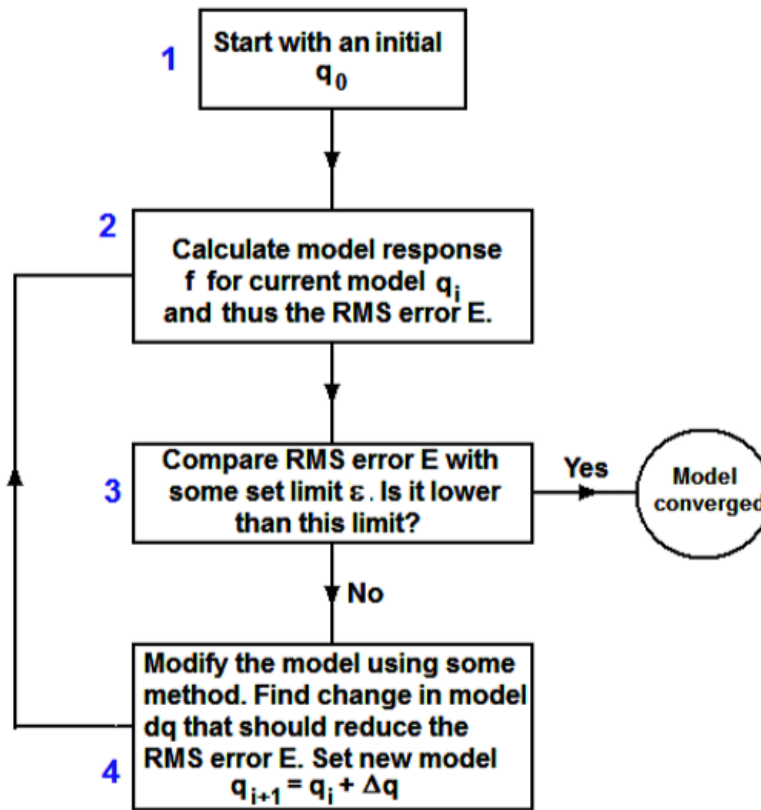


Figure 4.12 The iteration circle for inversion procedures (Loke, 2015)

Many of inversion techniques can be used for inverse modeling. Quasi-Newton, Gauss-Newton and the smoothness constrained least square meth (Loke & Barker, 1996) (the modification of Gauss- Newton- deGroot-Hedlin and Constable, 1990; Sasaki, 1992; Loke & Barker, 1996):

$$[J_i^T J_i + \lambda_i W^T W] \Delta q_i = J_i^T g_i - \lambda_i W^T W q_{i-1} \quad (4.14)$$

Where,

W: roughness filters or weight matrix.

$\lambda$ : roughness filter damping factor.

$q_{i-1}$ : current inversion model.

$\Delta q_i$ : change in model resistivity to be calculated.

g: data misfit, difference between measured and calculated apparent resistivity values.

J: Jacobian matrix of partial derivatives, or sensitivity.



from sources to geophones will be measured and the subsurface structure will be determined depending on arrival time, amplitude, frequency and velocity. Recorded data will be subjected to post processing and interpretation in order to output useful information about the study medium. Seismology can be defined by study of elastic wave propagation through the earth, so we can say that there is such a deeply relation between elastic properties of materials and seismic waves in the medium. Different types of rocks and soil have different elasticity properties and that link result in variety in seismic wave velocities while propagating in the layers. As a result, we can define the physical properties (stiffness, rigidity and density, etc.) of the medium by determining the seismic wave velocities. Therefore, to clarify this relation, we will include elastic theory in this study.

#### ***4.5.1 Elastic theory***

As we can define the seismology by study of elastic wave propagation through the earth, we can say that there is such a deeply relationship between elastic properties of rock mass and seismic waves in the medium. Therefore, to clarify this relation, we will include elastic theory in this study. Elasticity defined by the change in shape and volume after applying a force to a medium. If the medium restore its original shape and volume after removing the action we refer to it as “Elastic medium.” Elastic properties depend on the medium feature. For instance, solid media characterized by shape and volume elasticity, however. The elasticity in liquids and gases media happens just in the volume (Lowrie, 2007).

##### ***4.5.1.1 Stress and strain***

Applied external forces result in deformations on the body and the relation between this forces and deformations expressed as terms “strain and stress”. Stress defined by ratio between the force  $F$  and unit of area which acting on it and it can be measured by  $N/m^2$

$$\text{Stress} = \text{force/area}$$

We have two compounds of stress; if  $F$  is perpendicular to the surface, the stress is considered to be normal stress. If  $F$  is tangential to the surface, the stress is considered to be shear force. Whereas, strain defined by change in volume and shape of the body resulting from stress (Lowrie, 2007).

#### 4.5.1.2 Hooke's Law

Hooke's Law in elasticity state that applied force  $F$  equals a constant  $k$  multiplied by the change in length or extension ( $x$ )  $F = kx$ . Also according to Hooke's Law, there is a linear relation between strain and stress according to the following equation (Lowrie, 2007):

$$\sigma = E \cdot \epsilon \quad (4.15)$$

Where,

$\sigma$ : The stress

$\epsilon$ : The strain

$E$ : Elastic constant.

And the object still behave as elastic body till reaching Yielding Point which can defined by large increases in strain without increase in stress (Figure 4.14).

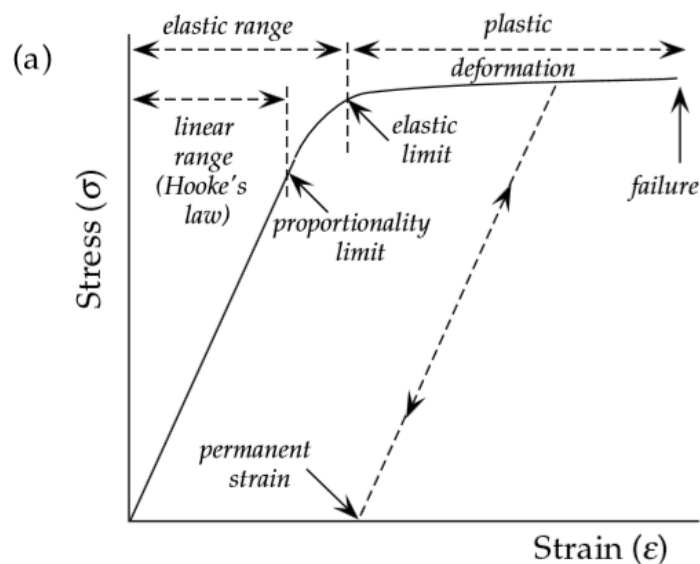


Figure 4.14 The relationship between stress and strain (Lowrie, 2007)



#### 4.5.1.2 Elastic Constants

There are five elastic constants which link between different types of strain and stress and describe the elastic properties in anybody (Lowrie, 2007).

Poisson's Ratio ( $\nu$ ) expresses the ratio between transverse and longitudinal strain (directions transverse to the direction of extension) (Figure 4.14). Practically this ratio is always between 0 and 0.5 and without unit.

$$\nu = \frac{\text{lateral (contractional) strain}}{\text{longitudinal (extensional) strain}} = \frac{\Delta b / b}{\Delta l / l} \quad (4.16)$$

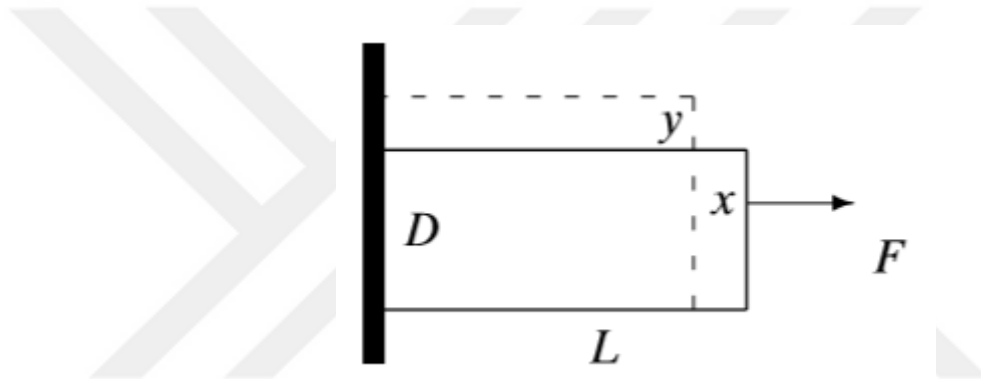


Figure 4.15 The Longitudinal and lateral strai (Lowrie, 2007)

- 1- Young's Modulus expresses the ratio between longitudinal stress and strain and the unit of Young's module is MPa

$$Y = \frac{F/A}{\Delta L/L} \quad (4.17)$$

Where,

$A$  = Area acted on by the shear force

$\Delta L$  = Increment of transverse displacement parallel to  $A$

$L$  = Original length.

- 2- Bulk Modulus (K): These parameters indicate to the change in the volume and can define by the ratio between the compressional stress and the change in volume. The unit of Bulk Modulus is  $N/m^2$

$$K = \frac{F/A}{\Delta V/V} \quad (4.18)$$

- 3- Rigidity or shear modulus ( $\mu$ ): indicate to the ratio between shear stress and shear strain and expresses the change in shape without volume. The unit of shear modulus is MPa.

$$\mu = \frac{F/A}{\theta} \quad (4.19)$$

$\theta$  : The angle of deformation

- 4- Lamé constants ( $\lambda, \mu$ ): These constants relate to Young's modulus ( $E$ ) and Poisson's ratio and describe the strength of isotropic medium and the elasticity properties in this medium are independent of direction. The name of  $\mu$  constant is modulus of rigidity; on the other hand  $\lambda$  constant has no name.

$$\lambda = K - \left(\frac{2}{3}\right)\mu \quad (4.20)$$

$$\mu = \frac{\Delta F/A}{\Delta L/L} \quad (4.21)$$

## 4.5.2 Seismic Waves

In the Early 1800's the main types of seismic waves were determined by Cauchy, Poisson, Stokes and Rayleigh. These waves were later described by Richard Dixon Oldham in 1900. There are two basic types of seismic waves; body waves which travel through the earth (invasive wave) and surface wave which propagates near the surface (non- invasive wave). Studying the properties of seismic wave depend on elasticity properties of layers (Shearer, 2009).

### 4.5.2.1 Body waves

If the medium of propagation is homogeneous, isotropic and unlimited medium, two types of body waves will be generated in this medium. First one is P-wave or compressional wave also it is called by primary wave because it arrives firstly to the seismogram. This kind of waves can propagate through solid and liquid medium. The second type of body waves is S-waves or shear wave which called by secondary wave because it arrives after P-wave. S-wave can propagate just through solid

medium but not through liquids because of the Lamé constant  $\mu$  which equal to zero in this media. The motion of P-wave is parallel to the propagation direction however the motion of S-wave is perpendicular to the propagation direction and has two polarizations; SH-waves and SV-waves. The velocity of S-wave is less than P-wave. These waves characterized by higher frequency than surface waves (Heisey, Stokoe, & Meyer, 1982).

The velocities of P-wave and S-wave are given by the following formulas: (Heisey, Stokoe, & Meyer, 1982)

$$a = \sqrt{\frac{\lambda + 2\mu}{\rho}} \quad (4.22)$$

$$\beta = \sqrt{\frac{\mu}{\rho}} \quad (4.23)$$

Where,

$a$ : is a by primary wave velocity,

$\beta$ : is shear wave velocity

$\mu, \lambda$ : are Lamé constant,

$\rho$ : is the density.

#### 4.5.2.2 Surface Wave

When shallow earthquakes occur, damage and destruction will happen resulting from surface waves effects. Surface waves can be generated when the propagation medium is bounded. This kind of waves propagates along the surface of the earth and reaches to the seismogram later than P and S wave (Body waves) and characterized by a long period and low frequency. These waves can be classified into two types; Rayleigh wave which called also by ground roll waves and Love waves. The amplitude of this surface wave decays with depth faster than body waves. As the velocities of surface wave depends on frequency, surface waves are described as dispersive.

The wavelength of this wave is increasing with depth. Thus, surface waves are characterized by dispersion properties because of differing in frequencies versus the velocities.

*4.5.2.2.1 Love Wave.* Love wave named by British mathematician Augustus Edward Hough (1863-1940). The particles motion in this wave is horizontal and parallel to the surface (Figure 4.15). The new generation of the geophone can receive only the vertical motion, therefore Love wave rarely can be exist in seismic records. Furthermore, this kind of has no importance in seismic investigation methods (Telford, Geldart, & Sheriff, 1991).

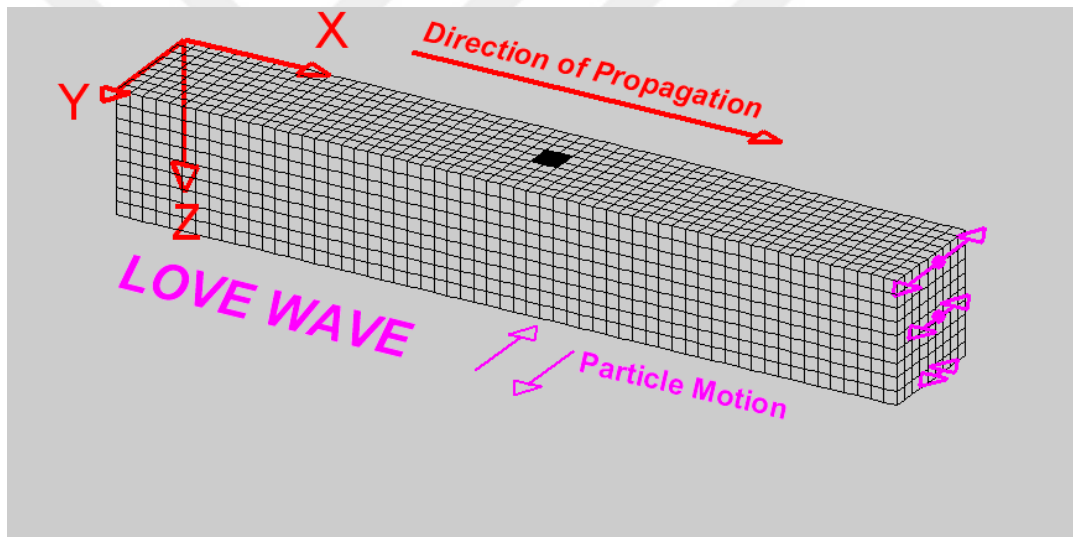


Figure 4.16 The particle motion of Love wave (Braile, 2015)

*4.5.2.2.2 Rayleigh Wave.* This wave which is known also by ground roll was found in 1885 by Lord Rayleigh. Rayleigh wave play such an essential role in geophysics and seismic explorations. These kinds of waves are generated in non- homogeneous medium (Telford, Geldart, & Sheriff, 1991).

Using vertical seismic sources and more than two third of generated wave energy is becoming a ground roll wave (Ólafsdóttir, 2014).

The particles motion (Figure 4.17) in this wave is an elliptical and retrograde motion in the same direction of wave (Telford, Geldart, & Sheriff, 1991).

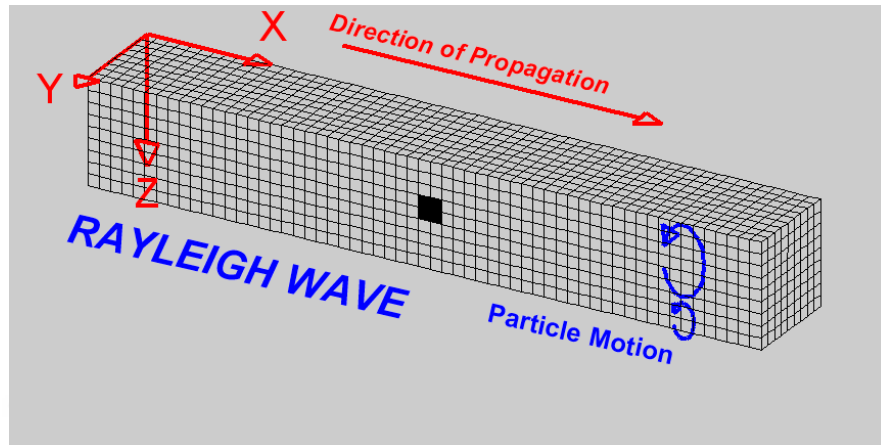


Figure 4.17 The particle motion of Rayleigh wave (Braile, 2015)

Rayleigh wave depends on frequency according to the following relationship (Heisey, Stokoe & Meyer, 1982):

$$V_R = f \cdot L_R$$

Where,

$V_R$ : Velocity of Rayleigh wave.

$f$ : Frequency of the wave.

$L_R$ : The wavelength of Rayleigh wave.

The propagation of the wave is near - surface with different wavelength because of the differences in soil rigidity properties which result in variation in velocities hence differences in wavelength travel and dispersion. Furthermore, the wavelength of Rayleigh is increasing with the depth and provides us more information about deep soil (Telford, Geldart, & Sheriff, 1991) (Figure 4.18).

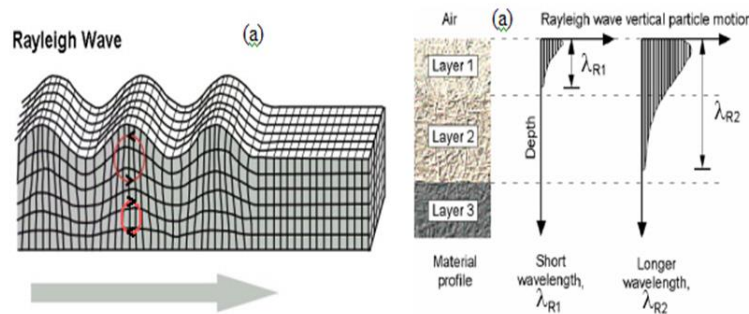


Figure 4.18 The relationship between wavelength of Rayleigh wave and the depth (Mullins, 2015)

### 4.5.3 Dispersion of Surface Wave

Surface wave characterized by dispersive properties and dispersion curve (Figure 4.19) defined by phase velocity versus frequency (Strobbia, C). Wave dispersion can be divided into two categories; material and geometric dispersion. Material dispersion occurs according to the internal structure, while geometric dispersion occurrence related to medium of the propagation. When the wave propagates through non-homogenous medium, the geometric dispersion happened and results in interference of waves. This type of dispersion is used in surface wave exploration methods and depends on mechanical properties of the test site (Park, Miller, & Xia, Hunter & Harris, 1996).

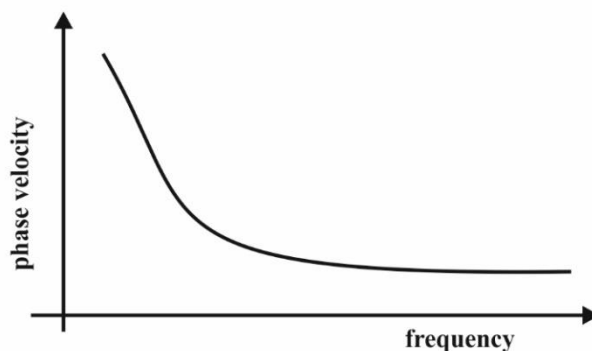


Figure 4.19 Dispersion curve (phase velocity versus frequency)

Having a variation in vertical velocity because of the difference between material properties in the site result in different propagation velocity for each frequency component of surface wave. The penetration depth of surface waves depends on

wavelength and frequency. The lower the frequency of Rayleigh wave (longer wavelength) the bigger the penetration of depth (Novotny, 1999).

Figure 4.20 illustrates the difference in propagation of surface waves in a vertically homogeneous medium and non-homogeneous medium. The phase of velocity is constant in homogeneous medium in the left and in the right of figure the phase of velocity depends on wavelength changes in non-homogeneous medium.

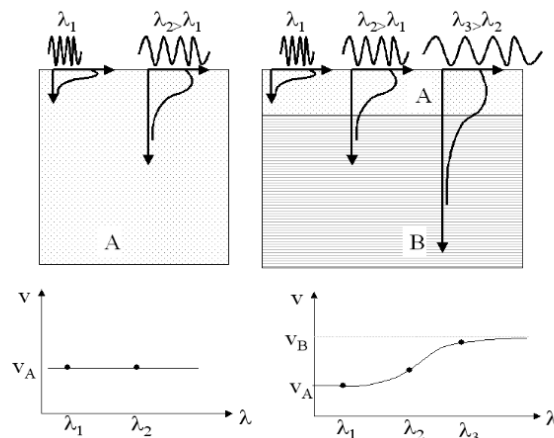


Figure 4.20 The difference in propagation of surface waves in a vertically homogeneous medium and non-homogeneous medium (Garofalo, 2014)

#### 4.5 Surface Wave Methods for Estimating the Stiffness of Soil

The stiffness of geometrical determination is very essential to describe the structure in the test site. Recently, there are several methods are widely used for obtaining the stiffness of material whether in laboratory or in the field (Sawangsurii, 2012). In this study we are going to use surface wave measurements method. Surface wave methods are non-invasive techniques as it can give us information about the structure of earth by propagating along the boundary of surface depending on dispersion properties.

These methods are widely used to estimate shear wave velocity ( $V_s$ ) profiles near-surface depending on Rayleigh wave dispersion curves. Surface wave methods have many advantages. These methods are low-cost and have no harmful causes for

environment. Spectral Analysis of Surface Waves (SASW) and Multichannel Analysis of Surface Waves (MASW) are two basic methods which utilizes the dispersion characteristics of Rayleigh waves for estimating S- wave velocity profiles (Ólafsdóttir, 2014). In SASW method two receivers are used with dynamic sources (hammer, weight drops, electromechanical shakers, vibroseis and bulldozers) in order to generate seismic energy. Using a few numbers of receivers lead us to repeat the test field with several configuration of sources to insure that the required depth in the field investigation is covered and reduce the noise influence .Therefore, we can say that SASW method is time and labor consuming. On the other hand, MASW test is less time consuming because of using for (12 - 24) geophones with multiple seismograms in the field (Park, Miller, & Xia, 1996). In this study, MASW method will be used and widely discussed.

#### ***4.6.1 Multi-channel Analysis of Surface Wave (MASW)***

Using of multi-channel analysis of surface wave method is increasing day by day because of several advantages. Less time consuming and money saving, decreasing the number of geophysical surveys and reducing in noise which leads us to accurate wave velocity profile as signal to noise ratio can easily achieved. There are two types of MASW method sources, passive and active. Active MASW method depends on impulsive or vibrating seismic sources while passive MASW method depends on natural sources, cultural noise, traffic, factories, wind, wave motion, etc. Multichannel Analysis of Surface Waves (MASW) is applied for obtaining Rayleigh wave dispersion curves from surface wave seismic records which provide us information about near-surface materials properties for estimation of shear wave velocity profiles of top layers in test site (Park, Miller, & Xia, 1996).

Multi-channel analyses of surface wave consist of three procedures:

- Acquisition of field data for Rayleigh wave.
- Obtaining the dispersion curve.

Finally, estimating S- shear wave velocity profiles depending on inversion methods (Park, Miller, & Xia, 1996).



- MASW method has been applied for many geotechnical problems by using multiple receivers and vertical (impulsive) seismic or natural sources for generating surface wave (Park & Penumadu, 2005)

MASW method is classified into two types of sources; active and passive sources and it is employed for producing 2D VS profiles by setting the receivers as linear array in active sources and circular, linear, cross and square in passive sources (Park, Miller, Xia, & Ivanov, 2007).

#### 4.6.1.1 Passive and Active MASW Sources

There are two types of active sources MASW method using Vibroseis (MASWV) and MASW method using impulsive source (MASWI) like sledge and hammer (Figure 4.21). If the MASWV is the method which will be used in the field so the processing technique will be done in a time-domain using the software. On the other hand for MASWI the processing procedures by software will be done in frequency-domain. MASWI is cheaper and faster than MASWV only there are some drawbacks in data processing while using MASWI method. (Park, Miller, Xia, Hunter, & Harris, 1999).

Also surface waves can be generated using passive sources such as natural and cultural activates traffic, wind and noise, etc. the penetration depth can be reached till hundred meters in passive but 10- 30 m in active sources and this depend on the kind of used sources and field site. The greater investigation depth is required for many geometrical problems and passive MASW method is providing as this advantage by using low frequencies 1- 30 Hz and long wavelength (Park, Miller, & Ivanov, 2004).

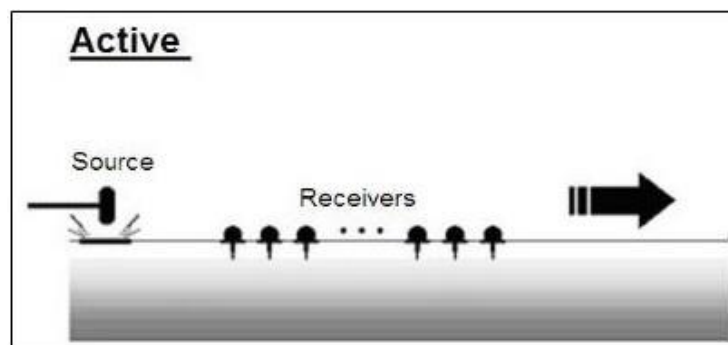
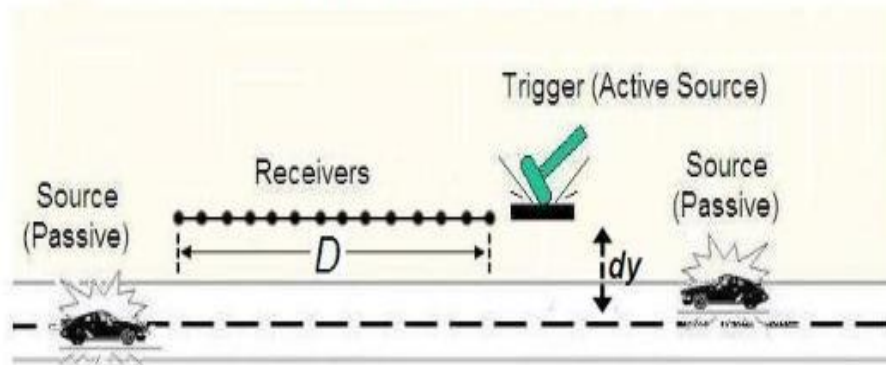


Figure 4.21 The active source of MASW Survey (Park, Miller, & Ivanov, 2004)

In passive MASW method we are using more than 24 geophones to get more resolution in data processing and need less manpower than active method. Passive sources can be divided to two types; passive remote and passive roadside (Baglari & Dey, 2017). In passive roadside the receivers are set as linear array to generate surface wave depending on cultural noise especially traffic sources and obtain 2D VS profile (Biswa & Dey, 2014). The other type is employed by setting the receivers as circular, cross and triangular arrays which need wide space in the study site for recording surface wave s then obtaining 1D shear wave velocity (Figure 4.22). 2D arrays are commonly more frequency used in passive survies than 1D array (Linear arrays). However, sometimes 1D arrays become prefered in some small space areas (Baglari & Dey, 2017).

## Passive Roadside MASW



## Passive (Remote)

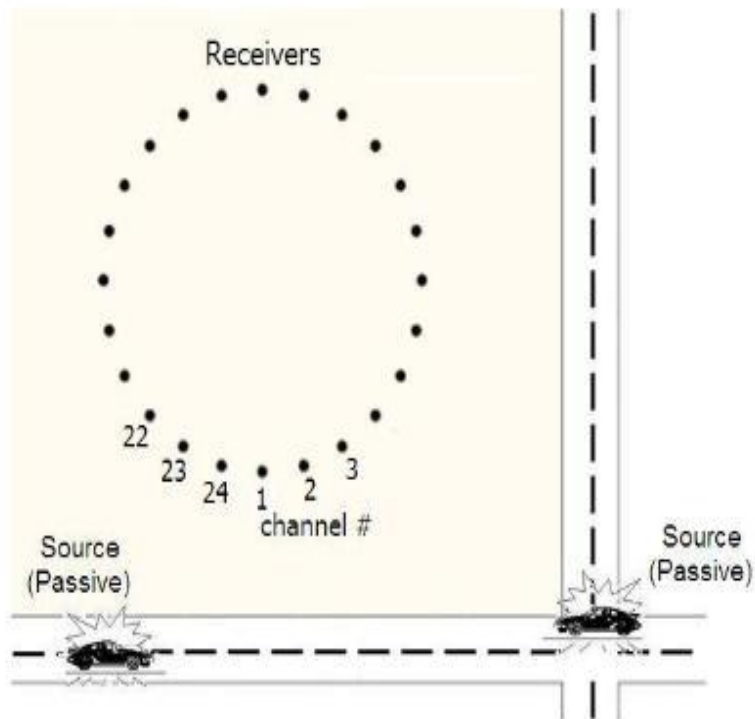


Figure 4.22 Schematic of passive remote and roadside MASW field survey (Biswa & Dey, 2014)

**CHAPTER FIVE**  
**CASE STUDY**  
**HARMANDALI WASTE DISPOSAL SITE, İZMİR TURKEY**

**5.1 Study area**

The Harmandalı waste disposal site is located in north of İzmir gulf – north east of Çiğli district between 38.32-38.33 longitude and 27.05-27.10 North latitude (Figure 5.1). It is placed on the slopes of Çakalhasan ridge which is in between two branches of Tokluağıl River. It is far from the İzmir city center (appr. 30 km) and has an area of approximately 900 000 m<sup>2</sup>. The dominant climate in the area is the Mediterranean climate which characterized by warm and rainy weather in winter and with hot weather and dry in summer. Since 1992, domestic, industrial, medical and demolition waste has been stored. At an approximate rate of 4000 tons/day, 12×10<sup>4</sup>tons /month and 1.5 million ton /year have been brought into this landfill site. Totally amount of the solid waste in 2010 was 1,100,000 ton. In 2015, daily disposal in Harmandalı landfill was received about 3400 tons/day. As a result, there are approximately 1.5 million tons extra waste loads in 1.2 km<sup>2</sup> area. A new disposal waste site is planning in İzmir city center, Harmandalı waste site is planned to continue working till 2020 (DEU, 2016).

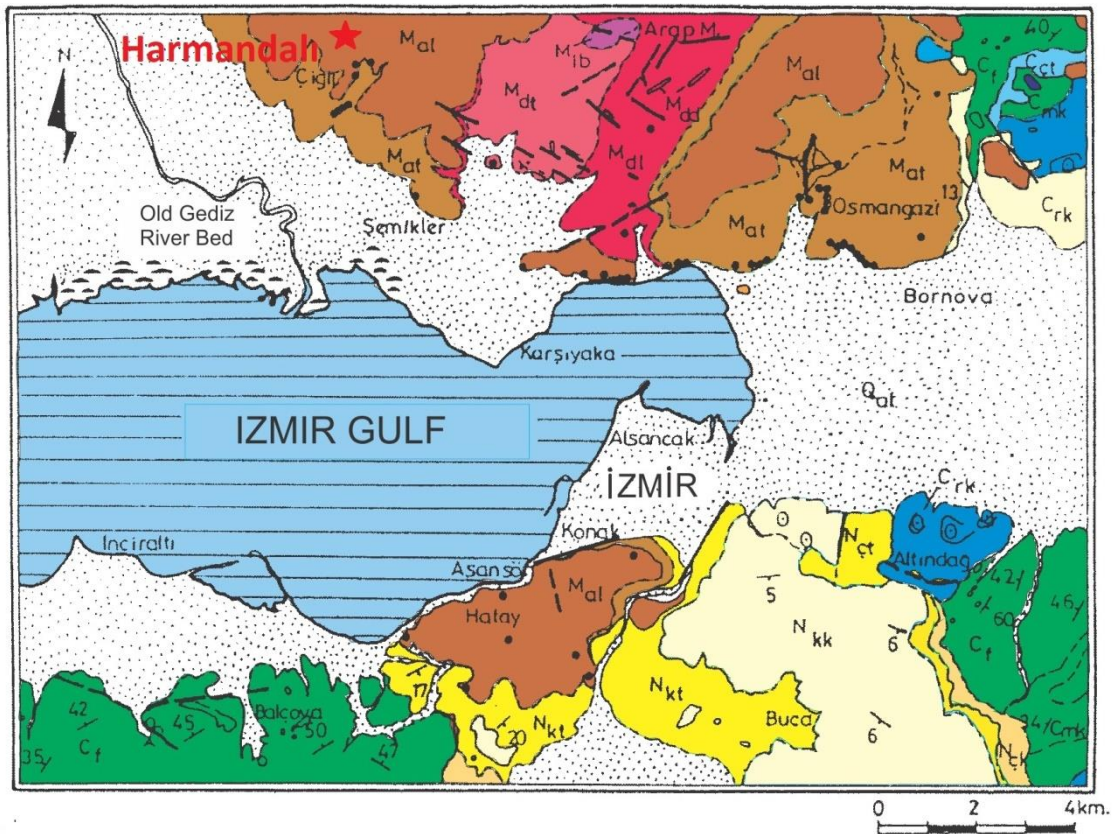


Figure 5.1 Harmandalı Location Map (Koca, 1995)

## 5.2 Propose of Study

Providing image for the subsurface is a good technique by using ERT method which enable us to determine the lithology of the area and water content which are essential causes of landslide occurrence. Besides, velocity determination of the rock is a good indicator of the material strength in landslide body. The main objectives of this study are to determine the affected area, structure, geometry of the landslide body and determination of groundwater table effecting on the landslide by using geological and geotechnical observations and geophysical investigations.

## 5.3 Method

Two surveys of resistivity tomography (ERT) using Wenner - Schlumberger configuration (Figure 5.2) and 7 surveys of multichannel analysis of surface wave (MASW) were carried out in the field (Figure 5.3). 2D resistivity model were

produced in order to determine the distributions of the resistivity in landslide area. Also, shear wave velocity profiles were produced for velocity zones and ranges achievements. Obtained results were compared with previous geological studies.



Figure 5.2 Electrical resistivity tomography surveys in Harmandalı waste disposal site (Google Earth, 2018)



Figure 5.3 Multichannel analyses of surface wave surveys in Harmandalı waste disposal site (Google Earth, 2018)

#### **5.4 Previous Studies and History of the Landslide in the Study Area**

Harmandalı waste disposal site were planned by İzmir Metropolitan Municipality and International Karst Water Resources Application and Research Center (Hacettepe University) (UKAM, 1990) to be a landfill for domestic and industrial wastes which have been received from Izmir metropolitan. On August 1990, many researches had been started about the readiness of the site and its conditions to make sure that chosen area is suitable for landfilling. The 1/5000 scaled geological map had been prepared. Some in situ experiments were applied such as Standard Penetration Test (SPT) which aims to estimate the penetration resistance (N-value) and water pressure test (Lugeon) for estimating hydraulic conductivity and permeability by measuring the volume of water under specific pressure. Also, laboratory tests had been performed such as soil moisture content test and density and unit weight of the soil test. The geological studies of geotechnical properties, boreholes studies, laboratory and data analysis had been finished on December 1990. The results showed that the clay classification in the slope wash is hard - so hard and the sand particles were coherent.

According to the Rock Quality Designation (RQD)% classification, the quality of the flysch was poor (25 - 50), sandstone and andesite quality was fair (50 -75).

According to the boreholes data and in situ tests results, the upper part of the pyroclastic rocks was impermeable and sandstone zone was more permeability than the pyroclastic rocks, however, it was classified as impermeable zone.

In 2016, Dokuz Eylul university- Geological Engineering Dept. started a research project about the landslide mechanism in Harmandalı waste disposal site and the effects of the landslide event which hit the area in February, 2013 on administration buildings and a truck scale in this area taking to the account all the previous studies, observations and researches which had been done in the site. During the landslide researches and investigations, two of landslide were occurred in the Harmandalı waste disposal site the first one on Mart, 2016 and the other landslide had been

happened after five months. In D.E.U project, slope angle and height of the slope measurements had been done.

By using 1/5000 and 1/2000 geological map of the Harmandalı waste disposal site, SE-NW geological section (Figure 5.4) was prepared for estimation of slope stability of the study area and determining the relation between the formation, sliding model, fault zones and the thickness of the waste in the landslide area. Also, the height of the slope was determined. Before 2013, three boreholes had been carried out in the site.

Totally number of the boreholes which were opened in the area between 2013 – 2016 was 27 with depth ranging between (16.5 - 41 m). In D.E.U project, 2016 nine of boreholes were opened with greatest depth for SK-8 65 m. Four boreholes (SK-1, SK-2, SK-3 and SK-8) had been done in landslide direction SE-NW for lateral deformations determination. By using the boreholes data, the slip and slide area and groundwater table had been determined. Pressuremeter tests had been done for determining the zones with low strength along the borehole profile and the depth of the failure surface.

On July, 2013 Multi-channel of surface wave method (MASW) had been carried out in Harmandalı area. 16 of MASW profiles were lined up in West- East directions. The length of each profiles were ranging between 15 – 16 m. 4.5 Hz vertical geophone with 24 channel were used in the field with space 2.5 m between the geophones. Data analyses were made using SeisImager software. The initial model for Vs was involved on 15 numbers of layers and 30 m depth. The iteration number was 10 times. The results of this master research showed that the S-velocity decreases in the west of Harmandalı area and increases in east direction according to the geological formation in the site. S- Velocity was 50-200 m/s for Alluvium and increase until 300 – 700 in the east direction.

In 2016, nine of electrical resistivity tomography profiles were papered out in the Harmandalı site (DEU,2016). The length of these profiles was ranging between 112 - 300 m. The directions of ERT- 1, ERT- 2 and ERT- 3 were NE SW which is



perpendicular to landslide direction and the directions of ERT – 6, ERT – 8 and ERT – 9 were NW SE which is parallel to landslide directions.

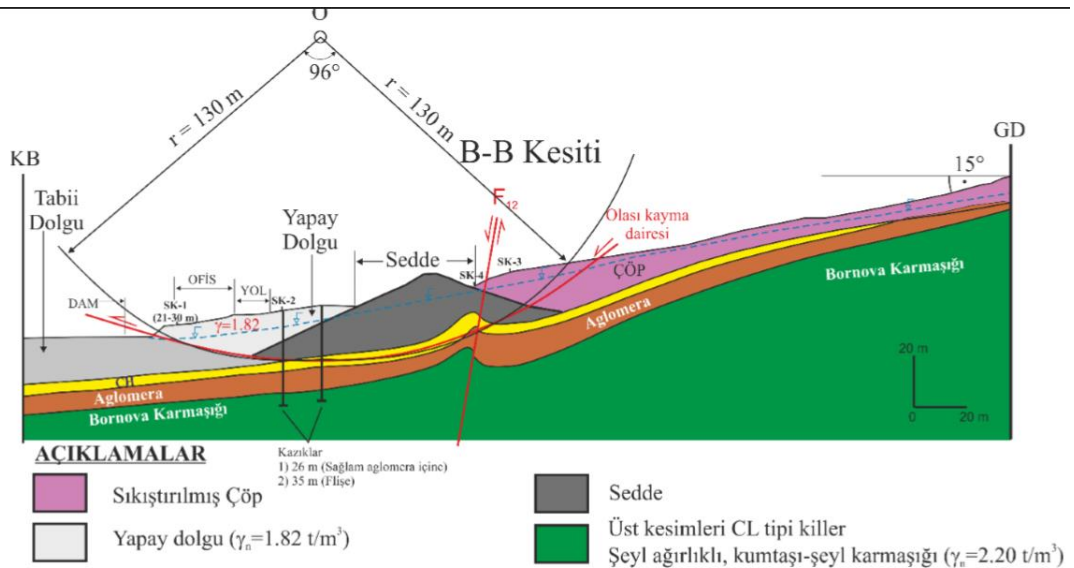
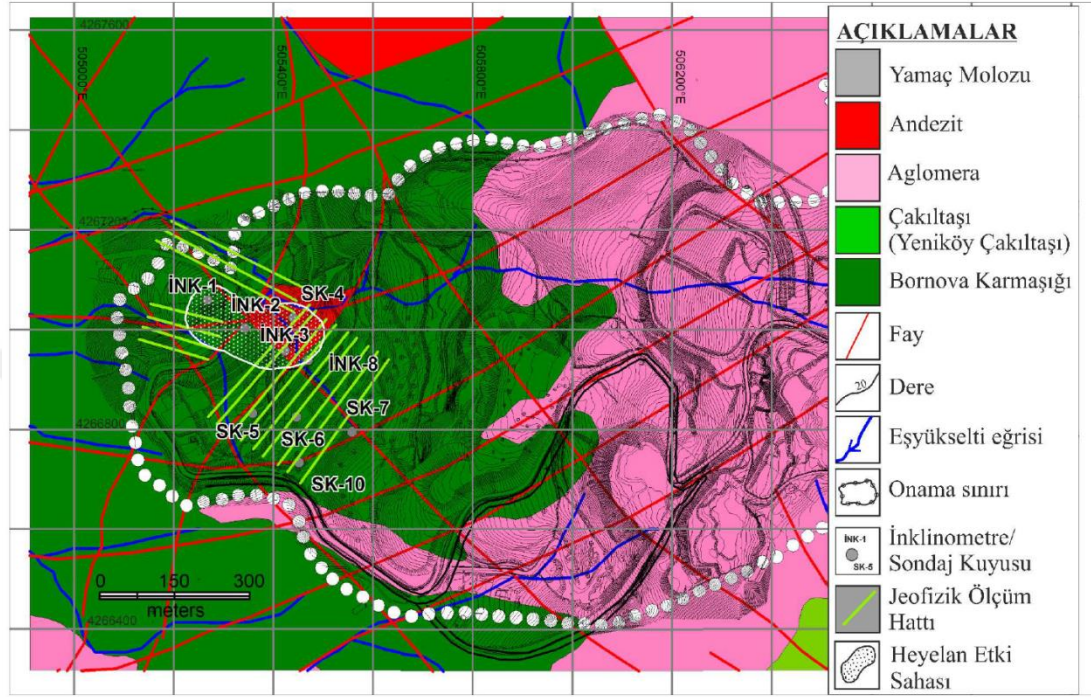


Figure 5.4 Geological section for landslide body in SE- NW direction (DEU, 2016)

## 5.4 Geological Settings

The geological settings of western Anatolia from east to the west are consists of three zones; Menderes massif, Izmir-Ankara and the Karaburun zones. İzmir Bay in the Aegean Sea is located in Izmir - Ankara zone which also called as Bornova flysch zone. Robert Brinkmann was the first who defined the Izmir - Ankara zone (1966, 1972 and 1976). The dimensions of this zone are 50 to 90 km wide and ~230 km long between Izmir and Balıkesir. The stratigraphic columns of the bornova flysch zone which overlies Menderes massif zone involved on the lower Triassic to upper Cretaceous in the lower part and deformed Lower Paleocene on the upper part of the column. The lithology in Harmandalı waste disposal site – study area from bottom to the top consists of three different formations (Figure 5.7). The basement rock is Bornova flysch and Neogen age lake sedimentary rocks (gravelstone, sandstone, marl and limestone) unconformably overlies the Bornova flysch formation. Sometimes claystone or mudstone could be found between sandstone and marl units. Then pyroclastic formation (tuff - agglomerate- dacitic and andesitic lava) unconformably overlies Bornova flysch formation and Neogen age lake sedimentary rocks. Alluvium and slope wash unconformably overlies all existing rock formations.

The geological units of Harmandalı waste disposal site from bottom to the top (From the oldest to youngest ages).

### 5.4.1 Bornova Flysch Formation

Bornova flysch formation is the basement of study area. Upper Cretaceous-Paleocene of deeper marine sediments is seen in this unit. Matrix of sandstone and shale can be recognized which is younger than the rocks itself. Sandstones have thin or moderate thickness of bedding planes and dip to northwestern. Also, it consists of different size of Mesozoic limestone blocks. Shale with gray, yellowish brown and greenish gray colors is the dominant lithology in Bornova flysch formation Harmandalı waste disposal site and that affect the weak rocks which founded in the site and lead to fractured structure. The clay had been exposed to the decomposition and weathering because of the weather condition and water and transformed to lean

clay (CL) which defined as clay of low to medium plasticity. This kind of clay is characterized by impermeability, water storage and absorption. The impermeability changes water content of clay and that increase the probability of failure occurrence in the site .The sandstone strength is higher than clay. The limestone had been observed in the north of the hill and the shale is injected into the cracks of limestone (Koca, 1990 and D.E.U, 2016).



Figure 5.6 Bornova flysch formation in the Harmandalı waste disposal site (Personal archive, 2018)

#### ***5.4.2 Yamanlar volcanic rocks***

Neogene volcanic rocks can be seen in this Yamanlar geological unit. Upper Miocene-Pliocene pyroclastic rocks are observed. The volcanics which are involved in the Yamanlar unit are; Andesite, tuff and agglomerate.

The agglomerates colors which observed in the field are grey and bordo. Agglomerate are considered as weak rocks that can be exposed to the weathering processes and easily transformed to the high plasticity clay (CH).

The observed Andesite in the site study is fractured and weathered Andesite with brown and purple colors (Koca, 1990) (D.E.U, 2016) (Kıncal, Akgün, & Koca, 2009).



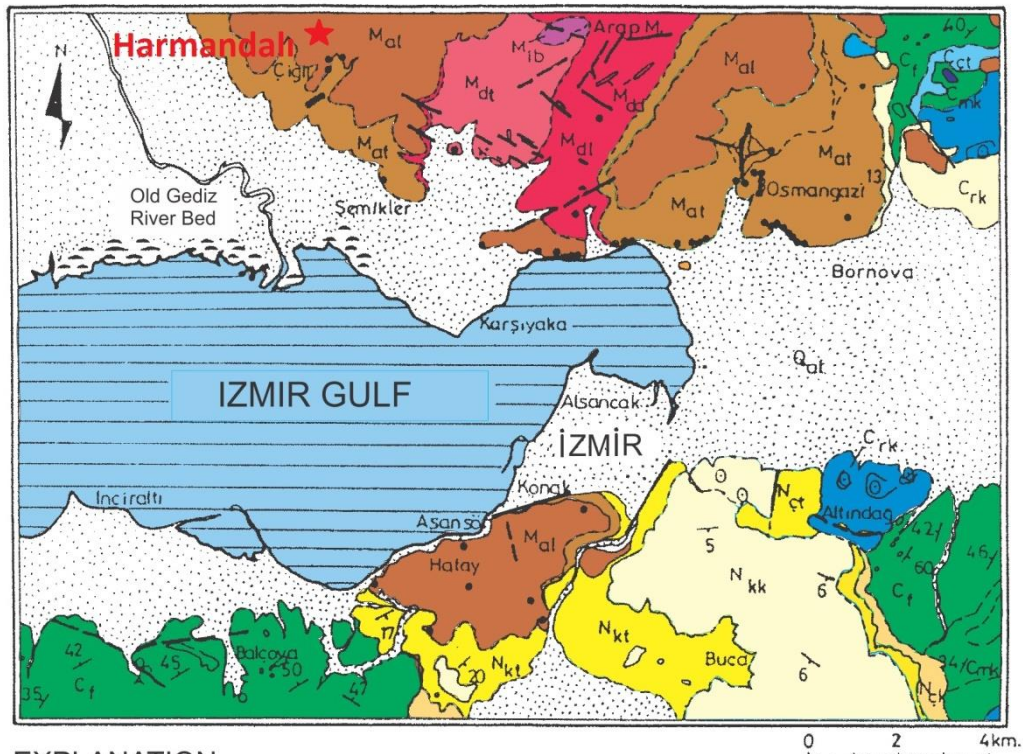
Figure 5.6 The volcanic rocks in the Harmandalı waste disposal site (Personal archive, 2018)

### **5.6.3 Slopewash**

Slopewash is the unit which covered the study area and made up of pyroclastic rocks – Andesite, clay, sand and gravels (Koca, 1990, D.E.U, 2016, Kınca, Akgün, & Koca, 2009).

### **5.6.4 Faults**

Three types of faults had been noticed in the study site: NEE – SWW faults and NW SE faults. Third type direction is NE - SW cut the previous faults and younger than them. First and second types of faults are noticed in the north of Izmir gulf. The third type had been noticed in İzmir-Menemen highway. Almost, 14 numbers of faults were noticed in Harmandali waste disposal site and their locations had been determined on 1/5000 and 1/2000 maps and the most important fault in Harmandali waste disposal site is F1- fault with SW direction. F1 - fault stretches along the sinikle dere and cut the track scale (Koca, 1990) (D.E.U, 2016) (Kınca, Akgün, & Koca, 2009).



EXPLANATION

N E O G E N E	M I O C E N E	Quaternary	Q <sub>al</sub>	Slope wash/Alluvium	<b>BORNOVA MELANGE</b> Upper Cretaceous Paleocene Upper Cretaceous Upper Triassic C <sub>f</sub> C <sub>mk</sub> C <sub>ct</sub> C <sub>rk</sub> T <sub>mdk</sub> Limestone Olistolithes Micritic Limestone Conglomerate <b>Allochton</b> Rudist shale fragments bearing limestone Megalodonti bearing limestone
			M <sub>ib</sub>	Intrusion breccia	
			M <sub>ds</sub>	Silicified dasitic dykes	
			M <sub>ds</sub>	Felsic intrusion	
			M <sub>al</sub>	Andesite lava	
			M <sub>at</sub>	Agglomerate	
			M <sub>dl</sub>	Dasitic lava	
			M <sub>dt</sub>	Dasitic tuff	
			N <sub>kk</sub>	Limestone	
			N <sub>kt</sub>	Marl/Clayey limestone	
	N <sub>ck</sub>	Conglomerate			
	T <sub>ckl</sub>	Basal conglomerate			
		●	Quarries in volcanic rocks		
		○	Quarries in limestone units		
		○	Quarries in Bornova Melange		
		↘ 34	Strike and dip of beds		
		↘	Main normal fault		
		⌌	Swamp areas		

Figure 5.7 Geological map of Harmandalı waste disposal site (Koca, 1995)

## 5.5 Solid Waste and Landslide in Harmandalı Landfill

The amount of solid waste has a daily increase in İzmir metropolitan city center because of high rate of population almost 3 Million people. The main goal of landfilling method is to dispose and bury the waste in order to decrease its effects on the environment and health. It is difficult to found a new landfill now in İzmir, Therefore, Harmandalı landfill will serve till 2020. Table 5.1 illustrates the types and amounts of solid waste in Harmandalı landfill

Table 5.1 Types and amount of solid waste in Harmandalı waste disposal site (Ürüt, 2003)

Year	Domestic	Industrial	Demolition	Medical	Biological Sludge	Ind. Sludge	Total
1994	285,000	25,431	3,519	1,118			315,068
1995	374,202	30,159	1,289	1,052			406,702
1996	466,945	41,210	1,911	1,027	4,345		515,438
1997	445,710	28,153	5,471	1,473	2,845	19.137	502,789
1998	575,239	26.735	6,543	1,953	4,251	16.364	631,085
1999	654,755	24,315	6,254	2,390	3,362	11.246	702,322
2000	644,801	25,156	11,329	3,180	1,795	16.676	702,937
2001	689.867	20.561	8.852	3.931	1.313	18.068	742,592
2002	618.145	19.004	6.492	896	235	15.187	659,959

According to D.E.U project, the occurred landslide in Harmandali waste disposal site had been classified into two types. Landslide in the waste (example: Landslide which happened on March, 2016) and landslide in the rocks and soil which is deeper than the first type (Example: the landslide which happened on February, 2013 and affected the administration buildings and a truck scale.

The types of failure occurrences in the Harmandali waste disposal site are presented as below (DEU, 2016):

1- Rotational slide (toe slide) and rotational slide (slope slide) (landslide on March 2016).

2- Rotational slide (Base failure) (landslide on February 2013).

The failures which had happened in the Harmandali deeply affected the area and the buildings also results in fractures and cracks (Figure 5.8, 5.9, 5.10 and 5.11).



Figure 5.8 The adminastiration buildings in The Harmandalı waste disposal site and landslide direction NW-SE (Personal archive, 2018)



Figure 5.9 The tension cracks and fractures which occurred resulting from landslide event in the Harmandalı waste disposal site (Personal archive, 2018)



Figure 5.10 The tension cracks and fractures which occurred resulting from landslide event in the Harmandalı waste disposal site (Personal archive, 2018)





Figure 5.11 The landslide effects in the Harmandalı waste disposal site (Personal archive, 2018)

## 5.6 Results belonging to boreholes data and in-situ tests

The results of boreholes data which were opened by Dokuz Eylul University between 2013 – 2016 in Harmandalı waste disposal site for 30 meters depth were used to compare it with the geophysical investigation. Seven profiles were compared with SK-2, SK-3, SK-8. Two of resistivity tomography profiles were compared with SK-7, SK-8, SK-9, SK-3 ,SK-4, SK-2.

According to the in-situ and laboratory studies which were performed by D.E.U project 2016, the stability properties of the site were determined (Table 5.2). The results showed that the groundwater tables are located at great depth and that mean there is no effect of groundwater on the sliding in the study area.

To determine the sliding surface of the landslide, inclinometer test apparatus were conducted in SK-1 (INK-1), SK-2 (INK-2), SK-3 (INK-3) and SK-8 (INK-8) boreholes (DEU, 2016). The inclinometer profile belonging to the SK-2 (INK-2) borehole is given in Figure 5.12.

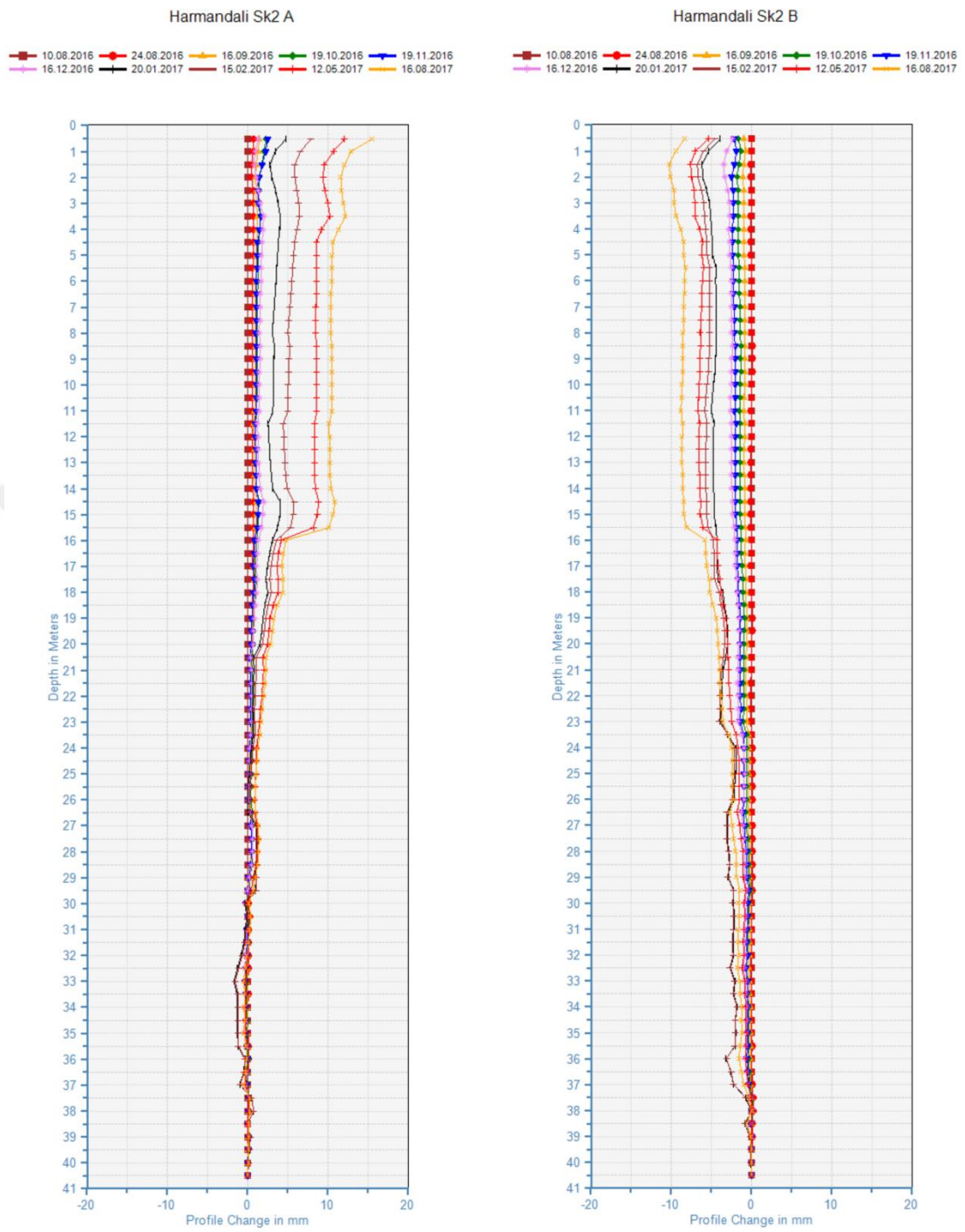


Figure 5.12 The inclinometer profile belonging to the SK-2 (INK-2) borehole

Table 5.2 The depth of the GWT level for different boreholes in the site and weathering grade determination of the rock units underlay the solid waste (D.E.U, 2016)

	Groundwater table (m)	Degree of weathering	Solid Waste
SK-1	5.30	Highly – completely weathered	
SK-2	6.80	Highly – completely weathered	
SK-3	5.3	9-36 m Agglomerate and tuff slightly weathered. Sandstone and clay completely weathered	
SK-4	1.40	Sandstone and clay Highly – completely weathered	Solid Waste 15-20m
SK-5	2	Highly – completely weathered	
SK-6	16.8	Agglomerate and tuff High weathered.	Solid Waste 0.00 -17.60m
SK-7	39	Agglomerate and tuff High weathered.	Solid Waste 5.00- 42.50 m
SK-8	17.80	Agglomerate and tuff High weathered. Sandstone and clay Highly – completely weathered	Solid Waste 1.00-20.60m
SK-9	20	Sandstone and clay Highly – completely	

## 5.8 Buffer Zone and Requirements for MSW Placing

There are some criteria which should be taken to the account in the Harmandalı waste disposal site in order to avoid the slope failures

- Leachate collection systems

In Harmandalı waste disposal site, there is a lot of leachate (Figure 5.12) have been produced due to solid waste decomposition processes and leads to decrease in the soil strength and stability. The borehole (Sk-4) which had been carried out near Sarlak stream (Figure 5.13) clearly illustrates the decrease in strength (D.E.U, 2016).



Figure 5.13 The leachate which occurred because of the waste in the Harmandalı waste disposal site (Personal archive, 2018)



Figure 5.14 Sarlak stream leachate in the Harmandalı waste disposal site (Personal archive, 2018)

- Gas collection system

There is a presence for methane gas in Harmandalı waste disposal site and the amount of this gas is depending on the waste properties, organic content and climate of site (D.E.U., 2016). Thus, the risk of methane gas explosion is increased in Harmandalı waste disposal site, and there are fears of Umraniye-Hekimbaşı accident can be also happened in the İzmir - Harmandalı landfill.

## CHAPTER SIX

### FIELD WORKS AND INSTRUMENTS

#### 6.1 ERT Field Measurements

##### *6.1.1 Data Acquisition and Processing*

Two dimensional (2D) Electrical Resistivity Tomography surveys were carried out along two profiles with NW-SE and NE-SW directions in the Harmandali (Çiğli/Izmir) waste disposal site. One of the surveys was parallel and other was perpendicular to the landslide direction (Figure 6.1 and Figure 6.2).



Figure 6.1 ERT-1 profile with NW-SE direction parallel to landslide body (Personal archive, 2018)

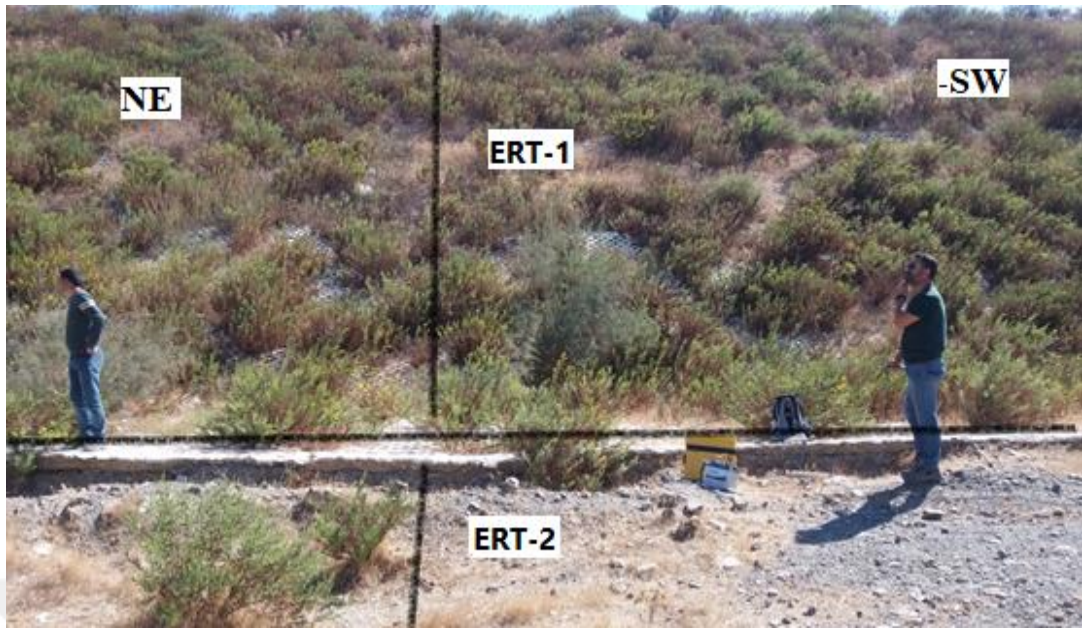


Figure 6.2 ERT-2 profile with NE-SW direction perpendicular to landslide body (Personal archive, 2018)

RVA-1 resistivity instrument (made in Turkey) had been used in ERT surveys (Figure 6.3 and Figure 6.4). RVA1 receiver characterized by 0.01 mV of sensitivity. This instrument has an accuracy of  $\pm 500$  mV. The power supply consists of two batteries (9 V).



Figure 6.3 RVA-1 resistivity instrument for ERT investigation (Personal archive, 2018)

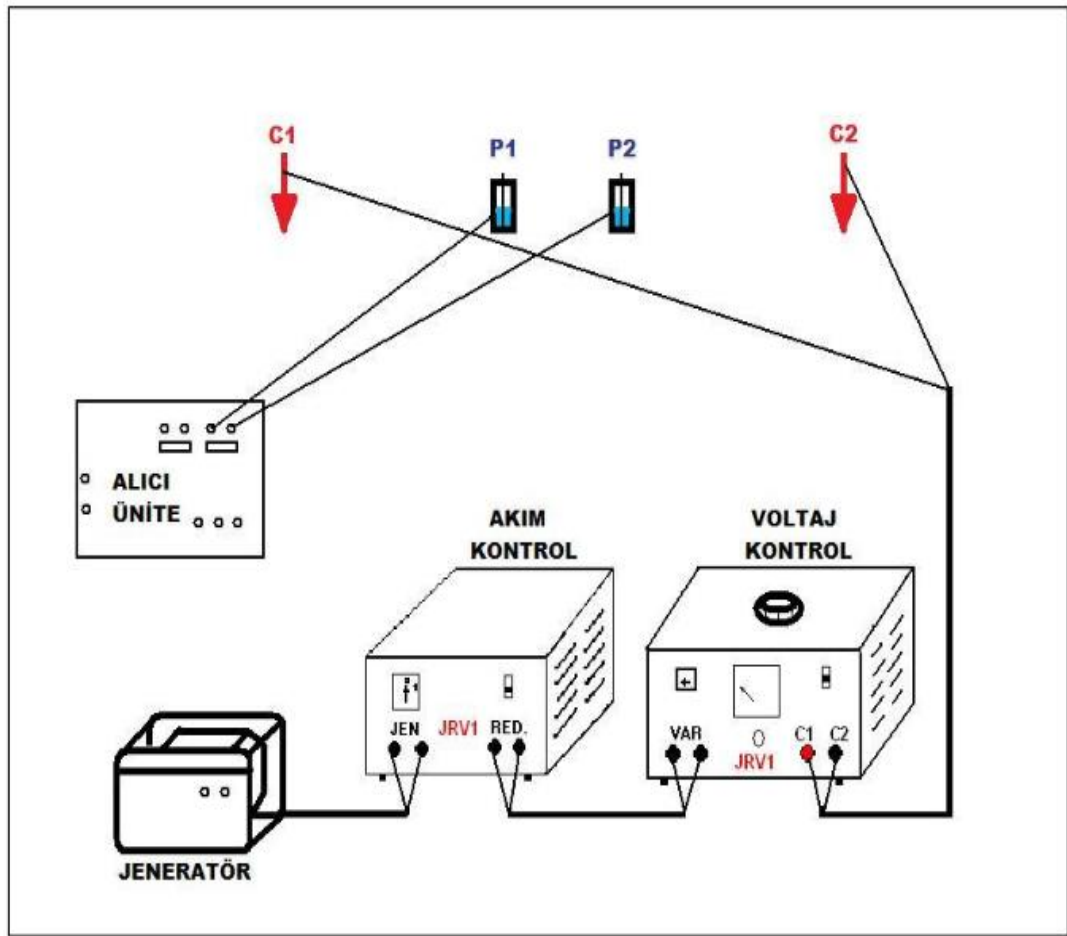
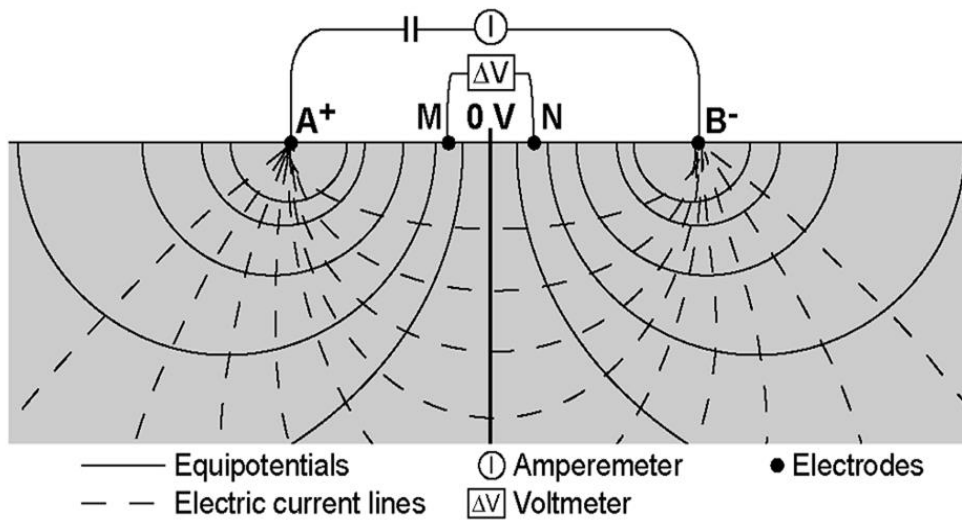


Figure 6.4 The technique of RVA-1 resistivity equipment working (Jeotermal Kaynak ve Mineralli Suarama Raporu)

Wenner- Schlumberger configuration (Figure 6.5) was performed in the test site. 55 electrodes had been used in the area with 5 m electrode spacing. The length of each profile was 275 m and the penetration was about 50 m depth. 2D resistivity models were produced through inversion of electrical tomography data. Low and moderate resistivity were observed in the study area (2-400  $\Omega\text{m}$ ) which was related to the water content, high plasticity of clay and waste in the area.





Wenner-Schlumberger

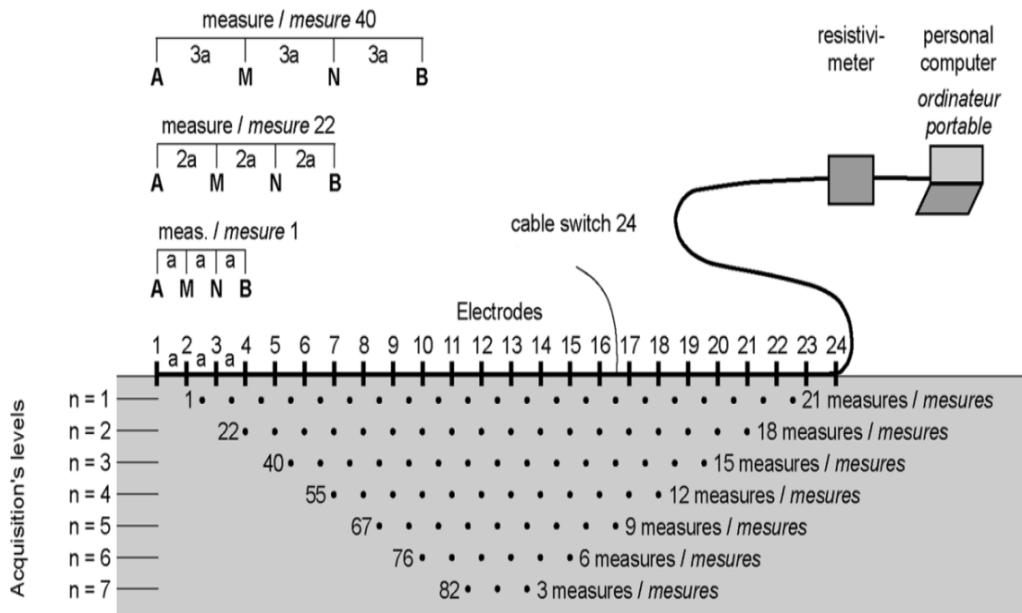
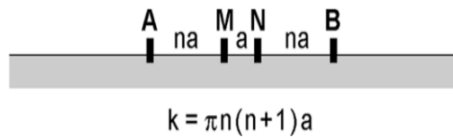


Figure 6.5 Wenner- Schlumberger configuration for 2D ERT investigation surveys (Laigne, 2014)

### 6.1.2 DC2DinvRes Software

DC2DinvRes software is suggested for ERT data analyses by applying smoothness constrained Gauss-Newton minimization

$$J_k^T J_k \rho_k^{GN} = -J_{ki}^T r_k \quad (6.1)$$

DC2DinvRes considered as inversion software and largely used for producing 2D model of the earth from the obtained ERT field data .

This software is used for different inversion and regularization schemes and provide us fast finite difference forward operator (Günther, 2007).

## 6.2 MASW Field Measurements

### 6.2.1 Data Acquisition and Processing

Multi-channel of surface wave method (MASW) measurements using Geometrics-SmartSeis ST device were carried out in Harmandali waste disposal site in order to obtain Rayleigh wave dispersion curves then estimating shear wave velocity profiles to 30 m depth of the area.

Passive source were used in this investigation which provide us (0 - 15 Hz) of frequency domain and great penetration depth. Seven profiles of MASW tomography survey in Harmandalı waste disposal site were performed on two directions. S1, S2, S3 profiles were positioned parallel to landslide direction (NW-SE) and S4, S5, S6, S7 profiles were positioned perpendicular to landslide direction NE-SW. 24 geophones (4.5 Hz vertical geophones) lined up in straight line with 5 m geophone interval. The length of each survey was about 120 m. Inversion methods (least square techniques) was applied to analyze collected data and derive shear wave velocity by inverting the dispersive phase velocity of surface waves using SeisImager software and generating two of S- wave profiles with depth using surfer software and make comparison between the results and the boreholes in study area (Figure 6.6) .

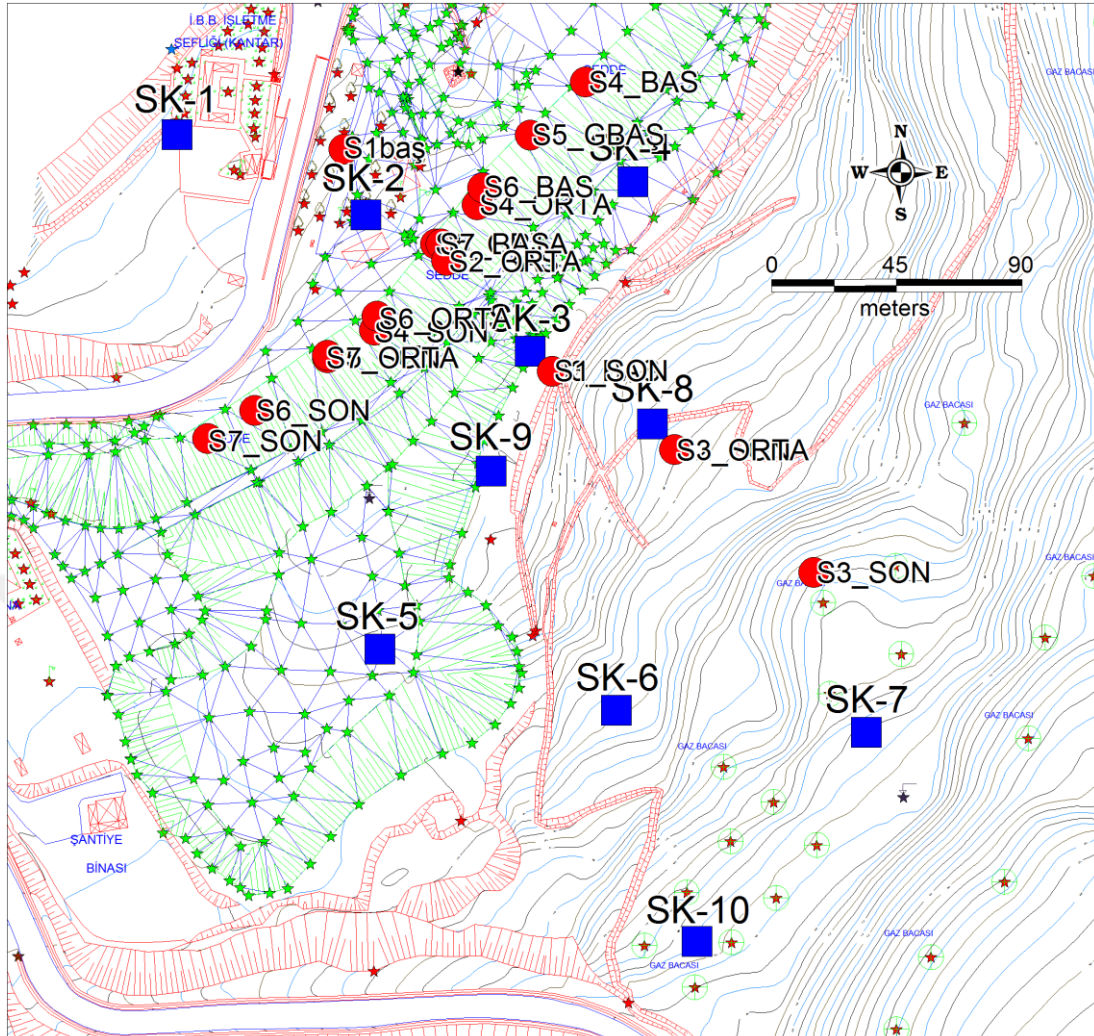


Figure 6.6 Location map of boreholes and MASW profiles in Harmandali waste disposal site

## 6.2.2 Fieldwork and Instruments (Hardware and software)

### 6.2.2.1 Smartseis ST Device

MASW method investigations were carried out in Harmandali waste disposal site by using Smartseis ST Device by Geometrics. SmartSeis seismograph is seismic exploration system which is characterized by a high performance exploration and high resolution. This device has many applications such as: bedrock determination, groundwater level determination, landside potential, stratigraphic mapping, mineral and gold exploration, hazardous waste migration and shear wave velocity profiles.

Smartseis ST is provided by PC, daylight-visible color LCD, keypad, printer and acquisition filters and noise reduction technology.

There are two of software which are commonly used with this device; SIPQC refraction analysis software which runs on seismograph and SeisImager/2D Lite refraction modeling and analysis software (time-term least squares, delay-time, and tomographic inversion methods) from OYO; runs separately. Normally numbers of Channels in this device are 12 or 24. In this study, we used cables with 24 channels (Figure 6.7).



Figure 6.7 SMARTSEIS ST Device (Geometrics,2018)

#### 6.2.2.2 4.5 Hz Geophones

4.5 Hz vertical geophone is an instrument used in seismic explorations (Figure 6.8). It is recommended especially in MASW data collecting field works for lower frequency investigations. The geophone is converting the ground motion into mechanical signal. Then, this signal will be employed to amplifiers and filtering. In this study geophones were set in linear arrays using cables with 24 channels.



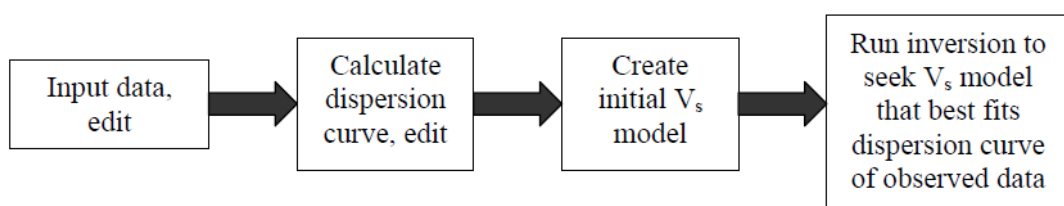
Figure 6.8 4.5 Hz vertical geophone (Geometrics, 2018)

### 6.2.2.3 SeisImager Software

This software is used to analyze MASW active and passive sources data by using three modulus Pickwin<sup>TM</sup>, Plotrefa<sup>TM</sup> and WaveEq<sup>TM</sup>. Then display it in windows and make us able to make corrections and save it then obtain a one-dimensional (1D) profile of shear-wave ( $V_s$ ) velocity with depth.

The processing in SeisImager software is following these procedures:

The processing flows as follows:



Field data were input into the SeisImager software for each survey in one time and make some corrections were made in the frequency domain following by return to time domain for processing. The phase velocity plot will appear after setting the geometry and the dispersion peaks will be determined. Then, by continuing the procedures of processing the dispersion curve will display. The next step is inversion after setting the initial model of  $V_s$  with depth and iteration number finally obtaining  $V_s$  model that best fits dispersion curve of observed data.

The field works faced many obstacles such as truck scale noise effect so while recording on seismograph we took care for this point and trying to start the seismic records when the ratio of noise was low as much as possible. Furthermore SeisImager software is characterized by low cut and high cut for the frequencies we could use it for removing high frequencies from the traces. The following Table 6.1 is illustrating used passive source acquisition parameters:

Table 6.1 Passive Source Acquisition Parameters

Parameter	Setting
Array configuration	Linear shape
Array size	120 m
Geophone type	4.5 Hz geophones
Seismic energy source	Ambient cultural activities
Total number of geophone	24 geophones
Geophone interval	5 m
Record length time	30 second for each record

### 6.3 MASW Data Analysis

MASW data which obtained from the field investigation were analyzed by SeisImager software using inversion method for obtaining 1D S- wave velocity models. Surface waves were recorded using the seismograph in the field. Then the changes in phase velocity for Rayleigh surface waves were estimated and the dispersion curves (phase velocity versus frequency) were obtained.

Shear wave velocity profiles derived by inverting the dispersive phase velocity and obtaining 1D S- wave profiles for 30 m depth by using non-linear least square method (Seisimager, 2005). Then make interpretation for identifying the stiffness and engineering parameters in the study area.

## 6.4 Inversion Analyses

The main aim of inversion analysis is finding S- wave velocity model whose observed dispersion curve match the calculated one as well as possible (Seisimager, 2005). Collected waves in the field can be transformed to dispersive curve using wave field transformation. By applying Fourier transform which converts data from x-t to f-k domain, this procedure enable us to calculate phase velocity using the following equation:

$$V = f / k \quad (6.2)$$

Where,

k: wave number

f: the frequency

V: phase velocity.

Then, the dispersion image will be obtained and the dispersion curve will be displayed as (phase velocity versus frequency) (Figure 6.9 and 6.10).

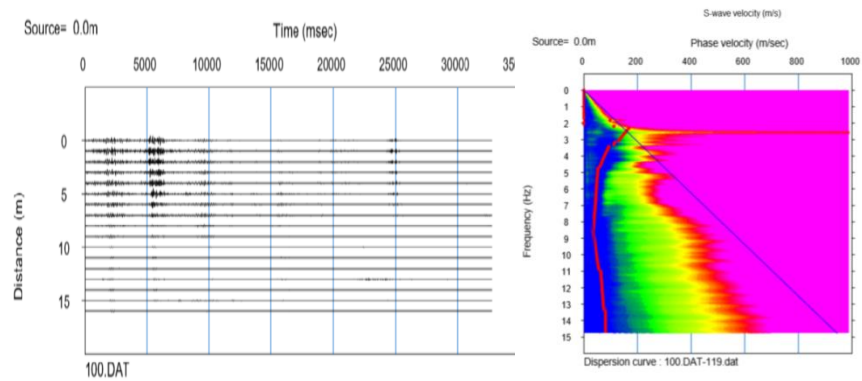


Figure 6.9 The dispersion image for the first survey of MASW

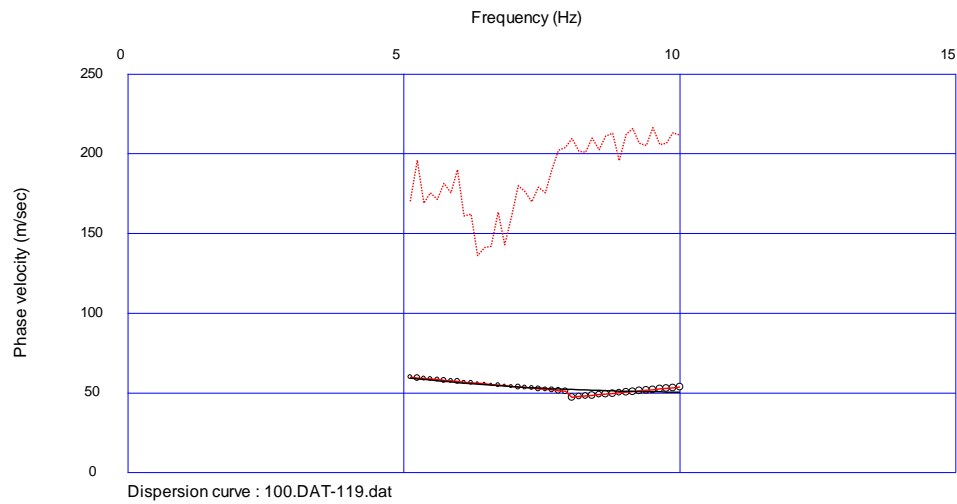


Figure 6.10 The dispersion curve for the first survey of MASW

Estimating of S-wave velocity model (model parameter) was estimated by applying inversion techniques to dispersion curve. For analyzing dispersion curve just surface wave will be consider as fundamental mode and all the other waves is noise (Seisimager, 2005). The first step for using inversion method is choosing the initial model of the earth by determining many parameters such as S- Velocity ( $v_s$ ), density ( $\rho$ ), the depth ( $Z$ ) and the number of layers (Table 6.2). Then the number of iteration was determined (15 times) and the inversion processing stopped when it reached the maximum number of iteration (Table 6.2). The inversion for dispersion curves result in vertical S- wave velocity with depth in the site (Figure 6.11, 6.12, 6.13, 6.14, 6.15, 6.16, 6.17 and 6.18).

Table 6.2 Initial model for  $V_s$

Maximum expected velocity in the site	1000 m/s
Minimum Frequency default	5 Hz
Maximum Frequency default	15 Hz
Number of layers	15
Iteration number	15



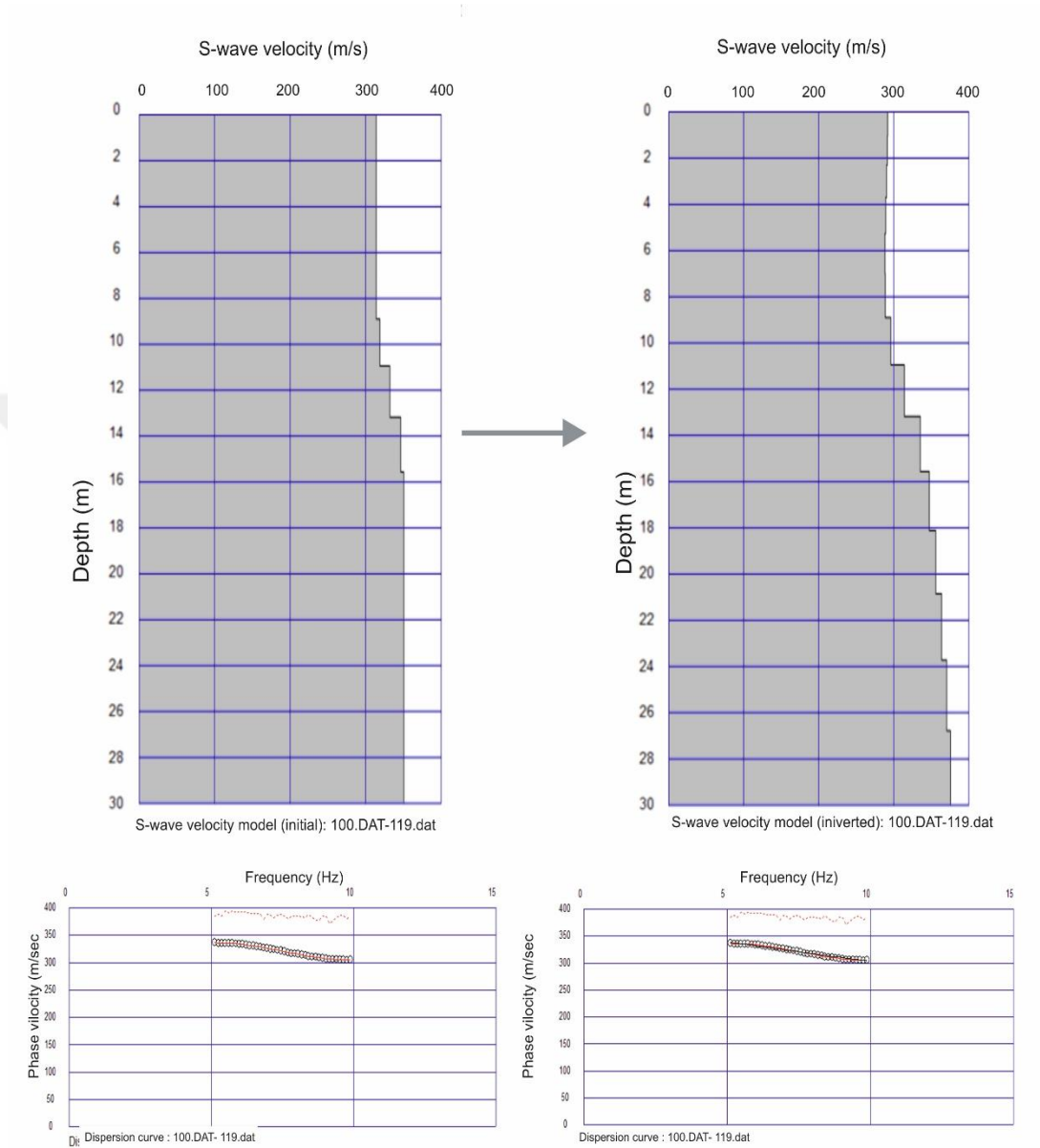


Figure 6.11 Illustration of the 1D S- wave velocity model for the first MASW survey before (on the left) and after iteration (on the right) and dispersion curve

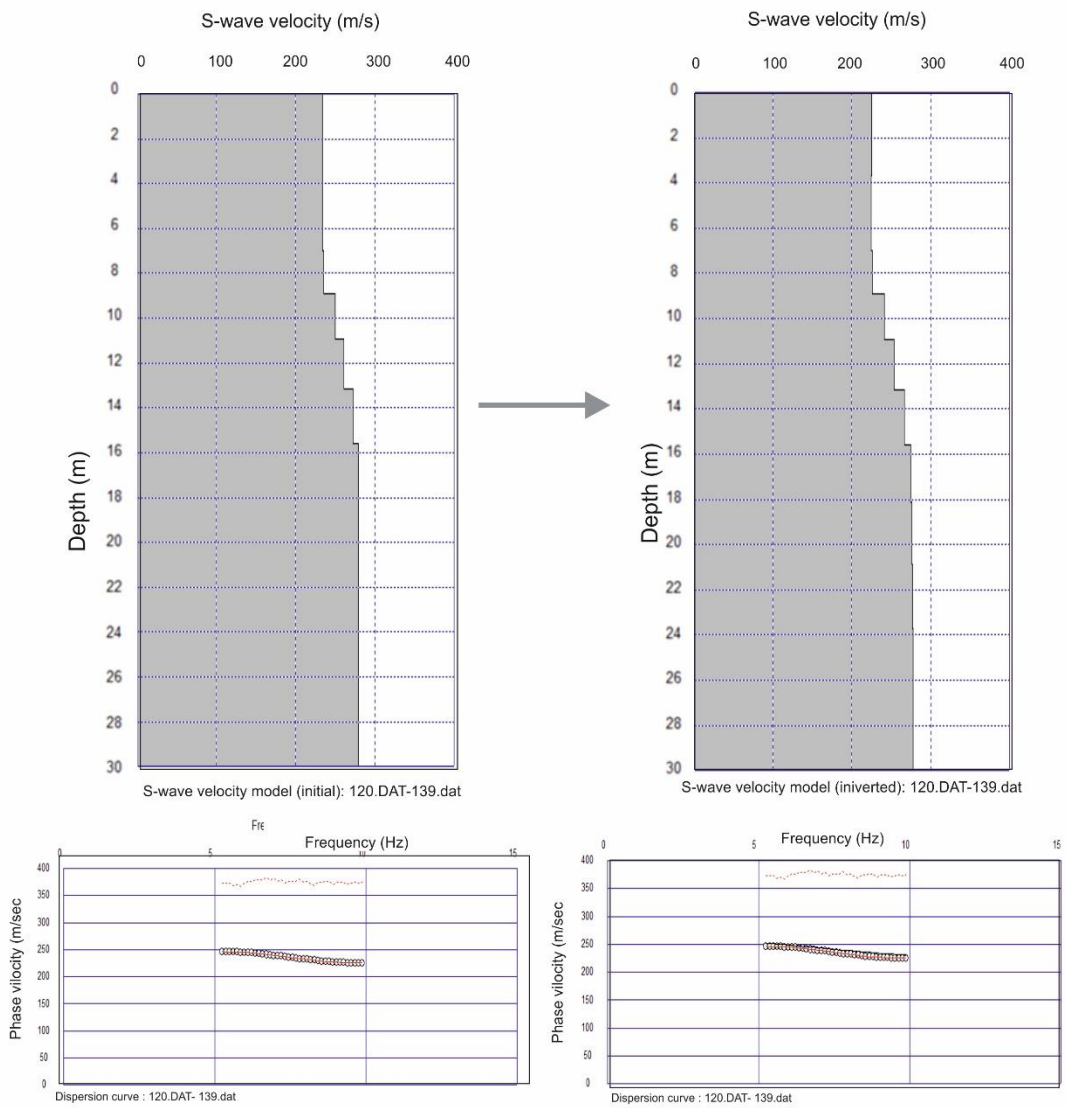


Figure 6.12 Illustration of the 1D S- wave velocity model for the second MASW survey before (on the left) and after iteration (on the right) and dispersion curve

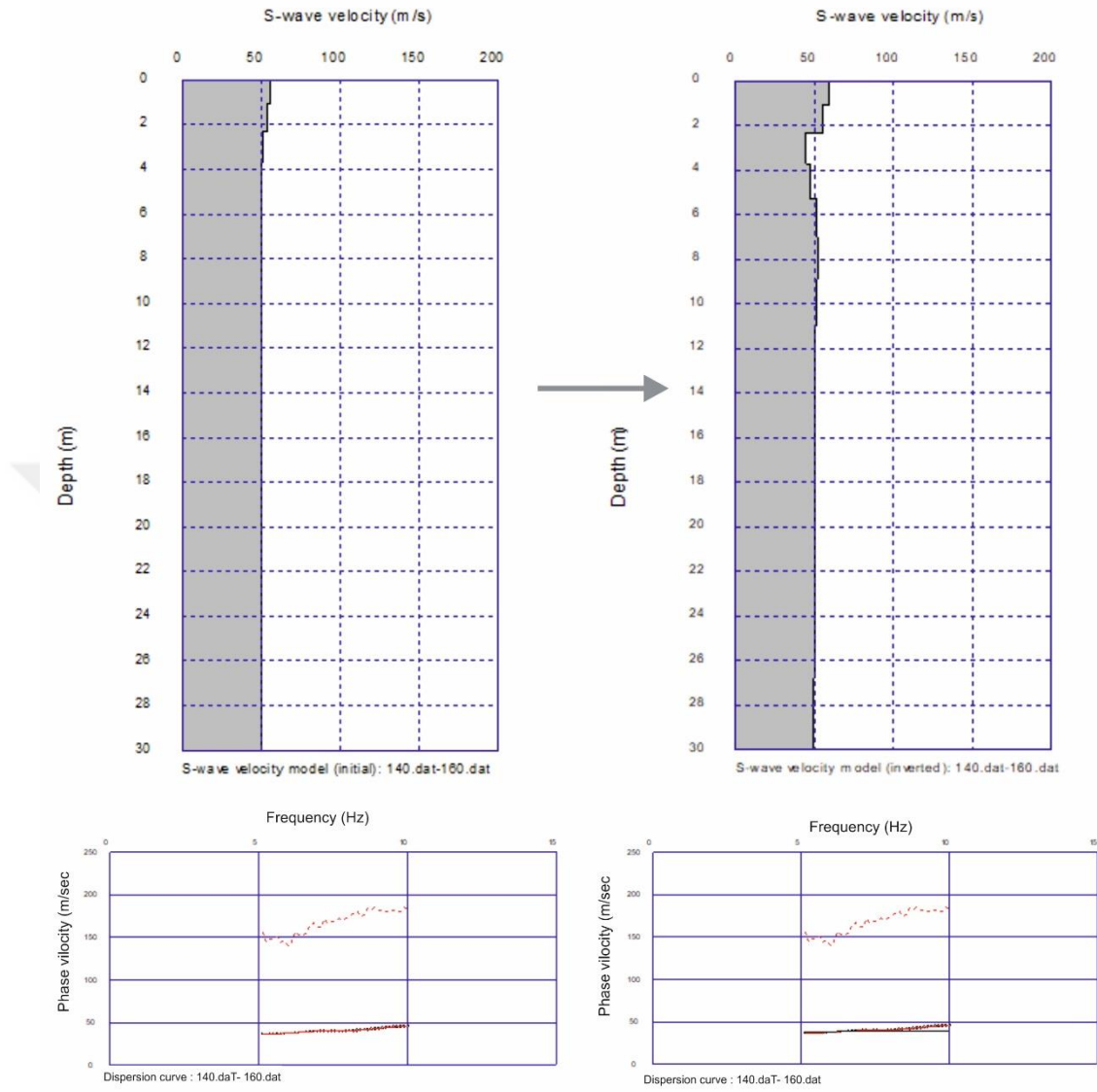


Figure 6.13 Illustration of the 1D S- wave velocity model for the third MASW survey before (on the left) and after iteration (on the right) and dispersion curve

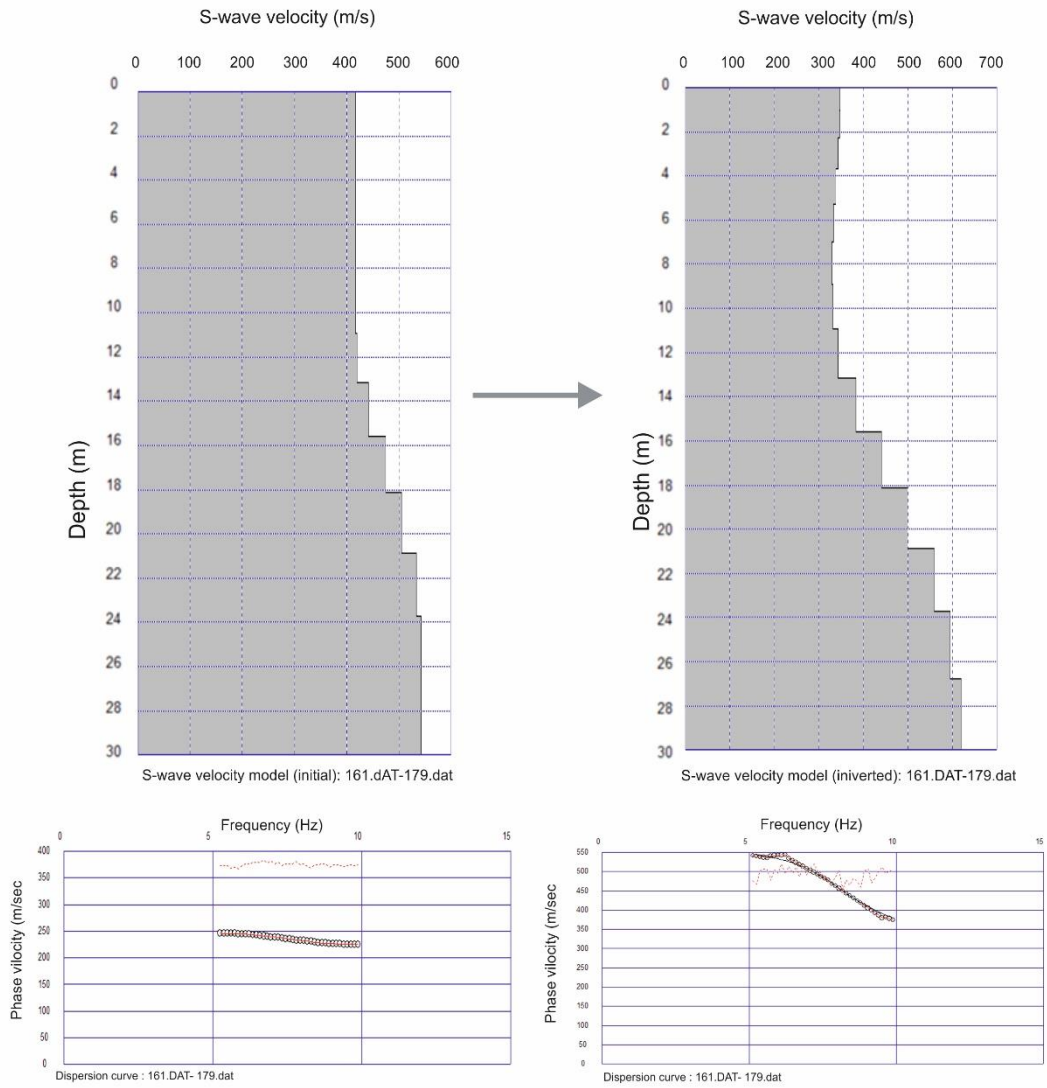


Figure 6.14 Illustration of the 1D S- wave velocity model for the fourth MASW survey before (on the left) and after iteration (on the right) and dispersion curve

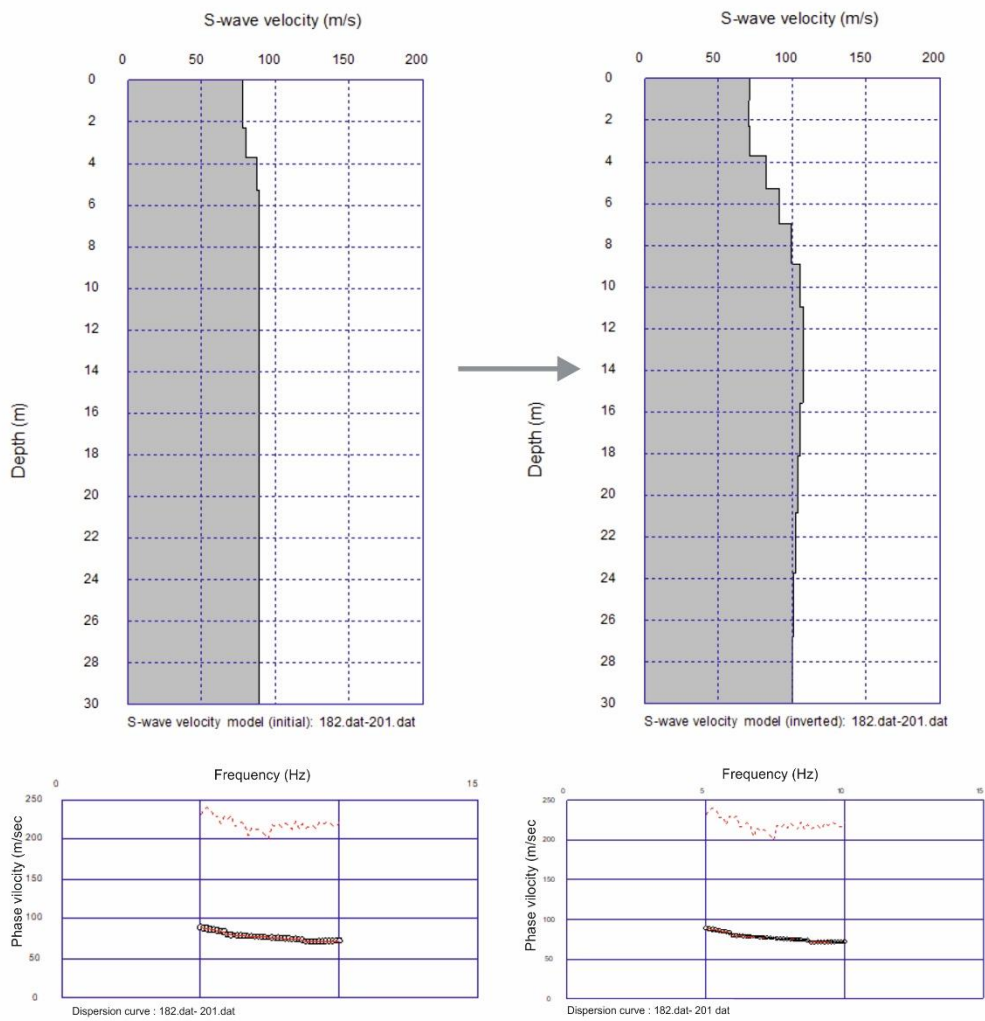


Figure 6.15 Illustration of the 1D S- wave velocity model for the fourth MASW survey before (on the left) and after iteration (on the right) and dispersion curve

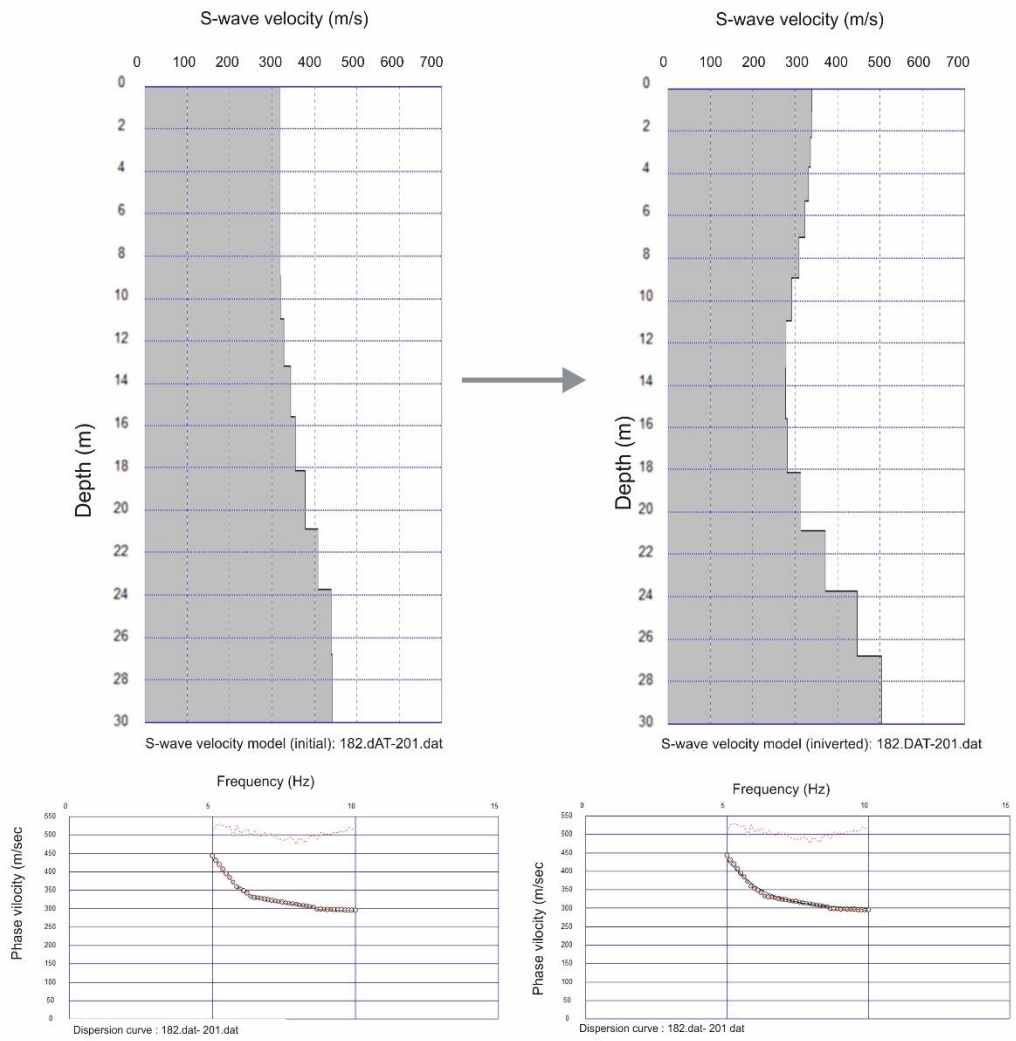


Figure 6.16 Illustration of the 1D S- wave velocity model for the fifth MASW survey before (on the left) and after iteration (on the right) and dispersion curve

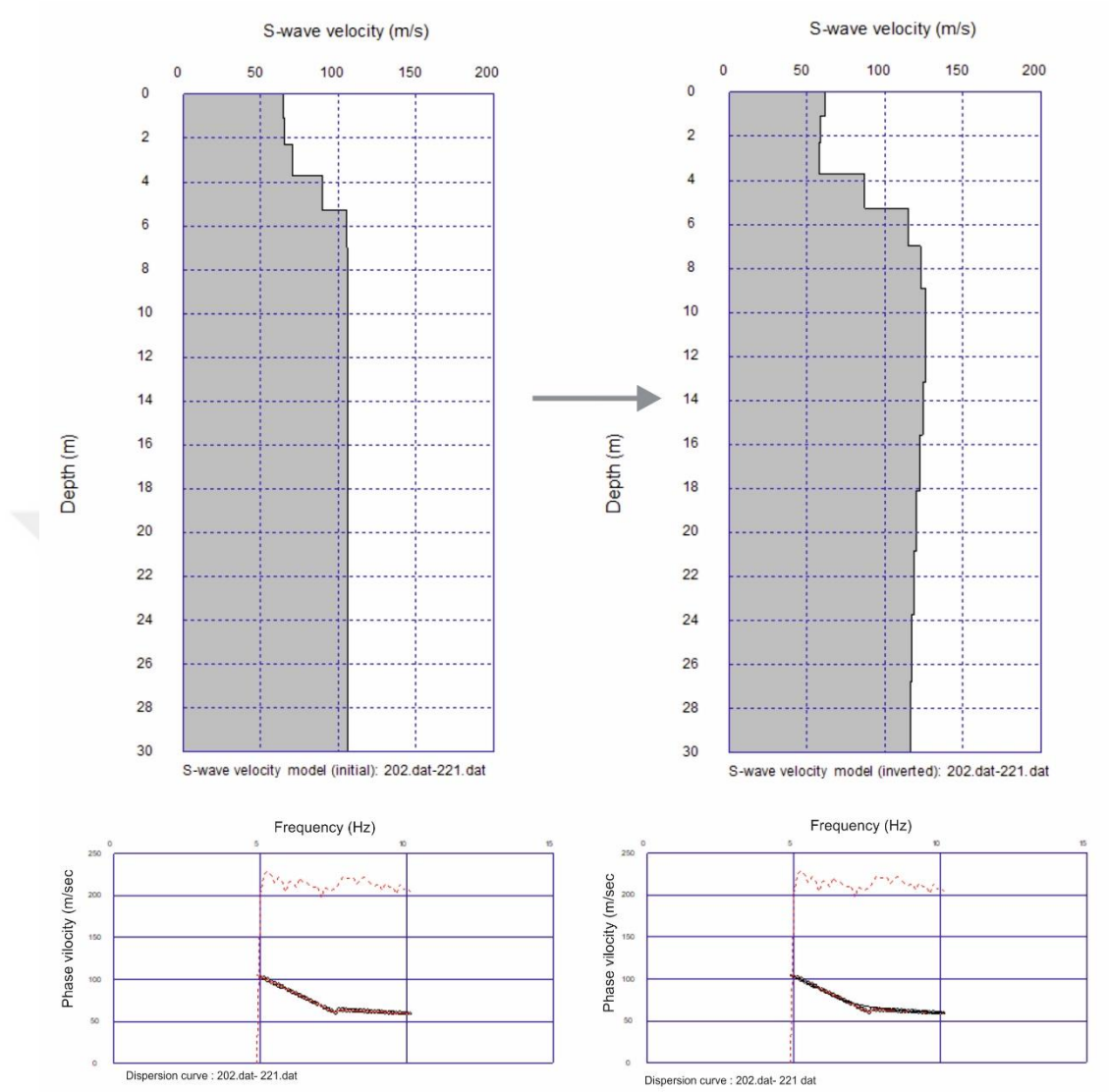


Figure 6.17 Illustration of the 1D S- wave velocity model for the sixth MASW survey before (on the left) and after iteration (on the right) and dispersion curve

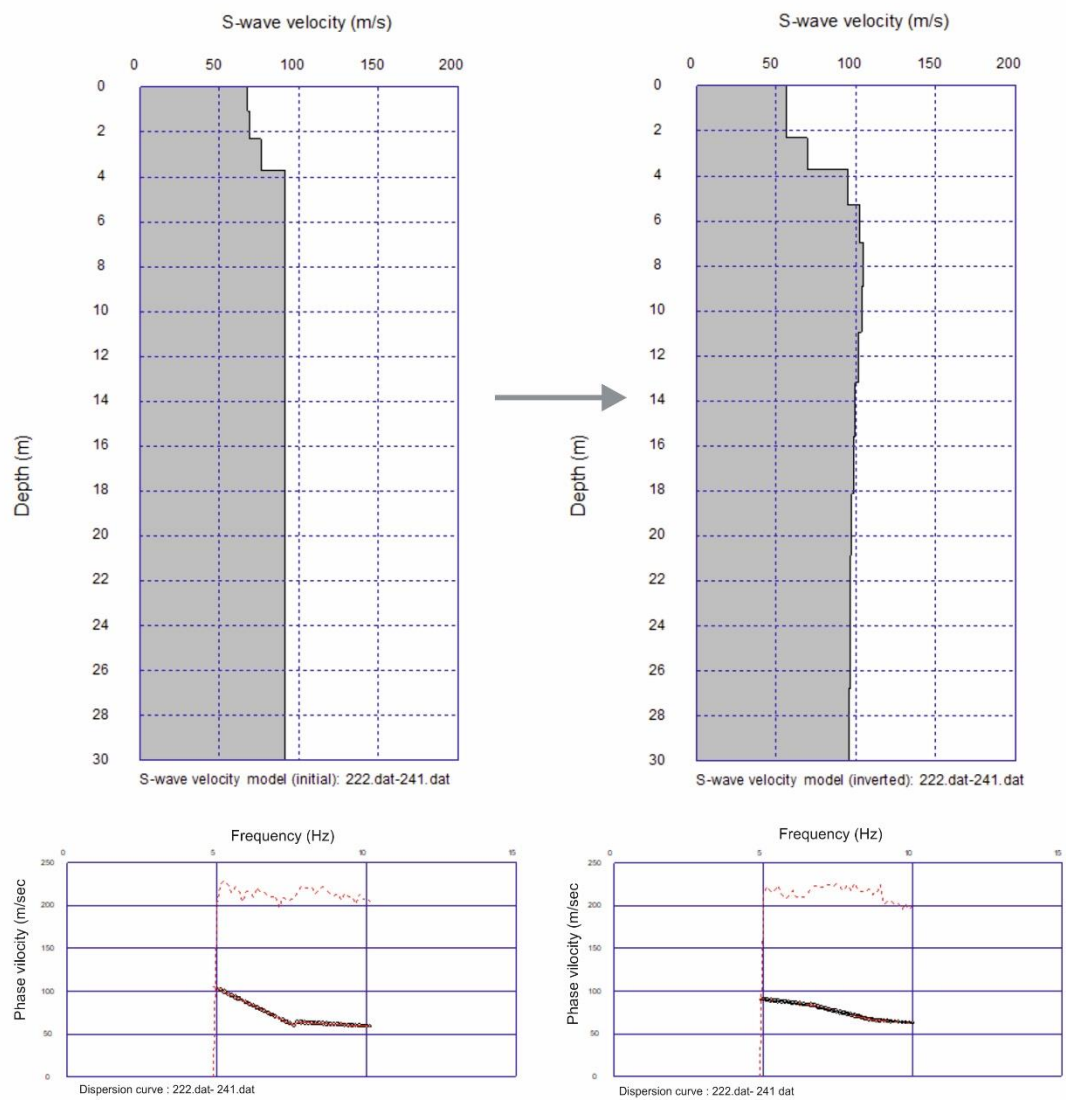


Figure 6.18 Illustration of the 1D S- wave velocity model for the seventh MASW survey before (on the left) and after iteration (on the right) and dispersion curve



## CHAPTER SEVEN

### RESULTS AND DISCUSSION

#### 7.1 ERT Investigations Results and Discussion

In Harmandalı waste disposal site, two resistivity models have been obtained using DC2DInvRes software. Finite difference technique was applied for ERT field data taking into the account the topography of the study site. Two resistivity models were obtained after applying inversion Gauss- Newton method. The penetration depth for the two ERT profiles was about 50 m. Table 7.1 and Table 7.2 showed the field and inversion parameters for the surveys of electrical resistivity tomography method.

Table 7.1 ERT-1 field and inversion Parameters

ERT-1 inversion Parameters	
Profile Direction	NW-SE (parallel to landslide)
Electrode Spacing	5 m
Electrodes Arrangement	Wenner- Schlumberger
Total Number of Datum Points	775
Minimum Electrode Location	0.0 m
Maximum Electrode Location	275
Total Number of Electrodes	55
Iteration Number	7
RMS Error	1.96 %

ERT-1 profile with NW-SE direction highlights low apparent resistivity values in the middle section ( $3.62 - 13.7 < 100 \Omega\text{m}$ ). The top section of ERT -1 profile concludes high apparent resistivity values ( $279 - 594 \Omega\text{m}$ ). The RMS error value of ERT-1 profile was 1.96 % after 7 times of iteration number (Figure 7.1).

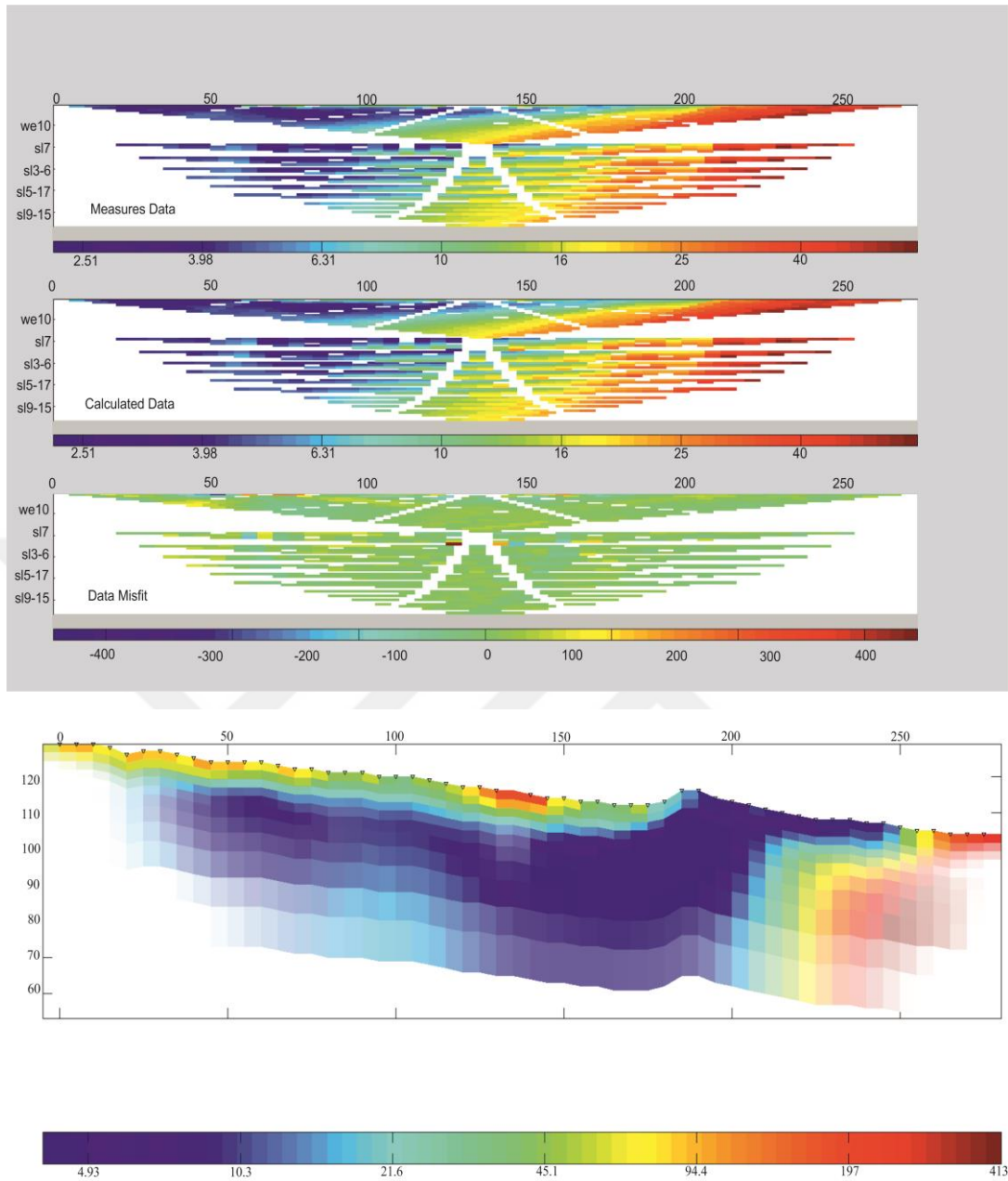


Figure 7.1 ERT-1 NW-SE (a) Measured data. (b) Calculated data. (c) Data misfit (d) Resistivity model with topography

Table 7.2 ERT-2 field and inversion Parameters

ERT-2 inversion Parameters	
Profile Direction	NE-SW( perpendicular to landslide)
Electrode Spacing	5 m
Electrodes Arrangement	Wenner- Schlumberger
Total Number of Datum Points	803
Minimum Electrode Location	0.0 m
Maximum Electrode Location	275
Total Number of Electrodes	55
Iteration Number	5
RMS Error	2.9 %

ERT-2 profile with NE-SW direction also shows low apparent resistivity values in the middle section ( $2.47 - 7.33 < 100 \Omega\text{m}$ ). The two left and right side section of ERT-2 profile show high values of apparent resistivity ( $>100 \Omega\text{m}$ ). The RMS error value of ERT-1 profile was 2.9 % after 5 times of iteration number (Figure 7.2). Low resistivity values in the landslide body in the two of ERT models indicate to clay material in the area and water content.

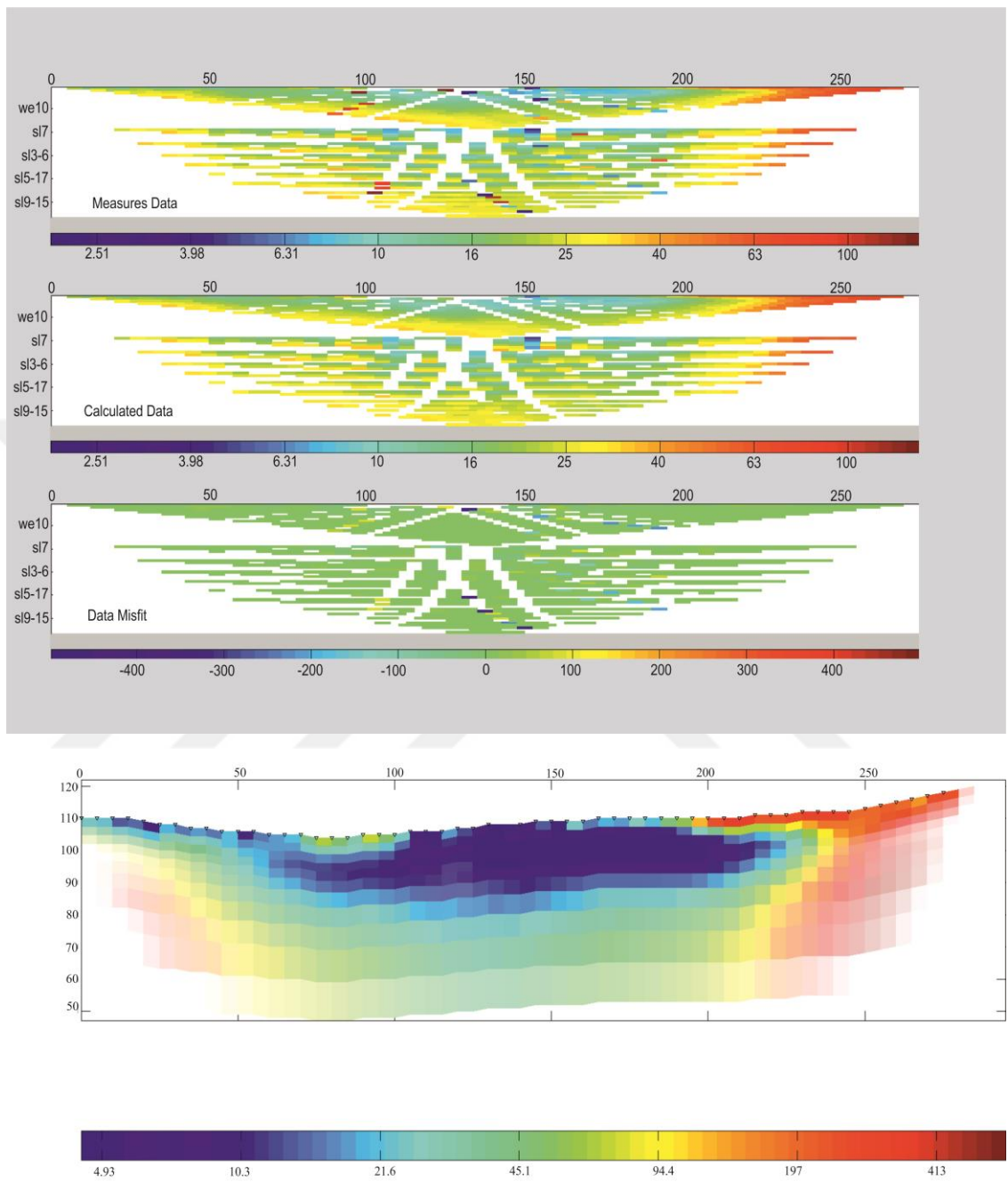


Figure 7.2 ERT-2 NE-SW (a) Measured data. (b) Calculated data. (c) Data misfit (d) Resistivity model with topography

ERT-1 IN SW- NW direction is in the same direction of landslide body. Therefore, this section had been compared with geological section (SW- NW) and boreholes (SK-8, SK-3, and SK-2) in the site. The result of comparison between the ERT method and previous geological studies showed that the potential sliding surface is indicated by low values of resistivity 2 – 10 ohm.m and it is clearly presented in ERT-1 profile (Figure 7.3).

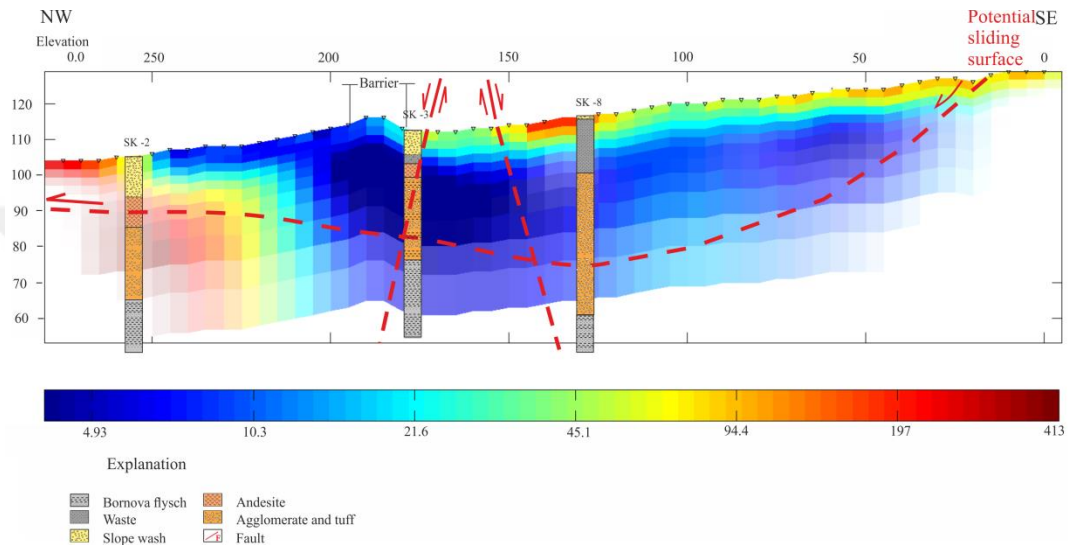


Figure 7.3 Comparison between ERT-1 profile and boreholes in the site

## 7.2 MASW Investigation Results and Discussion

The root-mean-square error (RMSE) values were determined for seven surveys and will be shown in the tables with the inversion results. The inversion results had been saved in to (\*.txt) files (Table 7.3, Table 7.4, Table 7.5, Table 7.6, Table 7.7, Table 7.8 and Table 7.9).

1D- S wave profiles had been compared to boreholes (SK-2, SK-3, SK-4, and SK-8). The results showed that the lowest velocity values are indicated in S3, S6, and S7 of MASW survey and comparing with geological studies it was noticed the presence of waste for 20m depth in SK-8 which compared with S3. For MASW survey – 6 and MASW survey -7 (S6, S7) the velocities were ranged between 50 – 180 m/s for S6 and between 50 – 120 m/s for S7. These surveys were compared with SK-3 which

include mixed of slope wash and waste from 9 – 12 m depth and includes Andesite unit with high plasticity clay from 12 – 17 m depth.

Two profiles for S- wave velocity with depth were prepared using Surfer software. S- Wave profiles showed presence of three velocity zones in the study site. The upper zone velocity is between 110 - 170 m/s, the middle zone velocity 200 - 290 m/s and the last zone velocity is ranged between 300 - 380 m/s (Figure 7.11 and 7.12).

Table 7.3 The inversion results of the first survey of MASW

Depth(m)	Vs (m/s)	Vp (m/s)	Den(g/cc)	N
0	291.615	1614.17	1.83176	33.2978
1.07143	291.351	1613.88	1.83176	33.2019
2.30769	290.434	1612.89	1.83176	32.8703
3.70879	289.132	1611.47	1.83176	32.403
5.27473	288.171	1610.43	1.83176	32.0614
7.0055	288.51	1610.8	1.83176	32.1817
8.9011	295.946	1618.97	1.8335	34.8982
10.9615	314.124	1639	1.83813	42.1941
13.1868	335.185	1662.18	1.84304	51.8812
15.5769	347.402	1675.51	1.84445	58.1467
18.1319	355.898	1684.73	1.84445	62.7973
20.8516	363.804	1693.37	1.84445	67.3487
23.7363	370.516	1700.77	1.84445	71.3864
26.7857	375.797	1706.66	1.84445	74.6772
36.4286	376.309	1707.46	1.84445	75.002

Table 7.4 The inversion results of the second survey of MASW

Depth(m)	Vs (m/s)	Vp (m/s)	Den(g/cc)	N
0	215.755	1529.42	1.80378	12.7556
1.07143	215.336	1528.98	1.80378	12.6769
2.30769	214.17	1527.7	1.80378	12.4595
3.70879	212.219	1525.52	1.80378	12.1015
5.27473	209.746	1522.79	1.80378	11.6582
7.0055	208.237	1521.19	1.80421	11.3932
8.9011	221.504	1536.08	1.80926	13.8697
10.9615	235.125	1551.39	1.81328	16.7728
13.1868	253.835	1572.24	1.81737	21.4048
15.5769	272.469	1592.8	1.81955	26.822
18.1319	289.505	1611.38	1.81955	32.5366
20.8516	309.374	1632.92	1.81955	40.1956
23.7363	329.952	1655.18	1.81955	49.3452
26.7857	349.809	1676.64	1.81955	59.4393
36.4286	359.577	1687.18	1.81955	64.888

Table 7.5 The inversion results of the third survey of MASW

Depth(m)	Vs (m/s)	Vp (m/s)	Den(g/cc)	N
0	19.57288	1311.774	1.727833	0.006113
1.071429	28.94897	1322.155	1.729947	0.021261
2.307692	37.30434	1331.271	1.731085	0.047677
3.708791	39.56524	1333.654	1.731085	0.057503
5.274725	39.11414	1333.158	1.731085	0.055441
7.005495	38.0653	1332.032	1.731085	0.050843
8.901099	37.09456	1330.992	1.731085	0.046828
10.96154	36.29542	1330.135	1.731085	0.04369
13.18681	35.65323	1329.447	1.731085	0.041275
15.57692	35.14401	1328.901	1.731085	0.039427
18.13187	34.74754	1328.476	1.731085	0.038028
20.85165	34.44794	1328.155	1.731085	0.036994
23.73626	34.23324	1327.925	1.731085	0.036264
26.78571	34.09486	1327.776	1.731085	0.035799
36.42857	39.56524	1333.654	1.731085	0.057503



Table 7.6 The inversion results of the fourth survey of MASW

Depth(m)	Vs (m/s))	Vp (m/s)	Den(g/cc)	N
0	331.232	1659.42	1.86293	49.9577
1.07143	330.08	1658.16	1.86293	49.4065
2.30769	327.127	1654.88	1.86293	48.0121
3.70879	322.2	1649.39	1.86293	45.7468
5.27473	317.053	1643.56	1.86293	43.4599
7.0055	314.508	1640.49	1.86293	42.3588
8.9011	317.603	1643.6	1.86293	43.7004
10.9615	331.064	1658.15	1.86365	49.8768
13.1868	370.273	1701.17	1.87026	71.2371
15.5769	436.409	1774.11	1.88384	120.228
18.1319	500.022	1844.34	1.89556	185.442
20.8516	560.858	1911.55	1.90637	267.306
23.7363	598.37	1952.98	1.91028	328.514
26.7857	619.417	1976.28	1.91028	366.748
36.4286	619.417	1976.28	1.91028	366.748

Table 7.7 The inversion results of the fifth survey of MASW

Depth(m)	Vs (m/s)	Vp (m/s)	Den(g/cc)	N
0	339.695	1665.9	1.83353	54.1372
1.07143	338.412	1664.58	1.83353	53.4884
2.30769	336.132	1662.24	1.83353	52.3494
3.70879	331.612	1657.47	1.83353	50.1404
5.27473	322.986	1648.2	1.83353	46.1035
7.0055	308.946	1633	1.83353	40.0188
8.9011	291.058	1613.63	1.83388	33.0956
10.9615	278.285	1600.01	1.83664	28.6879
13.1868	277.136	1599.18	1.8422	28.3124
15.5769	281.073	1603.66	1.84603	29.6134
18.1319	313.514	1639.24	1.85407	41.9339
20.8516	370.838	1701.84	1.86432	71.5841
23.7363	446.144	1783.94	1.87518	128.979
26.7857	504.026	1846.4	1.87597	190.213
36.4286	565.556	1913.11	1.87597	274.503

Table 7.8 The inversion results of the sixth survey of MASW

Depth(m)	Vs (m/s)	Vp (m/s)	Den (g/cc)	N
0	61.57716	1358.308	1.742652	0.235229
1.071429	58.30626	1354.869	1.74312	0.197696
2.307692	57.70023	1354.348	1.744907	0.191226
3.708791	86.56395	1385.794	1.751981	0.695929
5.274725	114.497	1416.6	1.75763	1.695785
7.005495	122.8311	1425.962	1.757757	2.121046
8.901099	125.7841	1429.415	1.757757	2.287747
10.96154	125.5799	1429.309	1.757757	2.275938
13.18681	123.9382	1427.546	1.757757	2.18253
15.57692	121.887	1425.291	1.757757	2.06956
18.13187	119.9387	1423.135	1.757757	1.966033
20.85165	118.312	1421.331	1.757757	1.882368
23.73626	117.0854	1419.969	1.757757	1.820918
26.78571	116.2734	1419.067	1.757757	1.781004
36.42857	125.7841	1429.415	1.757757	2.287747

Table 7.9 The inversion results of the seventh survey of MASW

Depth(m)	Vs (m/s)	Vp (m/s)	Den (g/cc)	N
0	56.14165	1352.505	1.744023	0.175256
1.071429	55.95291	1352.32	1.744339	0.173387
2.307692	69.25856	1366.934	1.747045	0.342044
3.708791	94.76926	1394.998	1.752447	0.928583
5.274725	102.1808	1403.154	1.752447	1.180231
7.005495	104.2572	1405.54	1.752447	1.258319
8.901099	103.227	1404.499	1.752447	1.219148
10.96154	101.3283	1402.454	1.752447	1.149158
13.18681	99.57501	1400.532	1.752447	1.08702
15.57692	98.20873	1399.02	1.752447	1.040228
18.13187	97.20156	1397.9	1.752447	1.006633
20.85165	96.40198	1397.009	1.752447	0.980498
23.73626	95.84027	1396.384	1.752447	0.962419
26.78571	95.48082	1395.983	1.752447	0.95097
36.42857	104.2572	1405.54	1.752447	1.258319

Multi-channel analysis of surface wave (MASW)  
(1)

SK -2 Borehole

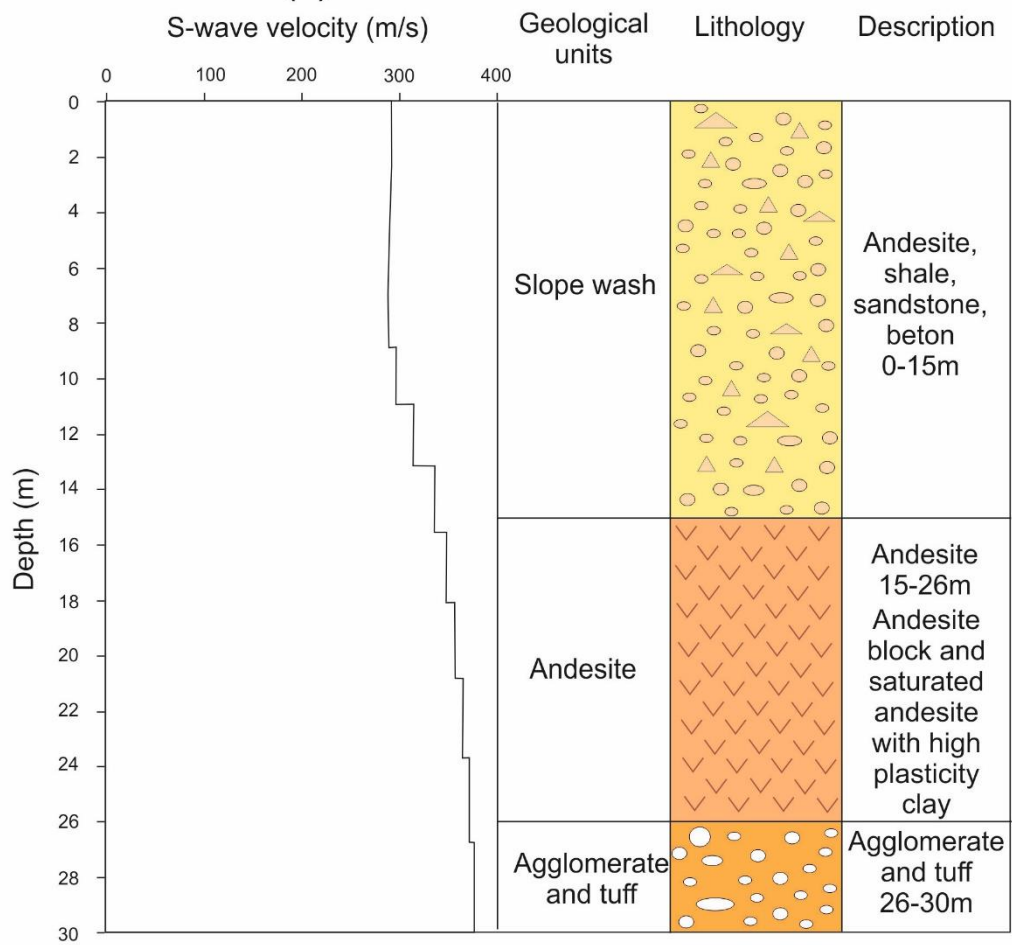


Figure 7.4 Comparison between the first survey of MASW and borehole SK-2

Multi-channel analysis of surface wave (MASW)  
(2)

SK -3 Borehole

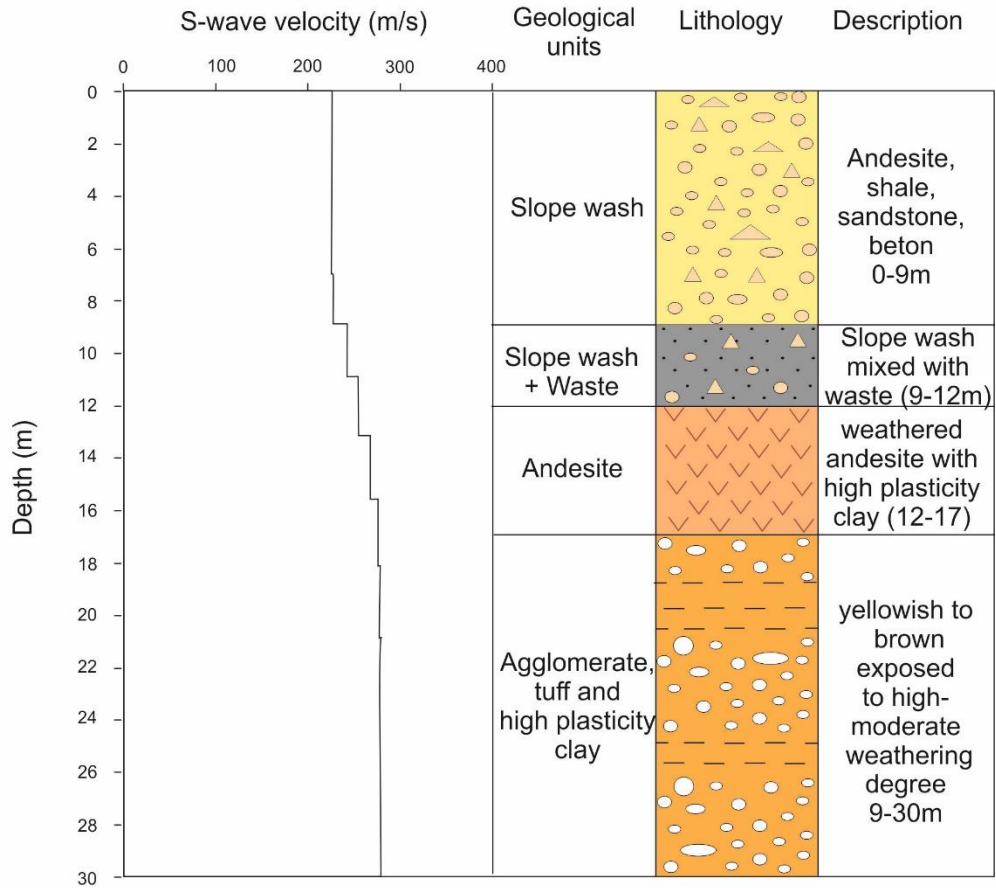


Figure 7.5 Comparison between the second survey of MASW and borehole SK-3

Multi-channel analysis of surface wave (MASW)  
(3)

SK -8 Borehole

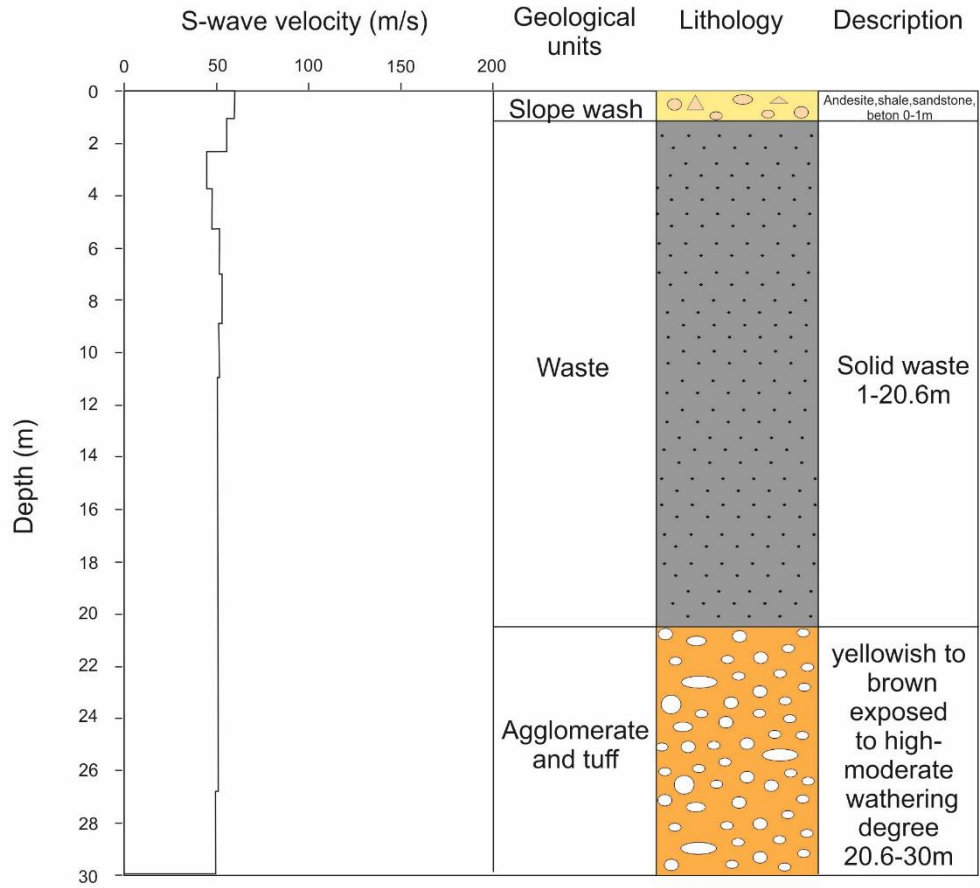


Figure 7.6 Comparison between the third survey of MASW and borehole SK-8

Multi-channel analysis of surface wave (MASW)  
(4)

SK -2 Borehole

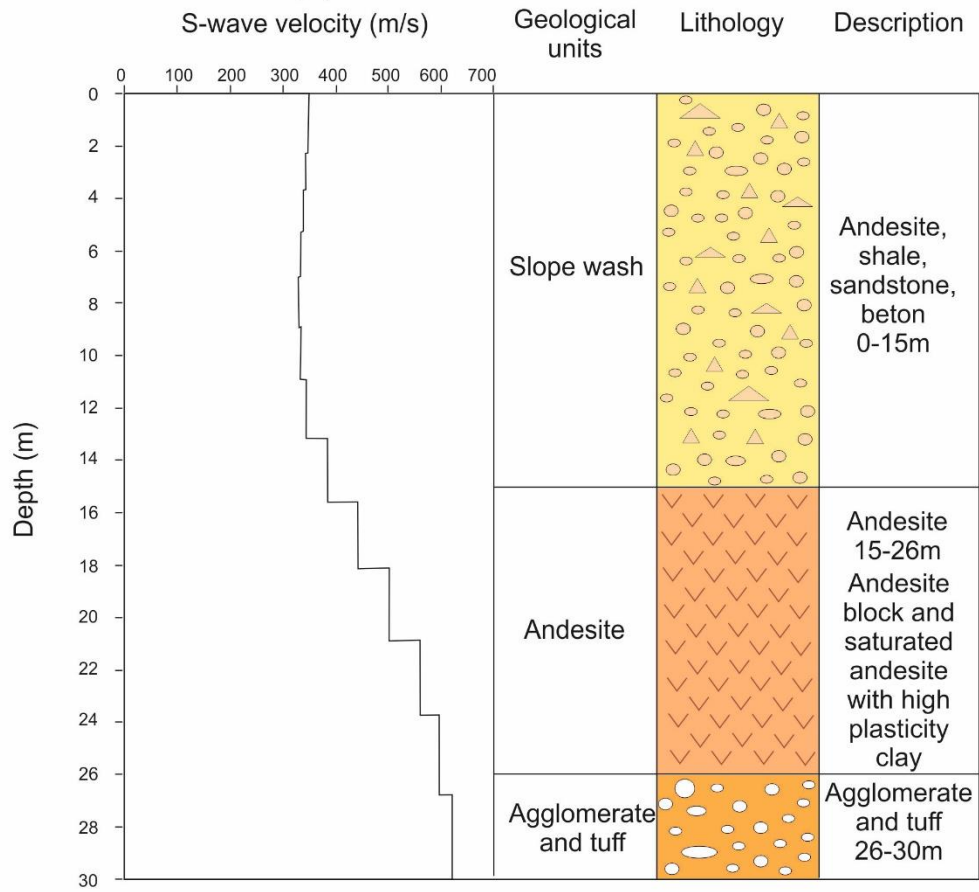


Figure 7.7 Comparison between the fourth survey of MASW and borehole SK-3



Multi-channel analysis of surface wave (MASW)  
(5)

SK -4 Borehole

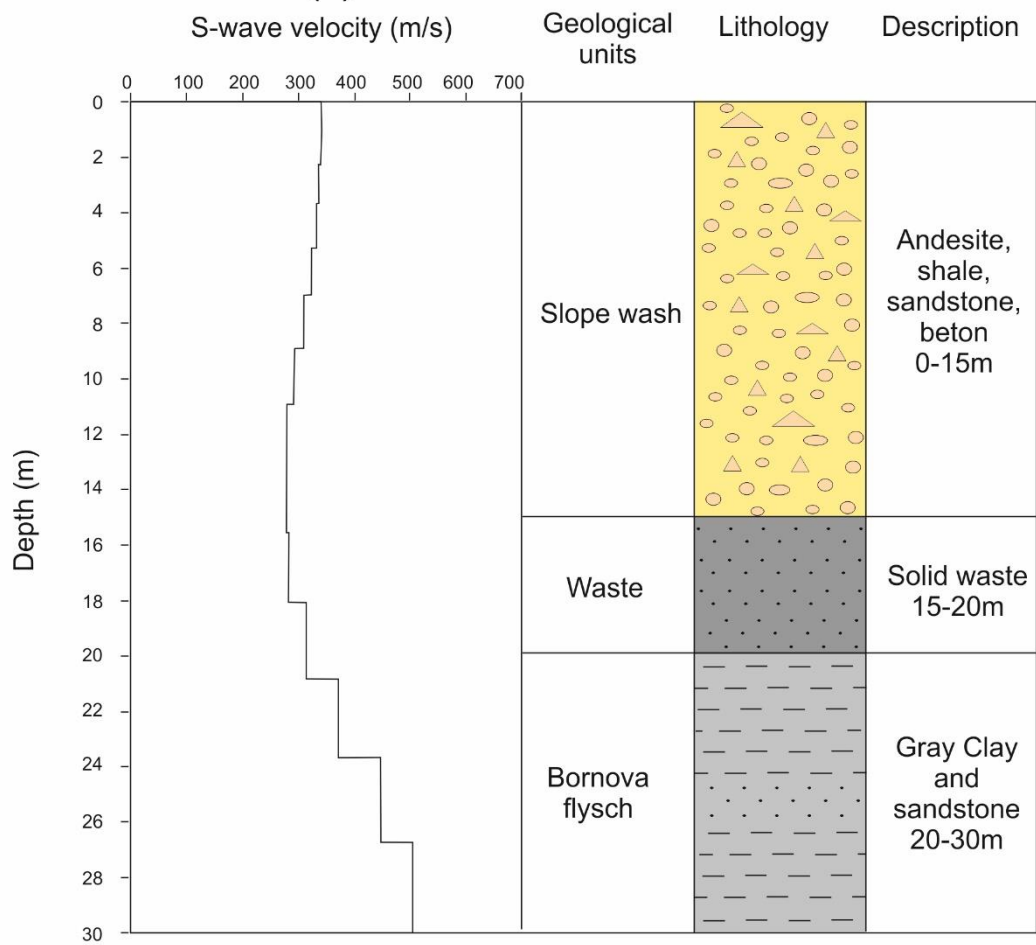


Figure 7.8 Comparison between the fifth survey of MASW and borehole SK-4

Multi-channel analysis of surface wave (MASW)  
(6)

SK -3 Borehole

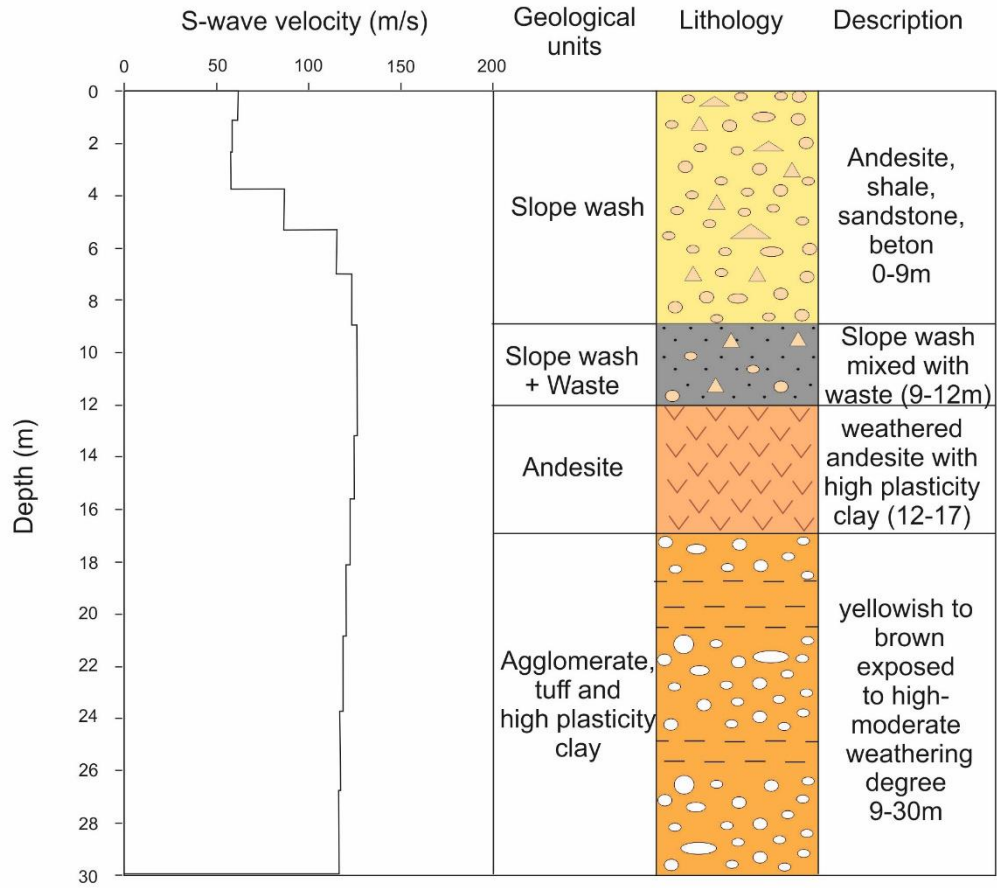


Figure 7.9 Comparison between the sixth survey of MASW and borehole SK-3

Multi-channel analysis of surface wave (MASW)  
(7)

SK -3 Borehole

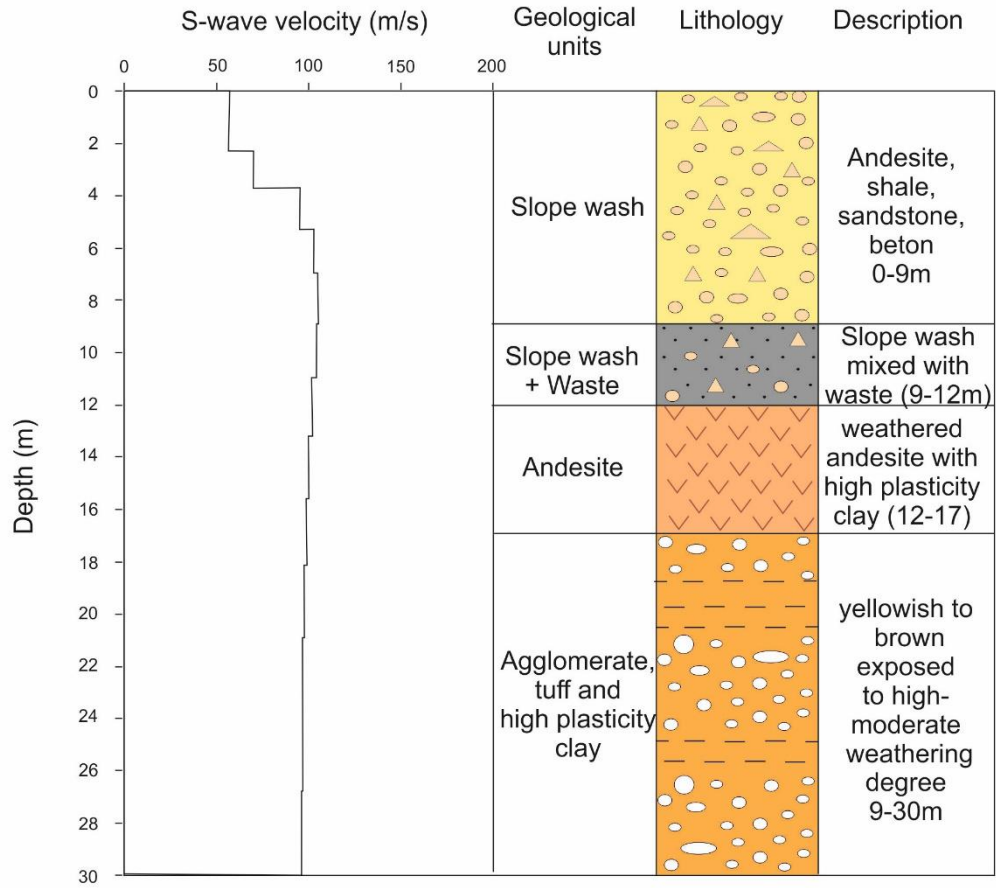


Figure 7.10 Comparison between the seventh survey of MASW and borehole SK-3

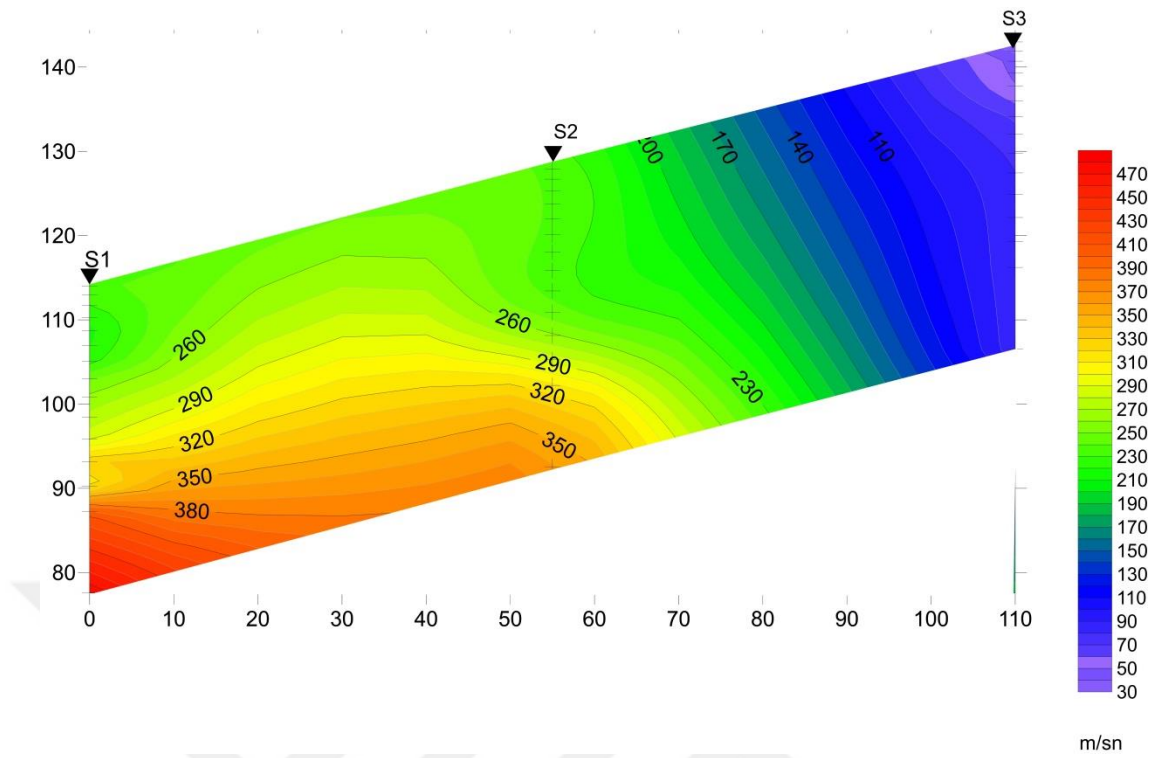


Figure 7.11 S- wave profile with depth parallel to landslide direction (NW-SE)

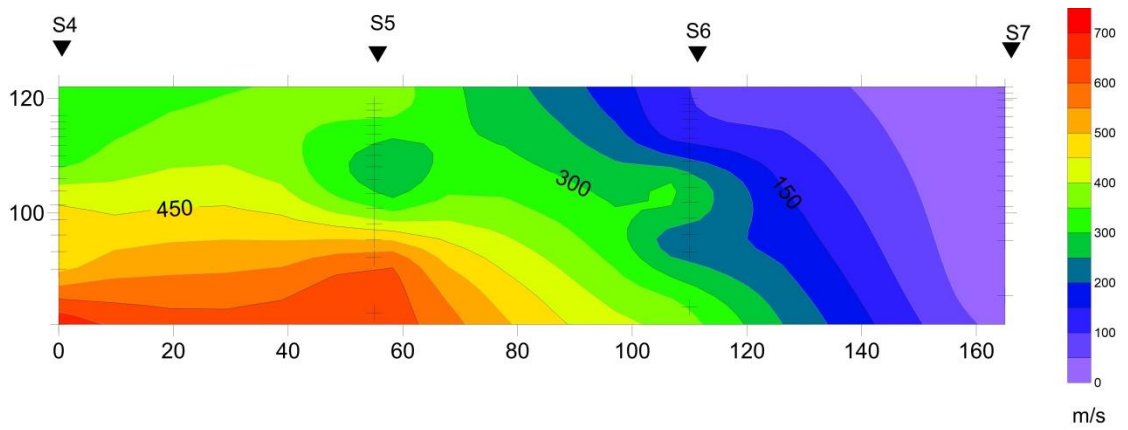


Figure 7.12 S- wave profile with depth perpendicular to landslide direction (NE-SW )

## **CHAPTER EIGHT**

### **CONCLUSION AND DISCUSSION**

#### **8.1 Conclusion**

In this study, shear wave velocity and resistivity distribution models were provided as well as physical properties and sliding surface of the landslide in Harmandali waste disposal site were determined using two of geophysical methods; electrical resistivity tomography (ERT) and multichannel analysis of surface wave (MASW). Both of geophysical methods provided us good results about the sliding surface which represent low resistivity and low S- velocity values. In terms of ERT method, the researches and site investigation indicate to the leachate effects in the site and the high plasticity of clay content (Clays with high plasticity occurred as a result of the weathering of andesite) and that was obvious in ERT-2 profile which is parallel to landslide direction supported by the geological settings and faults location.

ERT-2 profile was compared with the following boreholes SK-6, SK-8, SK-5, SK-3, SK2 and the results showed the lowest values of resistivity which basically existed in SK-6, SK-8, SK-3 which according to previous geological studies refer to the close leachates to the boreholes area and high plasticity clay content. The depth of the shear zone for each borehole according to the geophysical measurements in the study area is about 9 meter in SK-8, 22 meter in SK-3, 15 meter in SK-5 and 10 m in SK-2.

The results of MASW method were included in seven profiles of 1 D S- Wave velocity model which compared with the previous geological studies. Profile S1, profile S2 and profile S3 which are in landslide direction were compared to SK-2, SK-3, and SK-8 respectively. Profile S4, profile S5, profile S6 and profile S7 which are perpendicular to landslide direction were compared to SK-2, SK-4, and SK-3 for S6 and S7. Two of 2D S- wave velocity models were produced in the site. According to the comparison of 1D s- wave velocity profiles and 2D s- wave velocity models, it is clear that the velocity is decrease in profile S3, S6 and S7 which compared to the data obtained from boreholes SK-8 and SK- 3 respectively. The results of MASW method (Figure 7.11 and 7.12) are completely match ERT method results (Figure 7.1

and 7.2). By integrating the results of the both methods, the landslide body and potential sliding surface had determined through low velocity and resistivity values detection.

## **8.2 Discussion and Suggestions**

The Harmandalı waste disposal site is the only landfill in İzmir till now as there is no other available and suitable place for disposing the solid waste which produced in İzmir city center and it is expected to continue in work as landfill till the end of 2020. Therefore, many measures shall be taken to prevent further possible landslide events in the following years. Furthermore, administration buildings and the areas in vicinity of disposal site are under the threat of a slope failure, and the properties of stability problems should be well investigated. It was obvious that the main reason of the landslide is the number of leachates which existed in Harmandalı waste disposal site. So, some protection terms should be re-discussed in this domain of study. Landfill linear system design is the most important protection system in these cases and most be taken to the account during the landfill establishment. The liner system of Harmandalı waste disposal site is completely destroyed because of the reality that it becomes too old as it had been constructed since 1992. In Harmandalı waste disposal site there is no leachate collection system and the liquids which are produced from the waste are deeply affect the strength and lead to instability in the landfill. For that, it is suggested to provide permeable drainage layers and pipes for drain the water from the landfill and accordingly increase the strength in the area. Also, relocation the waste to more durable area in Harmandalı landfill is a good temporary solution and had been applied in the end of 2017 year by İzmir municipality.

## REFERENCES

- Adeyemo, I.A., Ojo, B.T., & Raheem, W.O. (2017). Comparison of Thickness and Depth Resolution Power of Wenner and Schlumberger Arrays: A Case Study of Temidire Quarters, Akure, Nigeria. *Journal of Geoscience and Environment Protection*, 5, 233-239.
- Aizebeokhai, A.B. 2010. 2D and 3D geoelectrical resistivity imaging: Theory and field design. *Scientific Research and Essays*, 5(23), 3592-3605.
- Anderson, N., Croxton, N., Hoover, R., & Sirles, P. (2008). Geophysical Methods Commonly Employed for Geotechnical Site Characterization. *Transportation Research Circular*, E-C130.
- Ayala, I.A. 2014. The spatial-temporal dimensions of landslide disasters. *Cambridge University press*, 61-77.
- Baglari, D. Dey, A. 2017. Effects of Source Characteristics in Passive Roadside MASW Survey. *Indian Geotechnical Conference 2017 GeoNEst*, 14-16 December 2017, IIT Guwahati, India.
- Batayneh, A.T., Al-Diabat, A.A. (2002). Application of a two-dimensional electrical tomography technique for investigating landslides along the Amman-Dead Sea highway, Jordan. *Environ Geol* 42:399-403
- Biswas, S., Dey, A. 2014. Passive MASW Survey and its Dispersion Imaging Scheme: A Review. *North East Student Geo – Congress on Advances in Geotechnical Engineering*. 18 October 2014, IIT Guwahati, India.
- Blight, G. 2008. Slope failures in municipal solid waste dumps and landfills: a review. *Waste Manage Res*, 26 (5).

Braile, L. (2015). *Love Wave Motions*, Retrieved May 23, 2018, from [https://media.oregonstate.edu/media/t/0\\_nmcsb56o](https://media.oregonstate.edu/media/t/0_nmcsb56o).

Braile, L. (2015). *Rayleigh Wave Motions*, Retrieved May 23, 2018, from [https://media.oregonstate.edu/media/t/0\\_nmcsb56o](https://media.oregonstate.edu/media/t/0_nmcsb56o).

British Columbia Bc Ministry of Environment .2016. Landfill Criteria for Municipal Solid Waste.

Caicedo, B., Giraldo, E., & Yamin, L. (2002). The landslide of Dona Juana Landfill in Bogota. A case study. Icon Engineering, Princeton, NJ, USA, Conference paper.

Camarero, P.L., Moreira, C.A. (2017). Geophysical investigation of earth dam using the electrical tomography resistivity technique. *International Engineering Journal*, 70 (1).

Capizzi,P., Martorana,R, Messina, P. & Cosentino, P.L. (2012). Geophysical and geotechnical investigations to support the restoration project of the Roman ‘Villadel Casale’, Piazza Armerina, Sicily, Italy. *Near Surface Geophysics*, 10, 145-160.

Chávez, R.E., Cifuentes-Nava, G., Tejero, A., Hernández-Quintero, J.E., & Geofísica, D.V. (2014). Special 3D electric resistivity tomography (ERT) array applied to detect buried fractures on urban areas: San Antonio Tecómitl, Milpa Alta, México. *Internacional*, 53, 4, 425-434.

DEU, (2016), Assessment of landslide and waste stability in Harmandalı waste disposal site report, In Turkish.

Dawson, C. (2016). Landslides - brittle failure Modeling Landslides - *Force Balance Rockslide spawns debris flow in British Columbia*, GSC.



- Dey, A., Morrison, H.F. (1979). Resistivity Modeling for arbitrarily Shaped Three-Dimensional Structures. *Geophysics*, 44(4), 753- 780.
- Drahor, M., Göktürkler,G., Berge, M. (2006). Application of electrical resistivity tomography technique for investigation of landslides: A case from Turkey, *Environmental Geology* 50(2):147-155.
- Duncan, J.M., Wright, S.G., & Brandon, T.L. 2014. *Soil Strength and Slope Stability*, (2.nd ed.). Canada.
- Evans, S.G., Roberts, N.J., Ischuk , A., & Morozova, G. (2007). Landslides triggered by the 1949 Khait Earthquake, Tien Shan, Tajikistan. *Engineering Geology*, 109, 195–212.
- Garofalo, F. (2014). *Physically constrained joint inversion of seismic and electrical data for near-surface applications*. Ph.D. Thesis, Engineering for Natural and Built Environmt.
- Geometrics, SmartSeis St, Retrieved June 2, 2018, from <http://www.geometrics.com/geometricsproducts/seismographs/smartseis-st/>.
- Ghosh, S., Hasan, S.E. (2010). Sanitary Landfill, *Environmental and Engineering Geology*, III.
- Gibb,J.P., Barcelona, M.J., Ritchey, J.D., & LeFaivre M.H.(1984). Effective porosity of geologic materials first annual report. *Illinois State Water Survey*.
- Gökhan Göktürkler, Çağlayan Balkaya, Zülfikar Erhan. (2008). Geophysical investigation of a landslide: The Altındağ landslide site, İzmir (western Turkey). *Journal of Applied Geophysics*, 65, 84-96.
- Günther, T.(2007). DC2DInvRes-Direct current 2D inversion and resolution, online documentation, Retrieved June 4, 2018, from <http://dc2dinvres.resistivity.net>.

- Guzzetti, F. (2000). Landslide fatalities and the evaluation of landslide risk in Italy. *Engineering Geology* 58(2), 89-107.
- Havenith, H.B & Bourdeau, C. ( 2010). Earthquake – Induced landslide hazards in mountain region : A review of case histories central Asia. *Geological Belgica*, 13 (3), 135-150.
- Havenith, H.B., Storm, A., Torgoev, I., Torgoev, A., Lamair, L., Ischuk, A., & Abdrakhmatov, K. (2015). Tien Shan Geohazards Database: Earthquakes and landslides. *Geomorphology*, 249, 16-31.
- Heisey, J.S., Stokoe, K.H., & Meyer, A.H. (1982). Moduli of Pavement Systems from Spectral Analysis of Surface Waves. *Transportation Research Record* 852.
- Hellman, K., Johansson, S., Olsson, P.V., & Dahlin, T. (2016). Resistivity Inversion Software Comparison. Conference Paper. DOI: 10.3997/2214-4609.201602016.
- Hughes, K.; Christy, A.; Heimlich, J. (2008). Landfill Types and Liner Systems; Ohio State University *Extension Fact Sheet CDFS-138-05*; The Ohio State University: Columbus, OH, USA, 4.
- Hungr, O., Leroueil, S., & Picarelli, L. (2013). The Varnes classification of landslide types, an update. *Springer Berlin Heidelberg*, 11 (2), 167-194.
- Jafari, N.H., Stark, T.D., & Merry, S. (2013). The July 10 2000 Payatas Landfill Slope Failure. *International Journal of Geoengineering Case Histories*, 2(3), 227.
- Jahanfar, A., Dubey, B., Gharabaghy, B., & Movahed, S.B. (2016). Landfill failure mobility analysis: A probabilistic approach. *International Journal of Environmental and Ecological Engineering*, 10 (5).
- Jahanfar, M.A. (2014). *Landfill Slope Stability Risk Assessment*, M.Sc. Thesis, The University of Guelph. Canada.

Jeotermal Kaynak ve Mineralli Surama Raporu, *RVA Device*. Retrieved April 20, 2018, from, <http://www.anatolyam.com.tr/ilgazrapor.pdf>

Jia, Y., Fu, B., Jolivet, M., & Zheng, S. (2015). Cenozoic tectono-geomorphological growth of the SW Chinese Tian Shan: Insight from AFT and detrital zircon U–Pb data. *Asian Earth Sciences*, *111*, 395-413.

Kanat, G. (2010). Municipal Solid waste Management in Istanbul. *Waste Management*, *30*, 1737-1745.

Karant, K.R. 1987. Ground Water Assessment: *Development and Management*. Tata McGraw- Hill Pub.Co, 720.

Keith Turner, A. & Schuster, L. (1996). *Landslide investigation and mitigation* (1.st ed.). USA: Transportation Research Board.

Kıncal, C. Akgün, A. & Koca, M. Y. (2009). Landslide susceptibility assessment in the Izmir (West Anatolia, Turkey) city center and its near vicinity by the logistic regression method. *Environmental Earth Sciences*.

Koca, M. Y., (1995). *Slope stability assessment of the abandoned andesite quarries in and around the Izmir city centre*. The Graduate School of Natural and Applied Sciences of Dokuz Eylul University, Izmir, PhD Thesis, 430.

Koelsch, F. (2001). Stability problems of landfills – The Payatas landslide. *Dr. Koelsch Geoenvironmental Technology LLC*.

Koelsch, F., Fricke, K., Mahler, C. & Damanhuri, E. (2005). Stability of landfills – the Bandung dumpsite disaster. In: Sardinia 2005, Tenth International Waste Management and Landfill Symposium, Cagliari, Italy.

- Laigre, C.S.E.L. (2014). The contribution of Electrical Resistivity Tomography (ERT) in Alpine dynamics geomorphology: case studies from the Swiss Alps. *Morphologie*, 20(1), 27-42.
- Lan, H. & Xu, Q. (2016). Some Issues on Strong Earthquake Induced Landslide in China. *Chile-China Workshop*. 16, Augustus.
- Lavigne, F., Wassmer, p., Gomez, C., & Pratomo, I. 2014. The 21 February (2005), catastrophic waste avalanche at Leuwigajah dumpsite, Bandung, Indonesia. *Geoenvironmental Disasters*, 1(10).
- Lawrence, M., & Jiang Y. (2017). Porosity, Pore Size Distribution, Micro-structure. *RILEM*. Department of Architecture & Civil Engineering BRE Centre in Innovative. Construction Materials (BRE CICM) Building Research Park, *Springer International Publishing*, 23, 39-7.
- Ling, S. (2015). *Landslide damming in Western Sichuan Province, China, with special reference to the 1786 Dadu River and 1933 Diexi events*. M.Sc. Thesis, University of Waterloo. Canada.
- Links, J.M. (2006). *Municipal, Industrial, and Hazardous Waste*. Johns Hopkins University. USA.
- Loke, M.H. (2000). *Electrical imaging surveys for environmental and engineering studies, a practical guide to 2D and 3D surveys*. Retrieved April 25, 2018, from, <http://geoelectrical.com>
- Loke, M.H. (2004). Tutorial : 2-D and 3-D electrical imaging surveys.

- Loke, M.H. (2015). 2-D and 3-D ERT surveys and data interpretation. *Piedmont Regional Order of Geologists Pasi Geophysics, Turin, Italy.*
- Loke, M.H., Barker, R.D. (1996). Rapid Least – Square Inversion of Apparent Resistivity Pseudosections By a Quasi –Newton Method. *Geophysical Prospecting* , 44, 131- 152.
- Lowrie, W. (2007). *Fundamentals of Geophysics* (2.nd ed.). USA: Camprdge University Press.
- Mihai,M., Paul,C., Cristian, M., Matei, M. (2017). MASW Seismic Method in Brebu Landslide Area, Romania. *Earth and Environmental Science*, 95 (032035).
- Mondal, SK., Sastry, RG., Pachauri, AK . (2007). High Resolution Resistivity Imaging of Naitwar Bazar Landslide, Garhwal Himalaya, India. *Symposium on the Application of Geophysics to Eng ineering and Environmental Problems*. 10.4133/1.2924721
- Mullins, C. (2015). Rayleigh wave propagation, *National Center for Physical Acoustics, The University of Mississippi*, Retrieved May 30, 2018, from <http://acoustics.org/2015/10/page/3/>.
- Novotny, O. (1999). Seismic Surface Wave.*Lecture Notes for Post Graduate Students*. Salvador, Bahia
- Ólafsdóttir , E.A. (2014). Multichannel Analysis of Surface Waves Methods for dispersion analysis of surface wave data. University of Iceland. Retrieved May 30, 2018, from file:///C:/Users/Lina/Desktop/New%20folder/Masw%20research/Fjölneamatíðnigre inng%20á%20yfirborðsbylgjum%20enskur%20texti.pdf

- Park, B., Miller, R.D., & Ivanov, J. (2004). Multichannel Analysis of surface waves (MASW) — active and passive methods. *Kansas Geological Survey, Lawrence, USA*.
- Park, B., Penumadu, D. (2005). Multichannel Analysis of Surface Wave (MASW) Method for Geotechnical Site Characterization. *Conference Paper, Geotechnical Special Publication*.
- Park, C. B., Miller, R. D., Xia, J. & Ivanov, J. (2007). Multichannel analysis of surface waves (MASW)- active and passive methods, *The Leading Edge*. 0106.
- Park, C.B., Miller, R.D., & Xia, J., 1996, Multi-channel analysis of surface waves using Vibroseis, Presented at the *66th Ann. Mtg. of SEG*, Denver, Expanded Abstracts, 68-71.
- Park, C.B., Miller, R.D., Xia, J., Hunter, J.A., & Harris, J.B., (1999). Higher mode observation by the MASW method. Exp. Abstrs. of Technical Program with Biographies, Society of Exploration Geophysicists, 69th Annual Meeting, Houston, TX. *Society of Exploration Geophysicists, Tulsa, OK*, 524–527.
- Pasierb, B. (2015). Numerical evaluation of 2d electrical Resistivity tomography for subsoil Investigations. *Technical transactions environmental engineering*, 2-Ś.
- Perrone, A., Lapenna, V., & Piscitelli, S. (2014). Electrical resistivity tomography technique for landslide investigation: A review. *Earth-Science Reviews*, 135, 65–82.
- Popesc, M., Urdea, P., Serban, R. (2014). Revealing the landslide structure using the electrical tomography technique case study: Buzad active landslide. *Geographica Timisiensis, XXIII*, 87 -96.

- Rambhatla, G., Suman, K., Ashok, K. (2006). 2D Electrical Resistivity Tomography of a Landslide in Garhwal Himalaya. *Conference: 6th International Conference & Exposition on Petroleum Geophysics*, Kolkata 2006.
- Ramke, H.G., (2008). Leachate Collection Systems. *1st Middle European Conference on Landfill Technology*, Szent István University. Budapest, Hungary.
- Robert, G., Nostrand, V., & Cook, K. (1966). Interpretation of Resistivity Data. *Geological Survey Professional Paper 499*. USA, Washington.
- Savoikar, P., Choudhury, D. (2011). Translational Seismic Failure Analysis of MSW Landfills Using Pseudodynamic Approach. *International Journal of Geomechanics* 12(2), 40-45.
- Sawangsuriy, A. (2012). Wave Propagation Methods for Determining Stiffness of Geomaterials, *Wave Processes in Classical and New Solids*, Chapter 7.
- Shanmugam, G., Wang, Y. (2015). The landslide problem, *Journal of Palaeogeography*, 4(2), 109-166.
- Shearer, P.M. (2009). *Introduction to Seismology* (2nd ed.). University of California, San Diego.
- SeisImager (2005): SeisImager/SWTM Manual, Pickwin v. 3.14 WaveEq v. 2.07 Manual v. 1.4.
- Stark, T. (1999). Stability of waste containment facilities. Urbana, 4818. Retrieved May 19, 2018, from <http://tstark.net/wp-content/uploads/2012/10/CP31.pdf>
- Stark, T.D. (1999). Stability of Waste Containment. *Municipal and Industrial Solid Waste Disposal Technology WasteTech '99*. New Orleans, Louisiana.

Strobbia , C. (2004). *Surface Wave Methods Acquisition, processing and inversion*. Ph.D. Thesis, Environmental Engineering at politecnico di Torino institution.

Telford, W.M. Geldart, L.B., & Sheriff, R.E. (1991). Applied Geophysics, (2.nd ed.), Campredge University Press, *Geological Journal*, 27(1).

UKAM, (1990), "Soil Investigation Report of Izmir-Harmandah Solid Waste Disposal Site" (In Turkish), *Hacettepe University International Karst WaterResources Application and Research Center*, 40, Ankara.

Ürüt, A., (2003). "İzmir Büyükehrinde Üretilen ve lenen Katı Atık Miktarları Hakkındaki statistiki Bilgiler", 2. *Ulusal Katı Atık Kongresi Bildiriler Kitabı*.

USGS, (2004). Landslide Types and Processes. Fact Sheet, U.S. Department of the Interior U.S. *Geological Survey* 3072.

Varnes, D. J. (1978). Slope movement types and processes. In R.I. Schuster & R.J.Krizek (eds.), *Landslide Analysis and Control*, National Academy of Sciences, National Research Council, Highway Research Board Special Report 176, 11–33.

Zohdy, A. A. R., Eaton, G. P., & Mabey, D. R. (1974). Application of Surface Geophysic to Ground – Warer Investigations. *Techniques of Water-Resources Investigations of the United States Geological Survey*, Chapter D1.